

**MULTIFUNCTIONAL SYNTACTIC
FOAMS: THERMAL, MECHANICAL AND
ELECTRICAL PROPERTIES**

DISSERTATION

Submitted in Partial Fulfillment of
the Requirements for
the Degree of

Doctor of Philosophy

at the
Polytechnic Institute of New York University
by

Vasanth Chakravarthy Shunmugasamy

January 2014

UMI Number: 3629561

All rights reserved

INFORMATION TO ALL USERS

The quality of this reproduction is dependent upon the quality of the copy submitted.

In the unlikely event that the author did not send a complete manuscript and there are missing pages, these will be noted. Also, if material had to be removed, a note will indicate the deletion.



UMI 3629561

Published by ProQuest LLC (2014). Copyright in the Dissertation held by the Author.

Microform Edition © ProQuest LLC.

All rights reserved. This work is protected against unauthorized copying under Title 17, United States Code



ProQuest LLC.
789 East Eisenhower Parkway
P.O. Box 1346
Ann Arbor, MI 48106 - 1346

**MULTIFUNCTIONAL SYNTACTIC FOAMS:
THERMAL, MECHANICAL AND ELECTRICAL
PROPERTIES**

DISSERTATION

Submitted in Partial Fulfillment of
the Requirements for
the Degree of

Doctor of Philosophy (Mechanical Engineering)
at the
Polytechnic Institute of New York University
by


Vasanth Chakravarthy Shunmugasamy

January 2014

Approved:


.....

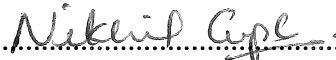
Department head signature


.....

Date

Approved by the Guidance Committee:

Major: Mechanical Engineering



.....
Nikhil Gupta, Ph.D.
Associate Professor of Mechanical
Engineering



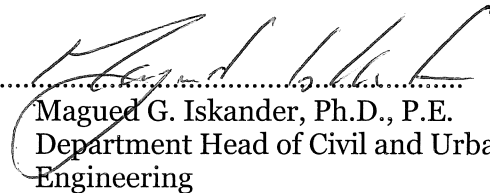
.....
Date



.....
Joo H. Kim, Ph.D.
Assistant Professor of Mechanical
Engineering



.....
Date



.....
Magued G. Iskander, Ph.D., P.E.
Department Head of Civil and Urban
Engineering



.....
Date



.....
Peter S. Walker, Ph.D.
Research Professor of Mechanical
Engineering



.....
Date

Microfilm or copies of this dissertation may be obtained from:

UMI Dissertation Publishing
ProQuest CSA
789 E. Eisenhower Parkway
P.O. Box 1346
Ann Arbor, MI 48106-1346

VITA

Vasanth Chakravarthy Shunmugasamy was born in Chennai, India on October 21, 1986. He completed his Bachelor of Engineering majoring in Mechanical Engineering in 2008 from the College of Engineering, Guindy, Anna University. He joined the Polytechnic Institute of New York University in 2008 for his Master's program in Mechanical Engineering. He completed his Master's program in 2010 and won the best Master's thesis award in the Department of Mechanical and Aerospace Engineering. He joined the Doctoral program in Spring 2011 and continued his research on lightweight polymer matrix composites, in the Composite Materials and Mechanics Lab (CMML) under the guidance of Dr. Nikhil Gupta.

ACKNOWLEDGEMENT

The author is thankful to Dr. Nikhil Gupta for patiently advising and guiding him throughout the entire research and for allowing him to be a member of the CMML. Special thanks to Dr. George C. Vradis for being a source of immense support. Dr. Dinesh Pinisetty, Dr. Jafar Al-Sharab and Dr. Joseph Borowiec are thanked for imparting knowledge through course work and valuable discussions while conducting this research. The author is also thankful to his CMML colleagues Dr. Dung D. Luong, Dr. Ronald Poveda, Sriniket Achar, Kevin Chen, James Cox, Harish Anantharaman, Matthew Labella and Steven E. Zeltmann for their valuable help and support. Alessandro Betti is acknowledged for helping in machining the samples. Last but not the least the author is thankful to his family for their blessings and support. The author would like to thank the Office of Naval research (grant N00014-10-1-0988) for funding this research.

DEDICATION

To my loving family.

Shunmugasamy Gurusamy: Dad, you are my true source of inspiration to do engineering degree in the first place. I will always remember the days when you taught me and Madan, Math and English for our school lessons.

Chandra Shunmugasamy: Mom, you are the binding force of our family. I'm in this position in my life, is because of you and the years you invested in teaching me about the good and bad in life.

MadanKumar Shunmugasamy: Madan, I have always looked upto you as my close friend and guide through-out my life. The one thing I always learnt from you is the brutal honesty you have always followed.

Last but not the least, I wish to thank my sister in-law Aishwarya MadanKumar and my nephew Baby Mahijit for all the love and affection they have showed on my family.

ABSTRACT

MULTIFUNCTIONAL SYNTACTIC FOAMS: THERMAL, MECHANICAL AND ELECTRICAL PROPERTIES

by

Vasanth Chakravarthy Shunmugasamy

Advisor: Nikhil Gupta, Ph.D.

Submitted in Partial Fulfillment of the Requirements
For the Degree of Doctor of Philosophy (Mechanical Engineering)
January 2014

Syntactic foams are light weight closed-cell composite foams obtained by dispersing hollow filler particles in a matrix medium. The existing applications of syntactic foam are mainly based on their compressive properties. The goal of the present research is to understand the fundamentals of structure-property correlations for syntactic foams that can help in developing multifunctionality in these composites, which can enable their applications in armors, electronic packaging, automobiles and aerospace structures. In this work, syntactic foams are characterized for thermal, electrical and mechanical properties. Experimental results obtained are helpful in identifying the relation between the syntactic foam microstructural parameters with the evaluated thermal, electrical and mechanical properties. Theoretical models are developed to obtain capabilities for predicting the properties and the model predictions are validated with experimental results. The model predictions are used to develop a method that can help in tailoring

two or more properties at the same time and make the material multifunctional. For example, hollow glass microballoon reinforced vinyl ester matrix syntactic foam that is designed for a dielectric constant of 3 can be designed to have coefficient of thermal expansion and density values in the range of 29.9 – 69.2 $\mu\text{m}/\text{m}/^\circ\text{C}$ and 800 – 925 kg/m^3 , respectively. This possibility of tailoring of syntactic foams makes them attractive multifunctional materials that can be used in imparting weight saving in structures.

TABLE OF CONTENTS

VITA.....	v
ACKNOWLEDGEMENT.....	vi
DEDICATION	vii
ABSTRACT.....	viii
TABLE OF CONTENTS	x
LIST OF FIGURES.....	xii
LIST OF TABLES	xvii
LIST OF SYMBOLS.....	1
CHAPTER 1. Composite materials	3
1.1 Introduction	3
1.2 Syntactic foams	4
1.3 Scope for the present work.....	6
CHAPTER 2. Objectives	8
CHAPTER 3. Thermal properties of syntactic foams.....	9
3.1 Introduction	9
3.2 Materials and Methods	11
3.3 Results	15
3.4 Discussion	17
CHAPTER 4. Dynamic mechanical properties of syntactic foams	26
4.1 Introduction	26
4.2 Literature Review	27
4.3 Materials and Methods	32
4.4 Results	34
4.4.1 Effect of temperature	34
4.4.2 Combined effect of temperature and frequency	46
4.5 Discussion	50
4.5.1 Effect of temperature	50
4.5.2 Temperature and frequency variation	57
CHAPTER 5. Electrical properties of syntactic foams	61
5.1 Introduction	61

5.2	Materials and Methods	66
5.3	Results and Discussion	68
CHAPTER 6. Unnotched Izod impact properties of syntactic foams		82
6.1	Materials and Methods	87
6.2	Results.....	88
6.3	Discussion	93
CHAPTER 7. Multifunctionality in syntactic foams		102
7.1	Multifunctionality modeling	102
CHAPTER 8. Conclusions		108
8.1	Thermal study	108
8.2	Dynamic mechanical study	108
8.3	Electrical study.....	109
8.4	Impact study.....	109
8.5	Development of multifunctional syntactic foams	110
CHAPTER 9. Recommendations for future work.....		111
9.1	Fatigue testing.....	111
9.2	Environmental study.....	111
9.3	High strain rate tensile behavior.....	111
9.4	Shock testing	111
REFERENCES		113

LIST OF FIGURES

Figure 1. Vinyl ester matrix syntactic foams containing 460 kg/m ³ hollow glass microballoon in (a) 0.3 and (b) 0.6 volume fractions and (c) a broken microballoon showing the wall thickness.	5
Figure 2. Illustration of change in wall thickness and radius ratio, η , in	6
Figure 3. DeepOcean Supporter ROV. Photo courtesy Ruth Clay, Trelleborg Offshore, Boston.	7
Figure 4. Scanning electron micrographs of (a) VE220-30 and (b) VE220-60 syntactic foams showing glass microballoons dispersed in vinyl ester matrix.....	14
Figure 5. Schematic of the experimental setup of thermomechanical	15
Figure 6. Thermal strain with respect to temperature for syntactic foams containing the same particle volume fraction (Φ_b) of (a) 30 % and (b) 60 % and for syntactic foams containing the same η of (c) 0.970 and (d) 0.936.....	16
Figure 7. Experimentally measured values of the CTE for the neat resin	17
Figure 8. (a) Comparison of theoretically calculated CTE values of syntactic foams using modified Turner's and Kerner's models and (b) and (c) validation of the models with data from literature [34, 56].....	21
Figure 9. CTE of syntactic foams normalized with the CTE of the matrix resin as a function of (a) wall thickness and (b) volume fraction of the HGM.	23
Figure 10. (a) Contour plot showing variation of CTE with respect to composite density. The composite density is varied from two different approaches on the horizontal axes. The scale bar represents both CTE and density in their appropriate units. (b) The same composite density variation is replotted with the volume fraction and wall thickness of HGM for clear illustration. The vertical scale bar represents density in kg/m ³	24
Figure 11. Storage modulus of (a) VE220, (b) VE320 and (c) VE460 syntactic foams containing $\Phi=0.3-0.6$. The temperature range 10-50°C is magnified in the inset graphs.	36
Figure 12. Variation of storage modulus (E') against temperature for neat vinyl ester resin. Regions I, II and III are identified by arrows and dash-dot lines. The dashed lines correspond to -50, 30 and 175°C where E' values are noted and presented in Table 5...	37

Figure 13. Loss modulus results for (a) VE220, (b) VE320 and (c) VE460 syntactic foams containing $\Phi=0.3-0.6$. The temperature range 10-50°C is magnified in the inset graphs.....	41
Figure 14. The damping parameter, $\text{Tan } \delta$, for (a) VE220, (b) VE320 and (c) VE460 syntactic foams containing $\Phi=0.3-0.6$. The temperature range 10-50°C is magnified in the inset graphs.	44
Figure 15. (a) Storage modulus of the neat vinyl ester resin obtained in the frequency range of 1-100 Hz for various temperatures, (b) master curve obtained using TTS at the reference temperature of 120°C and (c) the corresponding shift factors.....	47
Figure 16. The master curves for (a) VE220-30, (b) VE220-60, (c) VE460-30 and (d) VE460-60 syntactic foams at reference temperatures of 60, 90 and 120°C.	48
Figure 17. The shift factors for (a) VE220 and (b) VE460 syntactic foams, used for obtaining the master curves shown in Figure 16.	49
Figure 18. A comparison of Weibull distribution with the experimental data of storage modulus for neat vinyl ester resin.	52
Figure 19. Variation of the Weibull parameter m_2 with respect to (a) Φ and (b) syntactic foam density.....	54
Figure 20. Variation of the loss modulus at 30°C with respect to the syntactic foam density.....	55
Figure 21. Variation in maximum $\text{Tan } \delta$ with respect to the syntactic foam density.	56
Figure 22. Scanning electron micrograph indicating the presence of particle-matrix interfacial bond, which may be weak.	57
Figure 23. The Cole-Cole plot of syntactic foams and the neat vinyl ester resin.	58
Figure 24. Constants c_1 and c_2 of equation 5 plotted against syntactic foam density.....	59
Figure 25. The storage modulus values for syntactic foams and the vinyl ester resin obtained in the present work (represented by lines, extrapolated in the 100-150 Hz range) are compared with the existing data extracted from [78] (symbols).	60
Figure 26. The setup used in the measurement of impedance of syntactic foams.....	66
Figure 27. The variation of the impedance of neat vinyl ester resin with respect to frequency.....	69

Figure 28. Experimentally measured values (at 100 kHz) of the dielectric constant for the neat resin and twelve types of syntactic foams.	70
Figure 29. Variation of the experimentally measured dielectric constant at 100 Hz and 100 kHz with respect to the syntactic foams density.	71
Figure 30. Schematic of hollow glass microballoon to determine the dielectric constant.	72
Figure 31. Dielectric constant calculated for the glass microballoon using Equation (19), presented along with values obtained from the parallel and series model.	74
Figure 32. Comparison of theoretically calculated ϵ using J-S and Maxwell-Garnett model's with the experimental values (taken from [34]), at 1 MHz, for epoxy/HGM syntactic foams.	76
Figure 33. Dielectric constant of syntactic foams as a function of (a) volume fraction and (b) radius ratios of HGMs.	77
Figure 34. Variation of specific dielectric constant (normalized with respect to the syntactic foam density) as a function of (a) volume fraction and (b) the radius ratios of HGMs.	79
Figure 35. (a) Contour plot of variation of the dielectric constant with respect to the syntactic foam density. The syntactic foam density is varied with respect to both the volume fraction and the radius ratio of the microballoons. The scale bar represents both the dielectric constant and the foams density in their respective units. (b) The syntactic foams density plotted as a function of volume fraction and the radius ratio of the microballoons. The scale bar represents density in kg/m^3	80
Figure 36. Properties of hollow glass microballoons used in syntactic foams.	87
Figure 37. Schematic of the impact test setup along with the high speed camera used in the study.	88
Figure 38. Load-deflection plots for various types of syntactic foams containing microballoons of (a) 220, (b) 320 and (c) 460 kg/m^3 density, in $\Phi_{\text{mb}}=0.3-0.6$	90
Figure 39. Experimentally measured (a) impact strength and (b) impact strength with respect to syntactic foam density for the various syntactic foams tested.	91
Figure 40. Energy-deflection plots of for various types of syntactic foams containing microballoons of (a) 220, (b) 320 and (c) 460 kg/m^3 density, in $\Phi_{\text{mb}}=0.3-0.6$	92

Figure 41. Impact energy for various syntactic foams tested.	93
Figure 42. Macroscopic failure features of representative specimens of (a) VE220-30 and VE220-60 and (b) VE460-30 and VE460-60 syntactic foams tested under unnotched Izod impact test. The arrows indicate the direction of crack propagation.	94
Figure 43. (a) The model setup used in the simulation showing the loading and the boundary condition and (b) the normal stress distribution. The stress values shown in (b) are in Pa.....	95
Figure 44. Failure mechanisms observed in syntactic foams under impact loading conditions.....	96
Figure 45. Fractured surface on impact tested VE220-30 syntactic foam. The arrow in the top right image represents the direction of the crack propagation.....	97
Figure 46. SEM images of the fractured surface on impact tested VE220-60 type syntactic foam.	98
Figure 47. SEM images of the fractured surface on impact tested VE460-30 type syntactic foam.	99
Figure 48. SEM images of the fractured surface on impact tested VE460-60 type syntactic foam.	100
Figure 49. High speed images for (a) neat vinyl ester, and (b) VE220-30 and (c) VE220-60 syntactic foams. The time gap between two successive images in the sequence is 186 μ s. The arrows in the images indicate the crack propagating through the specimen.	101
Figure 50. High speed images for (a) VE460-30 and (b) VE460-60 syntactic foams. The time gap between two successive images in the sequence is 186 μ s. The arrows in the images indicate the crack propagating through the specimen.	101
Figure 51. The variation of the dielectric constant and the coefficient of thermal expansion of syntactic foams is plotted as a 3D-contour plot, while the syntactic foams density is plotted as a 2D-contour plot. The scale represents the CTE, dielectric constant and the syntactic foam density in their corresponding units.....	103
Figure 52. Selection of the elastic modulus and the CTE available in syntactic foams, for a constant dielectric value of $\epsilon=3$	103
Figure 53. Variation of the (a) CTE (μ m/m/ $^{\circ}$ C), (b) density (kg/m^3) and (c) modulus (GPa) of syntactic foams with respect to the HGM density and Φ_{mb} . The scale in (c) is the	

cumulative representation of the CTE, density and modulus in their corresponding units.
The dashed and dash-dotted lines represent CTE values of 40 and 60 ($\mu\text{m}/\text{m}/^\circ\text{C}$),
respectively. 106

LIST OF TABLES

Table 1. Theoretical and experimental densities and the matrix porosity volume fraction of the syntactic foams.	12
Table 2. Summary of available references on DMA testing of syntactic foams.	30
Table 3. Types and properties of hollow particles used in fabricating syntactic foams. ...	32
Table 4. Densities and the matrix porosity volume fractions for syntactic foams.	33
Table 5. Comparison of storage modulus values for syntactic foams at three representative temperatures.	38
Table 6. Maximum use temperature and glass transition temperature for various types of syntactic foams.	39
Table 7. Loss modulus at room temperature, maximum value over the test temperature range, and temperature at the maximum loss modulus for various syntactic foams.	42
Table 8. Tan δ at room temperature, maximum value over the test temperature range, and temperature at the maximum Tan δ for syntactic foams.	45
Table 9. Storage moduli values used in the Weibull distribution for syntactic foams.	53
Table 10. Existing studies on impedance and dielectric properties of syntactic foams.	63
Table 11. Existing studies on impedance and dielectric properties of syntactic foams, along with environmental effects.	64
Table 12. Theoretical and experimental densities, along with matrix porosity of the syntactic foams used in the study.	67
Table 13. Dielectric constant for the various types of syntactic foams along with the prediction from Maxwell-Garnett equation and J-S equation.	75
Table 14. Existing studies on pendulum impact testing of syntactic foams.	83
Table 15. Existing studies on drop weight impact testing of syntactic foams.	85
Table 16. Density, coefficient of thermal expansion and modulus of syntactic foams having a constant dielectric constant value of 3.	104
Table 17. Density and modulus of syntactic foams having a constant CTE value of 40 ($\mu\text{m}/\text{m}/^\circ\text{C}$).	107

Table 18. Density and modulus of syntactic foams having a constant CTE value of 60
($\mu\text{m}/\text{m}/^\circ\text{C}$)..... 107

LIST OF SYMBOLS

Symbol	Parameter
Φ	Volume fraction (subscripts m: matrix, g: glass, a: air, p: matrix porosity, mb: glass microballoon)
η	Radius ratio of hollow particle
R_i, R_o	Inner and outer radii of hollow particle
w	Wall thickness of hollow particle
R_e	Radius of surrounding medium
α	Coefficient of thermal expansion
E, K, G	Young's, bulk and shear modulus
ν	Poisson ratio
T_g and T_{max}	Glass transition and maximum use temperature
a_T	Shift factor
ρ^{th}, ρ^{exp}	Theoretical and experimental densities of syntactic foams
ε	Dielectric constant (subscripts o: vacuum)
Z	Impedance
R	Resistance
X_c	Reactance
ϕ	Phase angle
f	Frequency
C	Capacitance
t	Thickness of specimen
A	Contact area
Ψ	Electrical potential
ε_e	Dielectric constant of surrounding medium
$a_n, b_n, D_n, E_n, G_n, H_n, I_n$ and J_n	Constants
$P_n(\cos\theta)$	Legendre polynomial
r	Radial distance
$\delta_{m,n}$	Kronecker delta
Q, L and S	Constants

e_0

External applied field

χ

Polarization parameter

CHAPTER 1. Composite materials

1.1 Introduction

Composites are engineered materials which are a combination of two or more materials, wherein the constituents retain their physical structure, while resulting in enhanced properties over the individual constituents [1]. Although composites in general are considered engineered materials, materials available in nature have shown composites like structures. Some examples of natural composites are tree bark and human bones which have hierarchical microstructures. In usual practice, engineered composite materials consist of matrix medium (base material) with a reinforcing phase. The matrix material can be a metal or a polymer. The reinforcing phase (filler) can be in the form a fiber, particulate, platelets or interpenetrating phases [2-4]. The filler materials can be chosen from a wide variety of materials such as glass, polymers, metals, ceramics or natural available materials [2, 5]. The reinforcing phase is selected in such a way to provide augmented properties to the existing base materials.

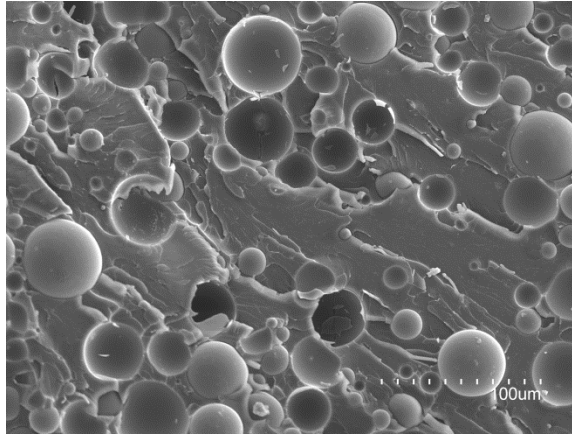
The demand for reducing emissions and improving the fuel efficiency while preserving safety has become top priority owing to the fast depletion of the natural resources. Aerospace, automotive and space industries are looking for innovative engineered materials to cope with this demand [6]. In this regard, polymer matrix composites are gaining attention owing to their higher specific properties, low water absorption, corrosion resistant, ease of fabrication and tailorability in properties [7, 8]. One of the easiest ways of decreasing the weight of the structures is to remove material from them. This can be done by imparting air packets inside the materials in the form of porosity. In this context these materials can be classified as open cell and closed cell foam composites. The open cell foams consist of channels or pockets of air structures throughout the materials microstructure [9, 10]. Although open cell foam method reduces weight, it can potentially undermine the structural integrity of the structure as there is lack of controllability of the pores.

1.2 Syntactic foams

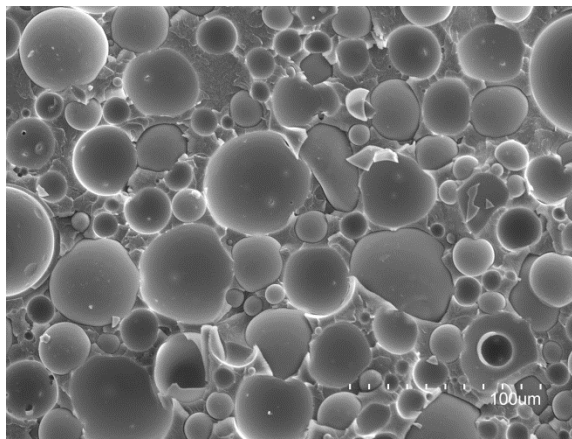
One of the novel ways of imparting porosity in structures is to enclose the porosity inside stiff shells. These materials are called syntactic foams, where in hollow microballoons are enclosed inside a matrix material [11]. The matrix materials that have been commonly used include metals, polymers and the filler materials include glass, polymers, ceramics, metals and fly ash cenosphere [7, 12]. The varying parameters in preparing syntactic foams include choosing the matrix and microballoon materials, the volume fraction and the density of the microballoons. Figure 1 shows the variation of the volume fraction of microballoons in syntactic foams and the wall thickness of a broken microballoon. The density of the microballoons is determined by the wall thickness parameter of the reinforcing microballoon. The microballoon wall thickness is characterized by radius ratio (η) as

$$\eta = R_i / R_o$$

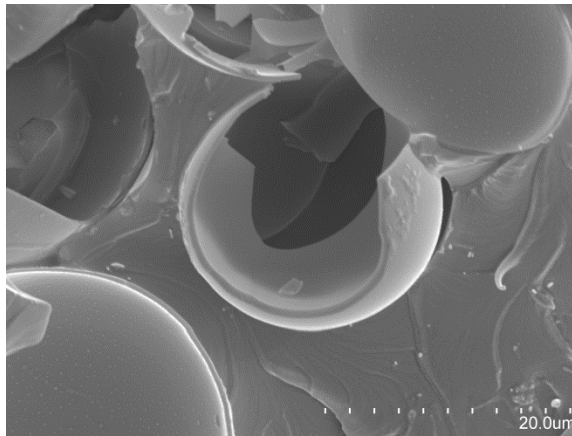
where R_i and R_o are the inner and outer radii of the microballoon. Figure 2 shows the illustration of the variation in the wall thickness parameter of the microballoon. So by controlling the volume fraction and wall thickness parameter of microballoon, the effective mechanical, thermal, electrical properties of the composites can be tailored. This tailorability capability of the syntactic foams makes it an ideal candidate to be used in weight saving applications.



(a)



(b)



(c)

Figure 1. Vinyl ester matrix syntactic foams containing 460 kg/m^3 hollow glass microballoon in (a) 0.3 and (b) 0.6 volume fractions and (c) a broken microballoon showing the wall thickness.

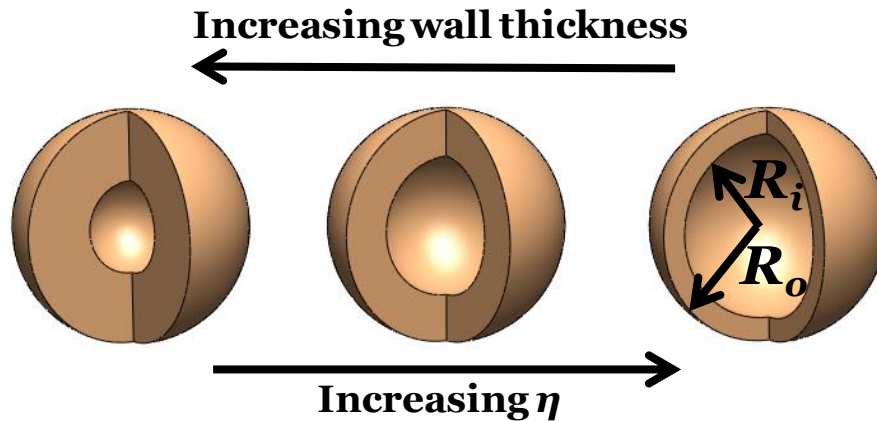


Figure 2. Illustration of change in wall thickness and radius ratio, η , in hollow particles (not to the scale).

1.3 Scope for the present work

The weight saving potential of syntactic foams is finding applications in aerospace, automotive and space structures. DeepOcean Supporter remotely operated vehicle (ROV) shown in Figure 3, used in deep sea exploration, contains hollow glass microballoon (HGM) polymer matrix syntactic foams as buoyancy aids. Airplane manufactures Airbus® and Boeing® utilizes structural members made from syntactic foams for weight saving applications [13]. The electronic device industry requires materials to be used as underfills and protection layers for the semiconductor chips. This application requires materials with low moisture absorption and tailorable coefficient of thermal expansion (CTE). The tailorability of CTE is important as the thermal stress mismatch between the substrate and the encasing cover could cause failure of the structure. One another application in the electronic field is the demand for materials with low and tailorable dielectric constant. The low dielectric constant materials help in increasing velocity of signal propagation while reducing attenuation [14].

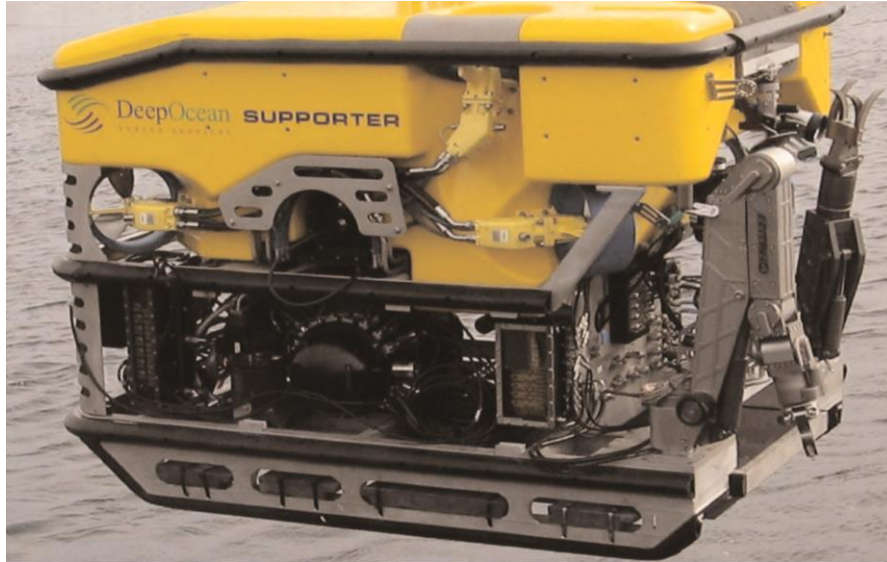


Figure 3. DeepOcean Supporter ROV. Photo courtesy Ruth Clay, Trelleborg Offshore, Boston.

The aerospace and marine applications require advanced composites which can be used as core materials for sandwich structures. These applications require the materials to be subjected to not only static loading at room temperature, but also dynamic loading under varying frequency and over wide variations of temperature ranging from cryo temperature to above glass transition temperatures. For syntactic foams to be used in these applications, a thorough understanding of the mechanical, thermal and electrical properties in terms of the variable parameters namely, volume fraction and wall thickness of the microballoon should be understood. The models developed for the variation of thermal and electrical properties of syntactic foams could be used in conjunction with the existing model for mechanical properties, to design syntactic foams for desired applications. So hollow glass microballoon reinforced vinyl ester matrix syntactic foams are evaluated for the CTE, dynamic mechanical and electrical properties.

CHAPTER 2. Objectives

The main objective of the current study is to understand the correlation between thermal, mechanical and the electrical properties of polymer matrix syntactic foams, with an aim to develop them as lightweight multifunctional composites. In particular, glass microballoon (HGM) reinforced vinyl ester matrix syntactic foams are utilized in the study. The following are the technical objectives of the study:

1. Experimental study of syntactic foams for
 - a. Thermal properties: coefficient of thermal expansion and glass transition temperature
 - b. Dynamic mechanical properties: storage and loss modulus
 - c. Electrical properties: dielectric constant
 - d. Impact properties
2. To develop theoretical understanding of the variation of the thermal (CTE) and electrical (dielectric constant) properties of the syntactic foams with respect to the material parameters. The theoretical models are developed with an aim to incorporate the two varying parameters namely, wall thickness and volume fraction of the HGMs.
3. Use the experimentally validated theoretical models for parametric studies to understand the correlations between various properties and develop methods to simultaneously modulate the mechanical, thermal, and electrical properties in the desired ranges.

CHAPTER 3. Thermal properties of syntactic foams

3.1 Introduction

Dispersion of hollow filler particles in matrix medium results in closed cell structured composite foams, called syntactic foams. Previous studies have characterized the mechanical properties of syntactic foams with respect to the properties and volume fraction of the filler particles [15]. Wall thickness and volume fraction of hollow particles (microballoons) are found to be very effective in tailoring the mechanical properties of syntactic foams [16]. These lightweight materials are suitable for weight saving applications in aerospace structures [17], undersea pipeline insulation [18], and electronic coating and packaging [19] because of their high compressive properties and low moisture absorption compared to other lightweight materials such as foams containing gas porosity. In these applications syntactic foams are often subjected to high temperatures, leading to interest in their thermal properties such as glass transition temperature [20] and thermal conductivity [21, 22].

In thermal applications, the coefficient of thermal expansion (CTE) is an important design parameter [23]. In applications such as electronic packaging or thermal insulation, matching of CTE between the insulation material and the substrate is important in order to minimize thermal stresses and the possibility of failure at the interface [23]. Thermal expansion behavior of foams used in space shuttle external fuel tanks has been studied extensively to minimize the possibility of failure due to thermal stresses [24]. Thermal expansion characteristics of polyurethane foams, used in insulating gas pipelines and refrigerated vehicles, have also been extensively studied [25, 26]. In addition, thermomechanical characterization of a special type self-repairing shape memory polymer-based syntactic foams has been explored previously [27]. Cell size, cell wall thickness, total porosity, and material properties are found effective in tailoring the thermal expansion characteristics of foams. Wouterson et al. [28] studied the thermal stability of short fiber-reinforced syntactic foams. Addition of a small weight

fraction (1–3%) of fibers did not measurably improve the thermal stability of the syntactic foams. The thermal stability of syntactic foams is generally better than that of the neat resin due to the presence of high volume fraction of ceramic particles in their microstructure [20]. Addition of ceramic fillers has shown to reduce the CTE of polymer and metal matrix composites compared to the matrix materials in previous studies [29–32]. It has been observed that addition of alumina particles in epoxy matrix decreases the CTE of the composite [33]. Although similar effects are also expected in syntactic foams due to the presence of ceramic microballoons, currently the published literature is severely lacking in understanding the relations between CTE of syntactic foams and material parameters such as volume fraction, wall thickness, and properties of particles. CTE of glass microballoon (HGM)/epoxy syntactic foams is found explored in two previous studies where up to 2 wt.% [16] and 51.3 vol.% [34] addition of HGMs reduced the CTE of epoxy by 5 and 54.3 %, respectively. However, despite indicating that HGMs will reduce the CTE of composites, these experimental studies are limited to studying only a few material compositions in a narrow range and do not provide general understanding between CTE and various material parameters.

Several theoretical models are available for predicting the CTE of particulate composites [35–39], fiber-reinforced composites [40], and composites with aligned axisymmetric [41] and non-axisymmetric [42] ellipsoidal particles. Gunes et al. [43] evaluated the effect of CTE on the shape memory performance of composites with different reinforcements and the experimental results were compared with theoretical models. One of the early works by Turner [38] assumed that the filler material is isotropic and the composite's CTE does not depend on the size and shape of the filler particles. It is also assumed that the dimensional changes of the constituent materials with respect to temperature are at the same rate as the bulk composite material. Although this model fits well with experimental data on several composite systems, deviations are also observed because of assumptions inherent to this model [37, 44]. Kerner's model is another widely used approach for CTE estimation, which accounts for shear and isostatic stresses developed in the component phases of the particulate composites [36, 39, 45]. This model does not deviate from the linear relation between the CTE of the components and volume fraction of each component [44]. Both Kerner's and Turner's models have been applied to a large number of polymer and metal matrix composite materials containing solid reinforcements with close matching with

experimental data. Including the wall thickness in these models can provide better predictions of CTE of hollow particle filled composites compared to the present approaches [46]. It is known that microballoon wall thickness can have a prominent effect on the properties of composites. Therefore, development of a predictive model that can account for both wall thickness and volume fraction of microballoons is desired.

In this study, experimental and theoretical studies are conducted to relate the CTE of syntactic foams with the volume fraction and wall thickness of HGM and gain insight into the possibility of designing lightweight materials for thermal applications.

3.2 Materials and Methods

HGM/vinyl ester syntactic foams are studied in this work. The manufacturing procedure is explained in detail in a published paper [47]. HGM of three different nominal densities (220, 320, and 460 kg/m³) are used in four different volume fractions (30, 40, 50, and 60%) to fabricate twelve types of syntactic foams. Syntactic foams containing less than 30 vol.% particles are usually not fabricated because of microballoon floatation issues during composite fabrication. In addition, higher density of such syntactic foams limits interests in such compositions because they do not lead to weight saving in their applications. Therefore, in line with the published literature, the HGM volume fraction is maintained in the range 0.3–0.6 in this study. The mean particle size and wall thickness are reported in Table 1 [48]. The microballoon wall thickness is characterized by radius ratio (η) which is previously defines as

$$\eta = R_i / R_o \quad (1)$$

where R_i and R_o are the inner and outer radii of the microballoon. The calculated values of η for the selected particles are also given in Table 1. The η values appear to be in narrow range for the selected particles. However, due to limited interest in high-density particles, the available literature mostly uses particles with density lower than 500 kg/m³. In addition, previous studies have shown that the mechanical behavior of syntactic foams containing 220 and 460 kg/m³ particles is different. With increasing volume fraction of lighter particles the composite modulus decreases, whereas the composite modulus increases with increasing volume fraction of higher density particles. Therefore, in syntactic foams these particles are defined as thin- and thick-walled, respectively.

Table 1. Theoretical and experimental densities and the matrix porosity volume fraction of the syntactic foams.

Specimen type ^a	Mean particle diameter (μm) ^b	Wall thickness (μm) ^b	Radius ratio (η) ^b	Theoretical density (kg/m ³)	Measured density (kg/m ³)	Matrix porosity (vol.%)
VE220-30	35	0.52	0.970	878	857.8	2.3
VE220-40				784	774.1	1.2
VE220-50				690	642.1	6.9
VE220-60				596	566.2	5.0
VE320-30	40	0.88	0.956	908	872.1	3.9
VE320-40				824	752.3	8.7
VE320-50				740	667.3	9.8
VE320-60				656	617.7	5.8
VE460-30	40	1.29	0.936	950	904.0	4.8
VE460-40				880	878.4	0.2
VE460-50				810	768.4	5.1
VE460-60				740	725.5	2.0

^a The nomenclature includes VE for vinyl ester, followed by the HGM density and then vol.%

^b Data taken from [48]

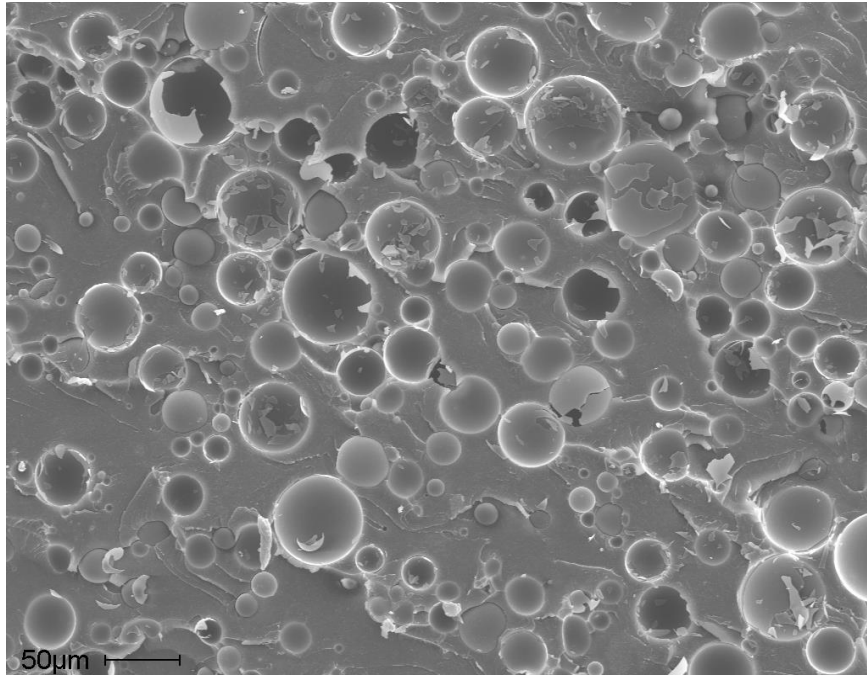
Apart from the porosity that exists inside hollow particles, some air is usually entrapped in the matrix during the composite material fabrication. This air porosity is termed as matrix porosity [15]. The presence of matrix porosity may also affect the composite properties. The matrix porosity (Φ_p) volume percentage is calculated by

$$\Phi_p = \left(\frac{\rho^{th} - \rho^{exp}}{\rho^{th}} \right) \quad (2)$$

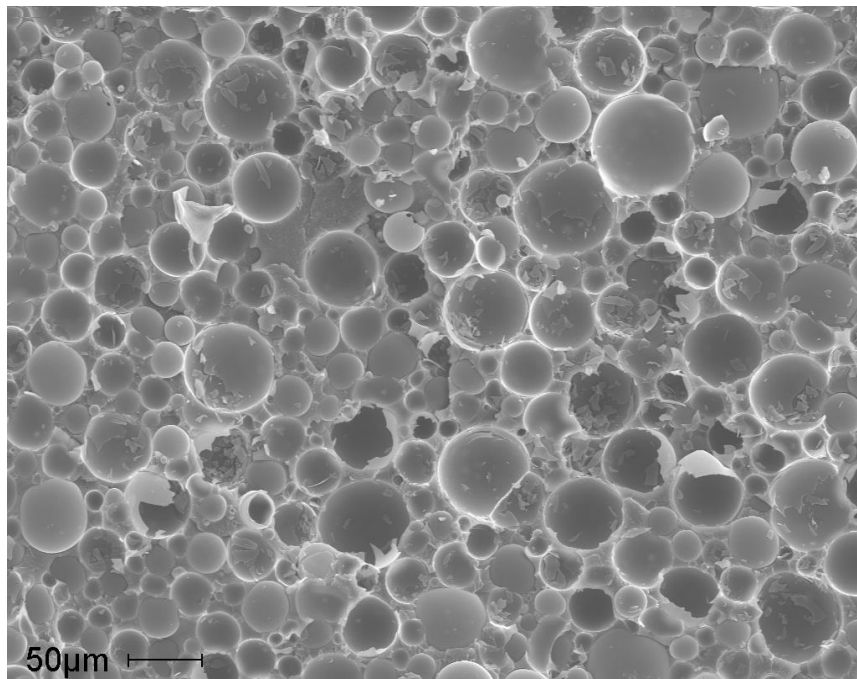
where ρ^{th} and ρ^{exp} are the theoretical and the experimental densities of the syntactic foam specimen, respectively. Table 1 shows the theoretical and the experimental densities of specimens along with the matrix porosity content. The matrix porosity values corroborate well with those reported in previous studies [47, 49]. In this study, the matrix porosity values are presented to establish the quality of fabricated composites.

These values are not related to the CTE of syntactic foam because in the small size specimens used for CTE measurement the specimens containing voids can be generally detected and avoided by careful surface inspection. In addition, weight and dimensions of each CTE specimens are measured to calculate their density. The presence of a large matrix pore leads to low density of specimen and it can be easily detected and excluded from the experimental scheme. The representative microstructures of syntactic foams containing 30 and 60 vol.% HGM of 460 type are shown in Figure 4a, b, respectively. Uniform distribution of HGMs can be observed in these figures. Similar microstructure is observed in foams containing 220 and 320 type particles. The particle diameter can vary over a wide range in a given sample of microballoons. In addition, the wall thickness of the same diameter particles can vary over a wide range. The effect of such polydispersivity of particle diameter and wall thickness has been previously studied by theoretical and experimental means and relations are available [48].

Specimens of nominal dimensions $11 \times 5.5 \times 3.5$ mm (length \times width \times height) were prepared for CTE measurement. The specimens were heated in a convection oven for 3 h at 70°C to remove any adhered moisture. The CTE characterization was conducted using a Q400 Thermomechanical Analyzer (TA Instruments, New Castle, DE, USA). The schematic of the experimental setup is shown in Figure 5. An expansion type probe was used for measuring the temperature-dependent dimensional changes. A preload of 0.02 N was applied for all the tests. The measurements were conducted from room temperature to 75°C at a heating rate of $3^\circ\text{C}/\text{min}$. Five specimens of each material type were tested. Time, temperature, and change in specimen height were recorded during the test and used for estimation of CTE. In initial experiments 1, 3, and $5^\circ\text{C}/\text{min}$ heating rates were tried. Based on the results, $3^\circ\text{C}/\text{min}$ was found to be suitable because the thermal equilibrium in the specimens was obtained at this rate and the results were consistent.



(a)



(b)

Figure 4. Scanning electron micrographs of (a) VE220-30 and (b) VE220-60 syntactic foams showing glass microballoons dispersed in vinyl ester matrix.

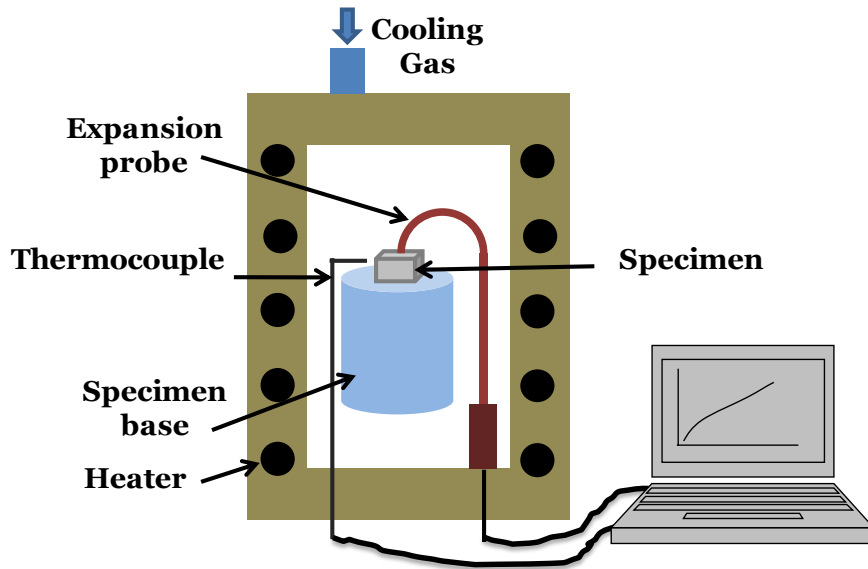


Figure 5. Schematic of the experimental setup of thermomechanical analyzer used for CTE measurement.

3.3 Results

Figure 6a and b depict representative plots of thermal strains with respect to temperature for syntactic foams having 30 and 60 vol.% HGM of different η , respectively. Similar trends are observed for other volume fractions as well. It is observed in these figures that the dimensional change is the steepest for the case of thin-walled particles, which indicates that the dimensional stability of the composite increases with the particle wall thickness. Figure 6c and d compare a representative set of results for composites containing HGM densities of 220 and 460 kg/m³ in different volume fractions. The trends for other type of particles are also similar. Figure 6c and d show that increasing the HGM volume fraction in syntactic foams increases their dimensional stability.

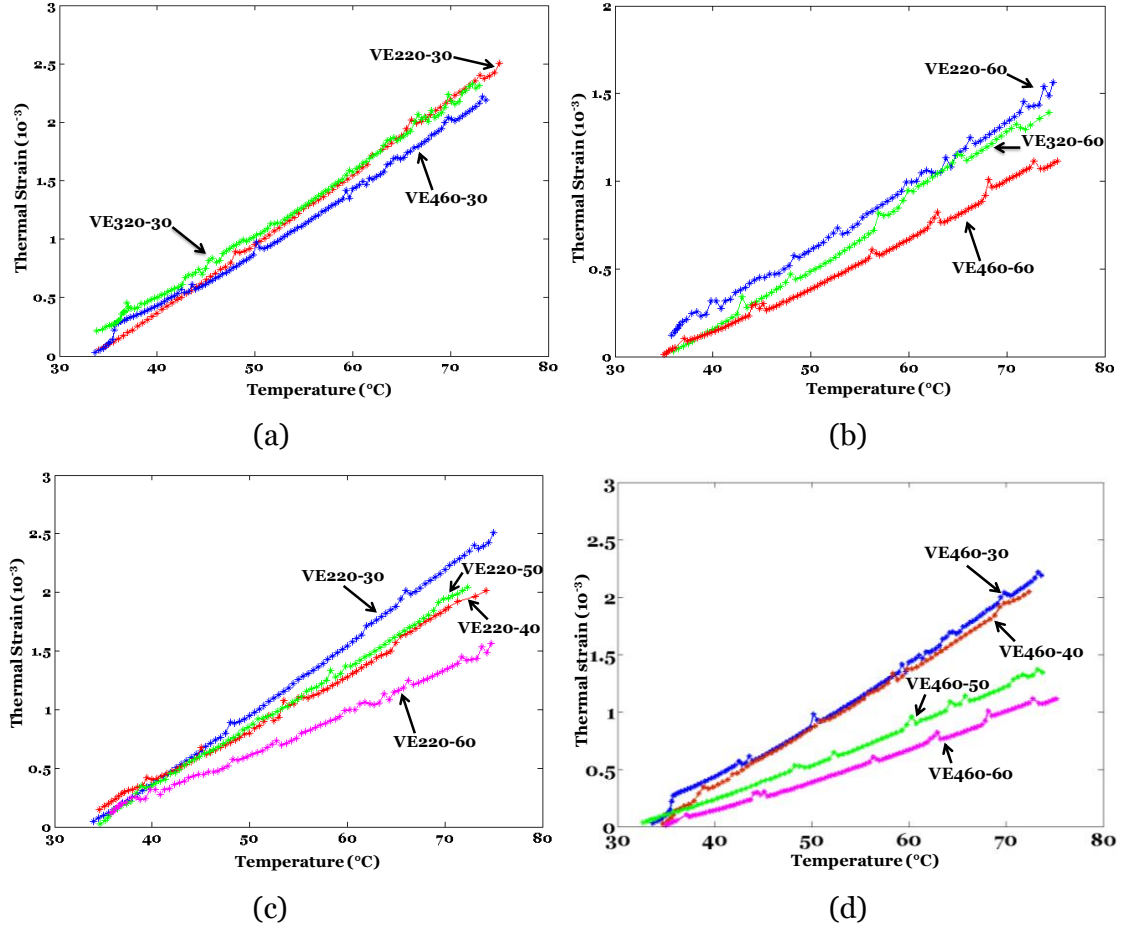


Figure 6. Thermal strain with respect to temperature for syntactic foams containing the same particle volume fraction (Φ_b) of (a) 30 % and (b) 60 % and for syntactic foams containing the same η of (c) 0.970 and (d) 0.936.

The slope of such graphs is used to calculate the CTE of syntactic foams (α) by

$$\alpha = \frac{1}{l} \times \frac{dl}{dT} \quad (3)$$

where l is the initial specimen length and dl/dT is the slope of the dimension change-temperature plot.

The experimental results of CTE are plotted in Figure 7. A clear trend is seen that the increase in the HGM volume fraction provides better dimensional stability to the composite. For comparison, the CTE of the neat resin is also plotted in the same graph. It is observed that the value of CTE of syntactic foams is up to 60.4 % lower compared to

that of the neat resin. The lowest CTE value is observed for VE460-60 syntactic foam, which contains HGM of the highest wall thickness in the maximum volume fraction selected in this study. While the experimental trend that increasing the glass content in the composite reduces the CTE of the composite is not surprising, the relations between the syntactic foam CTE and various material parameters such as wall thickness and volume fraction need to be developed to obtain a quantitative understanding of these parameters. Also, the relative effectiveness of microballoon wall thickness and volume fraction in tailoring CTE of syntactic foams and their effect on the composite's density need to be determined. These relations can help in engineering lightweight composites for applications where insulation material having a specific CTE value or the lowest possible density is required.

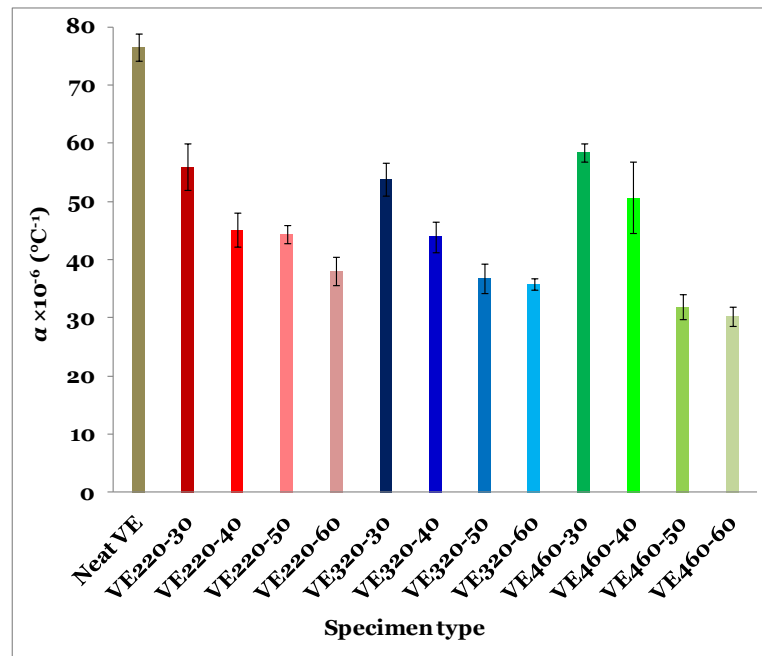


Figure 7. Experimentally measured values of the CTE for the neat resin and twelve compositions of syntactic foams. Error bars represent standard deviations in experimental measurements.

3.4 Discussion

The experimental results are analyzed to understand the effect of several parameters on CTE of syntactic foams. Figure 7 clearly shows that increasing the volume fraction and wall thickness of HGMs decrease the CTE of syntactic foams. It is observed

that increasing the volume fraction of 220 type particles from 30 to 60 vol.% decreases the CTE of composites by 27–50% compared to the neat resin. Similarly, 320 and 460 type HGMs lead to 30–53% and 23–60% decrease in CTE of syntactic foams compared to neat vinyl ester resin. In comparison to the volume fraction, microballoon wall thickness has a milder effect on CTE of syntactic foams within the range considered in this study. At the same HGM volume fractions, the syntactic foam CTE values show difference within 10 % for most particle types. Only VE220-50 shows deviation from this trend because of higher CTE value than that expected from the experimental trends for the entire set of compositions. The density of syntactic foams also follows qualitatively similar trends with respect to the microballoon volume fraction and wall thickness, as seen in Table 1. Among the present batch of composites, VE460-60 has the highest glass content, which also corresponds to the lowest measured CTE value. The experimental observations are limited to compositions characterized in this study. A broader understanding of syntactic foam CTE with respect to particle volume fraction and wall thickness can be obtained through developing predictive models and using them to conduct parametric studies. It is of interest to develop a correlation between composite density and CTE through these models because most applications of syntactic foams are based on their low density and the ability to tailor the mechanical and thermal properties as per the requirement of the application. Here, two different models applicable to solid particle-reinforced composites are analyzed for the possibility of modifying them for hollow-particle-reinforced composites and the predictions are validated with experimental results. The rule of mixtures (ROM) is widely used to obtain upper bound of various properties of composite materials. The ROM for the CTE estimation can be written as [40]

$$\alpha = \alpha_m \Phi_m + \alpha_b \Phi_b \quad (4)$$

where α_m and α_b are the CTE of matrix resin and HGM, respectively, and Φ_m and Φ_b are the volume fraction of the matrix and HGM, respectively. ROM is the basis for several theoretical models. Other theoretical models for predicting the CTE values of solid particle-reinforced composites are also available [32, 50]. These models are mainly applicable to composites containing solid fillers and do not include particle wall thickness, which is an additional parameter available for variation in syntactic foams. Turner's [29, 30, 32] and Kerner's [36, 39] models have been modified in this study to include the effect of wall thickness of hollow particles. Turner's model is given by

$$\alpha = \frac{\alpha_m \Phi_m K_m + \alpha_b \Phi_b K_b}{\Phi_m K_m + \Phi_b K_b} \quad (5)$$

where K_m and K_b are the bulk moduli of the matrix and microballoon, respectively. The bulk modulus can be estimated from the Young's modulus of the constituents as

$$K = E/(3(1-2\nu)) \quad (6)$$

where E is the Young's modulus and ν the Poisson's ratio of the respective constituents.

The effective modulus of HGM differs from the modulus of the glass and depends on its wall thickness. To determine the effective HGM modulus, an equivalent sphere with the same properties as the hollow HGM is assumed [51-53]. The radial displacement at the outer surface of the two systems are compared and the effective modulus (E^*) as a function of the microballoon radius ratio is found as [51]

$$E^* = \frac{E_g(1-2\nu)(1-\eta^3)}{(1-2\nu) + \left(\frac{1+\nu}{2}\right)\eta^3} \quad (7)$$

where E_g is the modulus of the microballoon glass material and is taken to be 60 GPa [54]. The modified Turner's model for CTE of hollow particle filled composites is given by substituting Eqs. (6) and (7) in Eq. (5) as

$$\alpha = \frac{\alpha_m \Phi_m E_m \left[(1-2\nu_g) + \left(\frac{1+\nu_g}{2}\right)\eta^3 \right] + \alpha_b \Phi_b E_g (1-\eta^3)(1-2\nu_m)}{\Phi_m E_m \left[(1-2\nu_g) + \left(\frac{1+\nu_g}{2}\right)\eta^3 \right] + \Phi_b E_g (1-\eta^3)(1-2\nu_m)} \quad (8)$$

where ν_g is the Poisson's ratio of the microballoon material and is taken to be 0.21, E_m is the modulus of the matrix and is taken to be 2.82 GPa [47] and ν_m the Poisson's ratio of the matrix material and is taken to be 0.35 [55].

The Kerner's model is given by

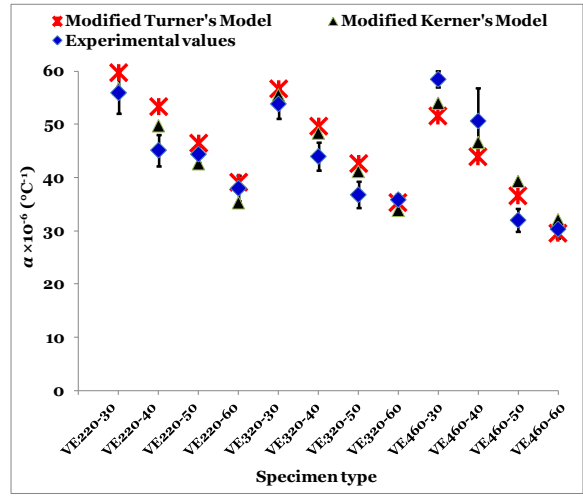
$$\alpha = \alpha_m \Phi_m + \alpha_b \Phi_b + \Phi_b \Phi_m (\alpha_b - \alpha_m) \times \left(\frac{K_b - K_m}{\Phi_m K_m + \Phi_b K_b + \frac{3K_b K_m}{4G_m}} \right) \quad (9)$$

where G_m is the shear modulus of the matrix material. The Kerner's model (Eq. 9) can be modified to obtain a new version (Eq. 10) for hollow-particle filled composites as

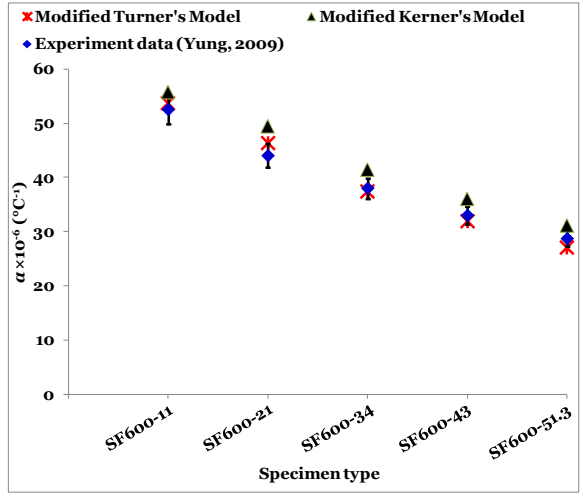
$$\alpha = \alpha_m \Phi_m + \alpha_b \Phi_b + \Phi_b \Phi_m (\alpha_b - \alpha_m) \left[\frac{E_g (1 - \eta^3)(1 - 2\nu_m) - E_m [(1 - 2\nu_g) + \frac{(1 + \nu_g)}{2} \eta^3]}{\Phi_m E_m [(1 - 2\nu_g) + \frac{(1 + \nu_g)}{2} \eta^3] + \Phi_b E_g (1 - \eta^3)(1 - 2\nu_m) + \frac{1}{2} E_g (1 - \eta^3)(1 + \nu_m)} \right] \quad (10)$$

The values of η have been calculated from the experimental data on particle density and size in a previous study [47]. Equations (8) and (10) are used to determine the theoretical estimates of CTEs of various syntactic foams and the results are presented in Figure 8a. The CTE of the resin is taken as 76.5 $\mu\text{m}/\text{m } ^\circ\text{C}$ from the experimental results presented in Figure 7 and the CTE of the microballoon glass is taken as 4 $\mu\text{m}/\text{m } ^\circ\text{C}$. A comparison shows that the theoretical values presented in Figure 8a closely match with the experimental values (Figure 7) and the difference is in the range of $\pm 15\%$ for the modified Turner's model and $\pm 18\%$ for the modified Kerner's model. There are several factors such as matrix porosity and use of literature values for Poisson's ratio that can lead to some difference in the theoretical and experimental results. In addition, polydispersion in particle size and volume fraction can also cause some variation in the measured properties [48]. Accounting for these parameters can provide closer theoretical estimates.

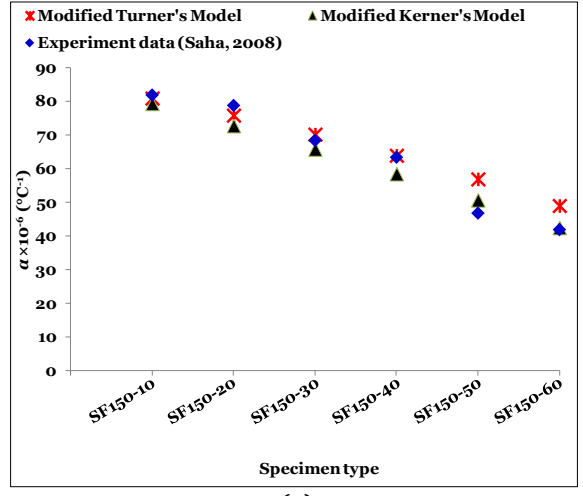
Since both modified Turner's and Kerner's models showed close match with the experimental results, they are also validated with experimental values of CTE taken from two previous studies [34, 56]. Syntactic foams with microballoon densities of 600 and 150 kg/m^3 were used to analyze the CTE by Yung et al. [34]. and Saha et al. [56], respectively. The comparison of theoretical and experimental values for these studies is shown in Figure 8b, c. Close matching between theoretical and experimental results provides further validation of the model to predict CTE of syntactic foams. Experimental data on syntactic foams containing $\Phi_b < 0.3$ is available only in Saha et al. [56]. Such data are not readily available on a wide variety of syntactic foams because high density of such syntactic foams makes them unsuitable for applications that look for weight saving through the use of lightweight materials.



(a)



(b)



(c)

Figure 8. (a) Comparison of theoretically calculated CTE values of syntactic foams using modified Turner's and Kerner's models and (b) and (c) validation of the models with data from literature [34, 56].

The modified Turner's model is selected to perform a parametric study on the variation of CTE with respect to radius ratio and volume fraction of HGMs. Figure 9a plots the normalized CTE as a function of η for various values of Φ_b . It is observed that in the case of $(1 - \eta) < 0.4$ (i.e., thin-walled particles), which is important for weight saving in structures, there is a steep change in CTE. Most existing studies on syntactic foams have used particles of $(1 - \eta)$ value in the range of (0–0.1), where CTE decreases sharply. However, rate of CTE change reduces substantially after $(1 - \eta) > 0.4$ (i.e., thick-walled particles). For $(1 - \eta) > 0.5$ the rate of CTE change is almost negligible. This trend suggests that for a fixed volume fraction of HGM, use of microballoons of $(1 - \eta) > 0.5$ only leads to increase in the composite density without further improving the dimensional stability of the composite. A comparison of trends in Figure 9b shows that increasing the volume fraction of HGM of the same wall thickness can cause over 80 % reduction in CTE of the composite compared to the matrix material. Within the range $0.8 < \eta < 1$, the CTE behavior of syntactic foams changes rapidly, but the rate of change decreases at $\eta < 0.8$. The line for $\eta = 0$ presents the case of solid particle-reinforced composite and is the lower bound on the CTE. The trends observed in CTE values need to be further analyzed with the syntactic foam density.

The weight saving potential through selection of material parameters is explored in Figure 10 for HGM/vinyl ester syntactic foams. The 3D contour plot in Figure 10a shows the CTE variation with respect to the composite density. The composite's density variation by means of HGM volume fraction and wall thickness (or density) is plotted on the bottom of Figure 10a as a 2D contour plot. The scale bar in Figure 10a demonstrates both CTE variation and the composite density variation in their appropriate units as indicated in the figure. The relation between the composite density and the microballoon volume fraction and density is further clarified in Figure 10b as a 2D contour plot. The syntactic foam density ranges covered in Figure 10a, b are the same. Reduction in the composite's CTE is evident with increase in the HGM volume fraction and wall thickness. A solid and a dotted line are drawn in Figure 10, for two representative constant values of $\alpha = 300 \times 10^{-7}$ and $\alpha = 500 \times 10^{-7} \text{ } ^\circ\text{C}^{-1}$, respectively. These lines are also projected on the density contour plot. It can be observed in Figure 10a that a variety of HGM/vinyl ester syntactic foam compositions having densities over a large range of 572–1050 kg/m³ can be used to obtain $\alpha = 500 \times 10^{-7} \text{ } ^\circ\text{C}^{-1}$. Correspondingly, Figure 10b shows that a

combination of HGM volume fractions in the range or 24–60 % with the HGM densities in the range of 180–700 kg/m³ can provide the same CTE value of $500 \times 10^{-7} \text{ }^\circ\text{C}^{-1}$.

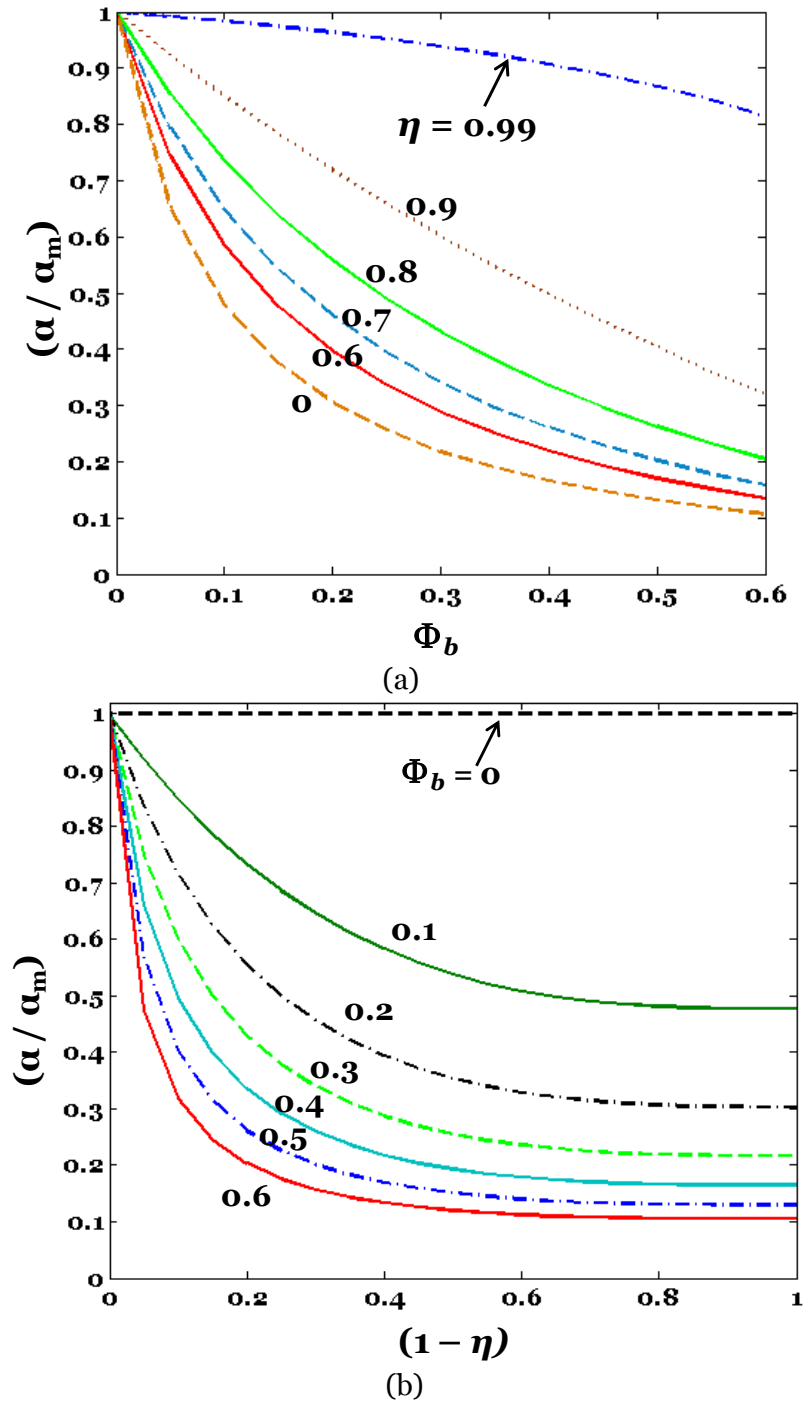
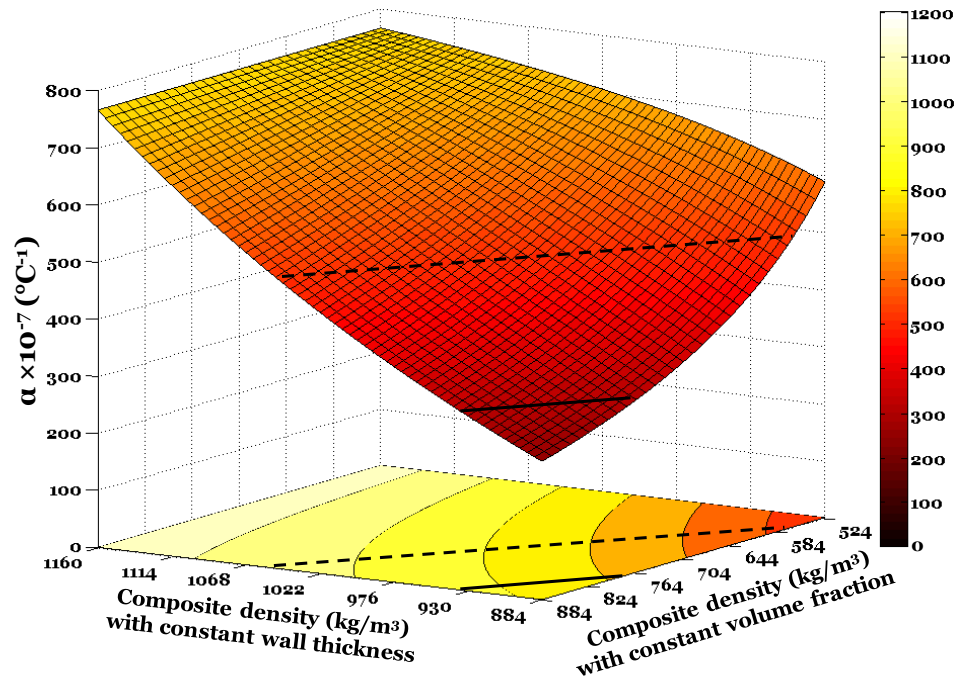
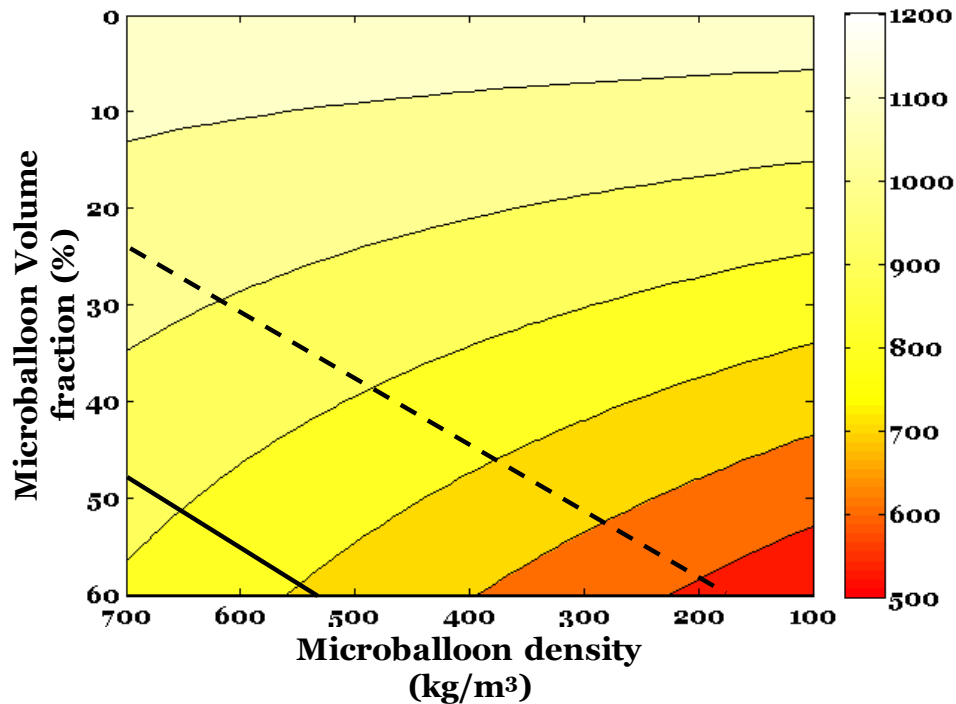


Figure 9. CTE of syntactic foams normalized with the CTE of the matrix resin as a function of (a) wall thickness and (b) volume fraction of the HGM.



(a)



(b)

Figure 10. (a) Contour plot showing variation of CTE with respect to composite density. The composite density is varied from two different approaches on the horizontal axes. The scale bar represents both CTE and density in their appropriate units. (b) The same composite density variation is replotted with the volume fraction and wall thickness of HGM for clear illustration. The vertical scale bar represents density in kg/m^3 .

Similar observations can be made for $\alpha = 300 \times 10^{-7} \text{ }^\circ\text{C}^{-1}$, where numerous syntactic foam compositions having densities in the range of 784–935 kg/m³ can be used to obtain the CTE value. Such flexibility helps in tailoring the properties of the composite for thermal applications. The parametric study results for CTE observed in Figure 10 can be combined with the existing understanding on mechanical properties of syntactic foams. Extensive information is already available on elastic modulus and Poisson's ratio variation with respect to the HGM volume fraction and wall thickness [47, 55, 57]. Such combination of mechanical and thermal properties will be helpful in selecting the best possible parameters in designing syntactic foams for a given application.

CHAPTER 4. Dynamic mechanical properties of syntactic foams

4.1 Introduction

Hollow particle reinforced composites, called syntactic foams, have gained significant attention in recent years due to their lightweight and high compressive energy absorption capability. Syntactic foams are classified as closed cell composite foams [11]. They comprise of two phases namely the matrix resin and the hollow filler particles (microballoons) [13, 16]. Syntactic foams are sometimes described as three-phase composites, considering interstitial voids within the matrix as the third phase [58, 59]. The high specific mechanical properties and the tailorability make them useful in weight sensitive applications [15, 60]. Several compositions of nanoscale reinforced syntactic foams are now developed for further enhancement in mechanical and thermal properties [61, 62]. The current applications of syntactic foams include aircraft components, spacecraft solid rocket booster nose cones fillings, and thermal insulation for deep sea pipelines [6, 63, 64]. While a wide body of literature is now available on room temperature mechanical properties of syntactic foams, relatively few efforts are found focused on thermal properties such as coefficient of thermal expansion [65], thermal conductivity [21, 22] and high temperature behavior [20]. Understanding of elastic and viscoelastic properties of syntactic foams is required under a wide range of temperatures and frequencies for their existing applications, which can help in developing composites with tailored vibration response, high temperature mechanical properties, and energy absorption capabilities.

Dynamic mechanical analyzer (DMA) is a widely used technique for characterization of viscoelastic material parameters [33, 66]. In this technique a sinusoidal force is applied on a specimen and the phase difference in the stress and strain response due to viscoelasticity is recorded. The in-phase and out-of-phase components of stress are used to calculate the storage modulus (E') and loss modulus (E''), respectively [67, 68]. The storage modulus provides a measure of energy stored in

the material while loss modulus refers to the amount of energy dissipated in each cycle of the sinusoidal deformation [67]. The ratio of the loss modulus to the storage modulus gives the damping parameter, $\tan \delta$. The loss modulus-temperature data can be used to measure the glass transition temperature (T_g). Developing correlations of these properties with the microballoon wall thickness and volume fraction (Φ) is desired for syntactic foams. Considering the wide variety of matrix and microballoon materials used in fabricating syntactic foams in the published literature, developing correlations between the fundamental microstructural features and dynamic properties can immensely help in engineering syntactic foams as per the requirements. The relevant past studies are summarized below to establish the scope of the present work.

4.2 Literature Review

The available past efforts of studying viscoelastic properties of syntactic foams are summarized in Table 2. A wide range of literature on compressive, tensile and flexural properties of syntactic foams is available [47, 69-71], but only a few studies of narrow scope are found focused on viscoelastic properties [28, 72-79]. Material compositions, test conditions, and main results are summarized for each available study on viscoelastic properties in Table 2. Single cantilever and three-point bending modes are the most commonly used test configurations.

Variation of dynamic mechanical properties of syntactic foams with respect to temperature has been studied [72-79]. Sankaran et al. reported the effect of hardener used with the epoxy resin on the properties of glass microballoon reinforced syntactic foams [73]. Syntactic foams of constant density ($\sim 450 \text{ kg/m}^3$) were prepared with three different hardeners. Room temperature (30°C) storage modulus values of 1354, 1500 and 1530 MPa were reported for the three syntactic foam systems, which demonstrate the importance of hardener and the cure chemistry on the viscoelastic properties of polymer matrix syntactic foams. Capela et al. and Ferreira et al. studied the dynamic mechanical properties of plain, glass fiber and carbon fiber reinforced syntactic foams [72, 75]. They observed a decrease in $\tan \delta$ from 0.872 to 0.559 for plain syntactic foams, as the weight fraction of the microballoons increased from 2 to 17%. The E' was found to increase with the addition of the short fiber reinforcement (both glass and carbon fibers), in comparison to the plain syntactic foams. The test parameters such as frequency and

amplitude are not specified in these papers. It is a common observation that syntactic foams have lower storage modulus at room temperature compared to that of the neat resin. Wouterson et al. studied the effect of three different lengths of carbon fibers on the dynamic mechanical properties of syntactic foams [28]. Increase in the storage modulus of 118%, at room temperature, in comparison to neat epoxy resin, was obtained for 3 wt.% short carbon fiber reinforced syntactic foam. The fiber content and length were found to have no effect on T_g of the syntactic foam.

John et al. studied the effect of temperature variation on the dynamic mechanical properties of plain and nanoclay reinforced cyanate ester matrix syntactic foams [76]. They observed an increase in storage modulus for 4 vol.% (21.5 GPa at 100°C) nanoclay reinforced syntactic foam in comparison to the plain syntactic foam (17 GPa at 100°C). The damping parameter, $\tan \delta$, was found to decrease with the addition of nanoclay, owing to the intercalation and exfoliation of nanoclay, which reduced the compliance of the polymer. Three types of syntactic foams having the same type of hollow particles in epoxy, polypropylene and polyurethane matrix resins were tested for the effect of hydrothermal exposure on storage modulus and $\tan \delta$ [77]. Results showed that the storage modulus decreased for all types of foams after ageing in sea water at 40°C temperature and 300 bar pressure. Polyurethane matrix syntactic foams displayed the worst performance with a decrease in storage modulus by 50%. These studies have been conducted at a single frequency (1 Hz) [28, 73, 74, 76]. To understand the effects of frequency, Tagliavia et al. studied the free vibration characteristics of syntactic foams, using a cantilever beam setup at room temperature [78]. A wide range of syntactic foam compositions were characterized for room temperature natural frequency response and a theoretical model was developed to estimate the viscoelastic properties of syntactic foams using microballoon volume fraction and wall thickness. However, effect of temperature and combined the effect of temperature and vibration were not included in this study.

Some of the common limitations observed in the existing references that utilized DMA testing technique are:

- Only up to three syntactic foam compositions are characterized, which does not provide comprehensive relationship between viscoelastic properties of syntactic foams and the numerous material parameters.

- No results are available that focus on relating particle wall thickness and volume fraction with the syntactic foam properties, except for one study on free vibration at room temperature characterizing the natural frequency.
- In most cases, a second phase reinforcement such as glass or carbon fibers or nanoclay is added to syntactic foams and the focus is to characterize the effect of this reinforcement.
- Results are available only at 1 Hz frequency. In some references the frequency is not specified, but it is not a study parameter and is maintained constant. The material behavior over a wide frequency range is not studied.
- Combined effect of temperature and frequency is not investigated in the available literature.

The present work aims at filling these critical gaps by focusing on the effects of variation in the temperature and loading frequency on the dynamic properties of syntactic foams. Twelve compositions of syntactic foams are fabricated with systematic variation in microballoon wall thickness and volume fraction to enable correlation between these parameters and the measured properties of the syntactic foams. The combined effect of frequency and temperature on the dynamic mechanical properties is analyzed. The Williams-Landel-Ferry (WLF) equation is used for the time-temperature superposition (TTS) to obtain the storage modulus of syntactic foams over a wide frequency range.

Table 2. Summary of available references on DMA testing of syntactic foams.

Author	Material	Test conditions*	Results
Sankaran et al. [73]	Neat epoxy and HGM**, $\Phi=0.62-0.72$. Three types of syntactic foams (constant density - 450 kg/m ³) hardener systems: cycloaliphatic amine, aromatic amine I and aromatic amine II.	Single Cantilever mode, $\omega=1$ Hz, $a = 40 \mu\text{m}$ and $T=R.T.-300^\circ\text{C}$	<ul style="list-style-type: none">• Reduction in use temperature for syntactic foams is up to 25%• 1.7-24.9% higher T_g for syntactic foams over the neat resin• $\text{Tan } \delta$ is the highest for cycloaliphatic amine based syntactic foam at room temperature
Capela et al. [72]	Neat epoxy resin, HGM (2-13 wt.%) and glass fibers (1 and 3 wt.%).	Tensile mode, ω and a =unspecified, $T=20-100^\circ\text{C}$	<ul style="list-style-type: none">• Reduction in $\text{Tan } \delta$:<ul style="list-style-type: none">- 27% at 13 wt.% of HGM- 41% at 13 wt.% HGM and 3 wt.% glass fibers• E' at 25°C<ul style="list-style-type: none">- 44% reduction at 13 wt.% HGM w.r.t neat resin- 30 % increase at 3 wt.% of glass fiber and 13 wt.% of HGM w.r.t. plain foams
Ferreira et al. [75]	Neat epoxy resin, HGM (2-17 wt.%) , glass fibers (1 and 3 wt.%) and carbon fibers (1 and 2 wt.%).	Three point bending mode, ω and a =unspecified, $T=20-100^\circ\text{C}$	<ul style="list-style-type: none">• Up to 56% lower E' of syntactic foams w.r.t. neat resin at 25°C• 39% and 28% increase in E' at 3 wt.% and 2 wt.% of glass and carbon fibers in 13 wt.% HGM reinforced syntactic foam in comparison to the plain foam at 25°C
John et al. [76]	Cyanate ester resin, nanoclay 2 and 4 vol.%, $\Phi=0.68$ and 0.64 (Total filler $\Phi= 0.7$).	Bending mode, $\omega=1$ Hz, $T=75-325^\circ\text{C}$	<ul style="list-style-type: none">• Increase in the nanoclay content<ul style="list-style-type: none">- increases the rate of decrease of E'- decrease in the syntactic foam T_g
Asif et al. [79]	Neat epoxy resin, PEEKMOH (1-5 wt.%), HGM (35-40 wt.%) and nanoclay (1-5 wt.%)	Three point bending mode, $\omega=1$ Hz, $T=R.T.-300^\circ\text{C}$	<ul style="list-style-type: none">• Increase in the nanoclay content increases E' and maximum use temperature
Lefebvre	Epoxy matrix, HGM of	Single Cantilever	<ul style="list-style-type: none">• Effect of ageing in seawater at 40°C and

et al. [77]	380 kg/m ³ density, Φ=unspecified	mode, ω=1 Hz, a=32 μm and T = R.T. , -120-150°C	300 bar <ul style="list-style-type: none"> • On ageing for 2,000 and 10,000 h <ul style="list-style-type: none"> - E' decreased by 6 and 12% - Temperature for maximum Tan δ changed from 157 to 155 and 163°C
Lefebvre et al. [77]	Polypropylene matrix, HGM of 380 kg/m ³ density, Φ=unspecified	Single Cantilever mode, ω=1 Hz, a=32 μm and T=R.T. , -120- 150°C	<ul style="list-style-type: none"> • Effect of ageing in seawater at 40°C and 300 bar • On ageing for 2,000 and 10,000 h <ul style="list-style-type: none"> - E' decreased by 10 and 36% - Temperature for maximum Tan δ increased from -36 to -34 and -30°C
Lefebvre et al. [77]	Polyurethane matrix, HGM of 380 kg/m ³ density, Φ=unspecified	Single Cantilever mode, ω=1 Hz, a=32 μm and T = R.T. , -120-150°C	<ul style="list-style-type: none"> • Effect of ageing in seawater at 40°C and 300 bar • On ageing for 2,000 and 10,000 h <ul style="list-style-type: none"> - E' decreased by 67 and 51% - Temperature for maximum Tan δ changed from 30 to 18 and 23°C
Hu et al. [74]	Neat epoxy resin and 4 different polymer microballoons: P(DVB- GMA), P(DVB-BA), P(DVB-St) and P(DVB- MMA). Φ=0.1.	Shear mode, ω=1 Hz, a=0.3 mm and T=-20-90°C	<ul style="list-style-type: none"> • Only Tan δ is studied • Maximum Tan δ increase of 40% due to P(DVB-GMA) particles
Wouterson et al. [28]	Neat epoxy resin, phenolic microspheres (Φ=0.3) and short carbon fiber	Three point bending mode, ω=1 Hz, a=unspecified and T=R.T.-110°C	<ul style="list-style-type: none"> • Increase in the fiber content increases E' • Variation in the fiber length and content had no effect on the glass transition temperature
Tagliavia et al. [78]	Vinyl ester matrix and HGM. 16 types of syntactic foams, HGMS of densities 220, 320, 380 and 460 kg/m ³ , Φ=0.3-0.6.	Cantilever beam, free vibration at R.T.	<ul style="list-style-type: none"> • E' increases with HGM wall thickness • Increase in Φ of thin walled HGM decreases the storage modulus, while the opposite is observed for thick walled HGM

*T: temperature, R.T.: room temperature, ω: frequency, a: amplitude.

**HGM: glass microballoons.

4.3 Materials and Methods

Vinyl ester resin (U.S. Composites, FL) was used as the matrix material for preparing syntactic foams. Vinyl ester resin has been used as matrix material for nano and micro-scale reinforced composites owing to its low moisture absorption and high resistance to chemicals [80-82]. Methyl ethyl ketone peroxide (U.S. Composites, FL) was used as the catalyst to polymerize the vinyl ester resin. Hollow glass microballoons (3M, MN) consisting of three nominal true particle densities, namely 220, 320 and 460 kg/m³, were used in 0.3 – 0.6 volume fractions. Since the density of microballoons is less than half the density of the resin system, flotation of microballoons becomes a concern and the quality of composite is not uniform at microballoon volume fraction lower than 0.3. The properties of the glass microballoons used in the current study are presented in Table 3. Since the particles have nearly the same outer diameters, the main varying parameter is their wall thickness (w), as illustrated in Figure 2. The radius ratio, η , defines the geometric properties of hollow particles by

$$\eta = R_i/R_o \quad (1)$$

where R_i and R_o are the internal and the outer radii of the microballoon. The particle wall thickness can be defined in terms of radius ratio as $w=R_o(1-\eta)$. This relation shows that η is lower for a thicker walled hollow particles of the same radius.

Table 3. Types and properties of hollow particles used in fabricating syntactic foams.

Specimen type*	Mean particle diameter (μm)	Nominal true particle density (kg/m^3)	Particle wall thickness (μm)	Particle radius ratio
S22	35	220	0.52	0.970
S32	40	320	0.88	0.956
K46	40	460	1.29	0.936

*Manufacturer's notation.

The detailed explanation on the manufacturing procedure for syntactic foams is available in a previously published paper [47]. Figure 1 shows microstructures of syntactic foams containing Φ of 0.3 and 0.6. The distribution of particles is confirmed to be uniform through microscopic observations in the fabricated syntactic foams. The

measured and the theoretical densities of the composites are shown in Table 4. The theoretical density is obtained using the rule of mixtures. Some unwanted voids, called matrix porosity, may be entrapped in the matrix due to the mechanical mixing process employed for manufacturing of syntactic foams. The volume fraction of the matrix porosity Φ_p is calculated by

$$\Phi_p = \left(\frac{\rho^{th} - \rho^{exp}}{\rho^{th}} \right) \times 100 \quad (2)$$

Table 4. Densities and the matrix porosity volume fractions for syntactic foams.

Specimen type*	Theoretical density (kg/m ³)	Experimental density (kg/m ³)	Matrix porosity (vol%)
VE220-30	878	852	3.0
VE220-40	784	765	2.4
VE220-50	690	683	1.0
VE220-60	596	538	9.7
VE320-30	908	877	3.4
VE320-40	824	786	4.6
VE320-50	740	704	4.9
VE320-60	656	632	3.7
VE460-30	950	918	3.3
VE460-40	880	850	3.4
VE460-50	810	772	4.6
VE460-60	740	703	4.9

*The nomenclature includes VE for vinyl ester, followed by the true particle density and then particle vol.%.

where ρ^{th} and ρ^{exp} are the theoretical and the experimental densities, respectively, of syntactic foams. The calculated matrix porosity content is given in Table 4, which is of similar level and below 5 vol.% in all syntactic foams except for VE220-60. The matrix porosity values calculated from Equation 2 do not provide an exact value because some microballoons may fracture during syntactic foam manufacturing and may increase the syntactic foam density and shift the calculation. The matrix porosity represented by

equation 2 is the resultant of the density increase due to particle fracture and the density decrease due to the presence of matrix voids. Therefore, the matrix porosity figure is only an indication of the material quality.

Specimens of nominal dimensions 30×11×1.75 mm (length×width×thickness) were prepared for all experiments. The specimen width and thickness were controlled within ±1% accuracy. The accuracy in specimen dimensions and tight measurement tolerance are extremely important for DMA testing. The specimens were cut using a low speed precision diamond blade saw (IsoMet®; Buehler Ltd., Lake Placid, NY) and then dried in a convection oven for 3 h at 70°C prior to testing. Q800 Dynamic Mechanical Analyzer (TA Instruments, New Castle, DE) was utilized to conduct the experiments. The experiments were performed in single cantilever mode with a span length of 17.5 mm to ensure that the specimen span length to thickness ratio is 10. Frequency of 1 Hz was used for studying the effect of temperature on dynamic properties. The temperature range used in the study was from -75 to 195°C, at the heating rate of 5°C/min and an isothermal soak time of 1 minute. The specimens were tightened in the cantilever clamp using a torque of 0.8 N.m.

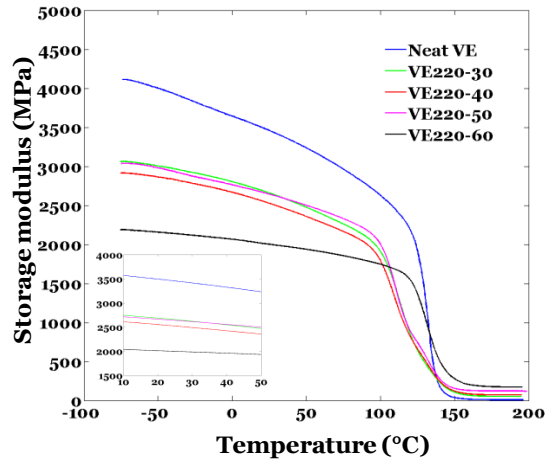
The TTS study was also performed under the single cantilever mode on the specimens of the same geometry. The experiments were conducted in a frequency range of 1-100 Hz, divided linearly into 20 divisions. The testing temperature range was 30-140°C, with an isothermal soak time of 1 minute and the frequency sweep at every 5°C. Due to small changes in the room temperatures, which is usually in the range 22-26°C, some variation is observed in the results if the specimens are conditioned at room temperature and the DMA testing is started. In order to obtain consistent results, the TTS testing was started at slightly elevated temperature of 30°C and this temperature is termed as room temperature in the present discussion.

4.4 Results

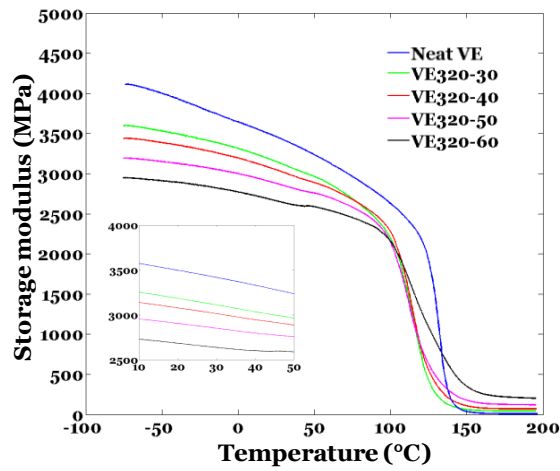
4.4.1 Effect of temperature

Figure 11(a), (b), and (c) show the representative sets of graphs for storage modulus (E') variation with respect to temperature in the range -75 to 195°C for VE220, VE320, and VE460 syntactic foams, respectively. Neat resin results are also plotted in each figure for comparison. As the general characteristic, the graphs have three distinct regions as illustrated in Figure 12. In region I, E' slowly decreases with increase in temperature. In region II, the rate of E' reduction drastically increases. This region appears around T_g . In region III, E' stabilizes to a very low value compared to that in region I. The region III defines the flow region where E' variation is negligible. The E' values at three representative temperatures, namely -50 , 30 and 175°C (marked in Figure 12), are presented in Table 5 to determine the extent of change with respect to temperature. Selection of these representative temperatures is based on the observations that (a) in region I, trend of E' is linear and the graphs are well separated in the temperature range -75 to 0°C , enabling selection of representative temperature of -50°C to demonstrate the dependence of E' on microballoon volume fraction; (b) 30°C is previously defined as the room temperature for this study and is important for a large number of applications; and (c) 175°C is a temperature in region III, where no variation is observed in E' with respect to temperature and any temperature value can be selected for illustration of the trends. Some of the notable trends observed for E' are:

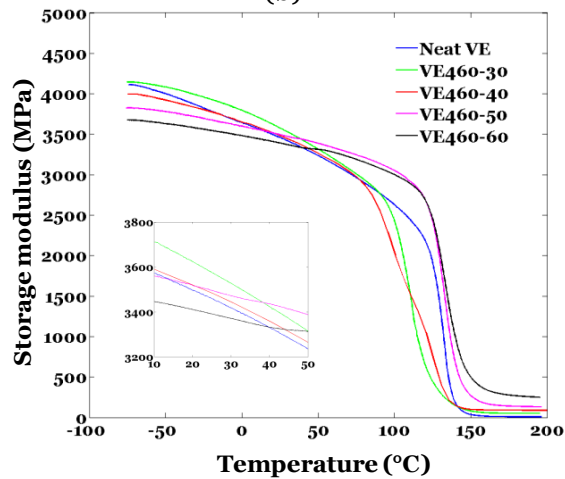
- E' for neat resin is higher than any composition of VE220 and VE320 syntactic foams at low temperatures (in region I). However, VE460 syntactic foams show E' comparable to that of neat resin (Table 5). These trends are similar to the room temperature tensile and compressive modulus values reported in literature for the corresponding syntactic foam compositions [47].
- At low and room temperature, increase in microballoon wall thickness at the same level of Φ results in increase in E' for all types of microballoons.
- In general, E' decreases with increasing Φ , but there are some exceptions to this trend and the standard deviations overlap with each other. The possibility of having a relation between E' and Φ will be further investigated.



(a)



(b)



(c)

Figure 11. Storage modulus of (a) VE220, (b) VE320 and (c) VE460 syntactic foams containing $\Phi=0.3-0.6$. The temperature range 10-50°C is magnified in the inset graphs.

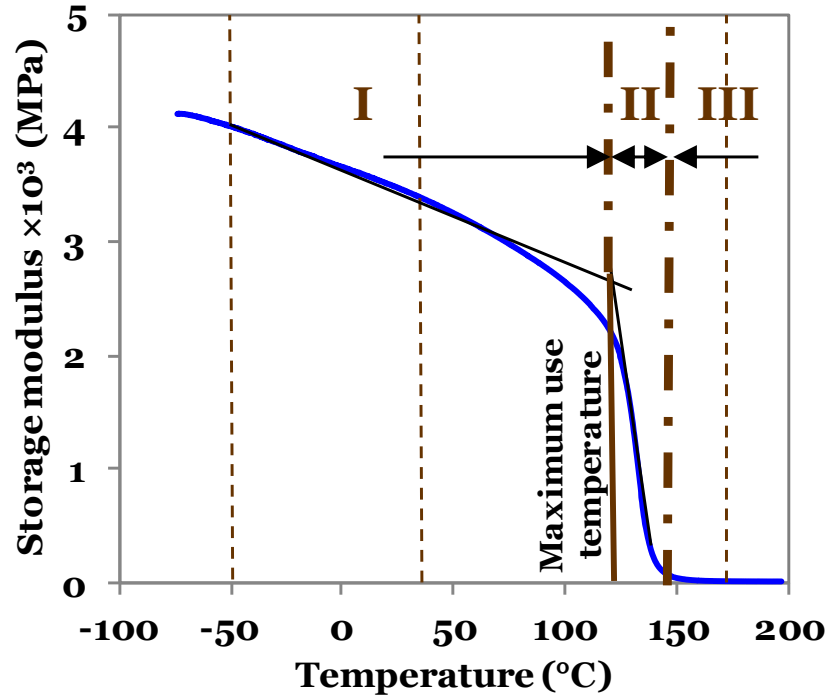


Figure 12. Variation of storage modulus (E') against temperature for neat vinyl ester resin. Regions I, II and III are identified by arrows and dash-dot lines. The dashed lines correspond to -50 , 30 and 175°C where E' values are noted and presented in Table 5.

- In region III, E' is lowest for the neat resin, which is measured to be 76-96% lower than any syntactic foam (Table 5). In this region, E' increases with Φ but has no apparent relation to microballoon wall thickness.
- Figure 11 (a), (b), and (c) show that the curves for different Φ of the same microballoon type cross over. The storage modulus of neat resin becomes the least after the cross over. The cross over points shifts to lower temperature as η increases.

The maximum use temperature (T_{\max}) is defined as the temperature at which the storage modulus starts to decrease drastically [72, 73]. The intersection point of the tangents drawn to the curve in regions I and II is defined as T_{\max} in Figure 12. The values of T_{\max} are presented in Table 6. The T_{\max} is higher for neat resin compared to any composition of syntactic foams. Compared to the T_{\max} of neat resin (122°C), most syntactic foams have T_{\max} below 96°C . The difference between E' , calculated at room

temperature and at maximum use temperature was found to be higher for neat resin (38% reduction) compared to that of any composition of syntactic foams (maximum reduction of 27% for VE460-30).

Table 5. Comparison of storage modulus values for syntactic foams at three representative temperatures.

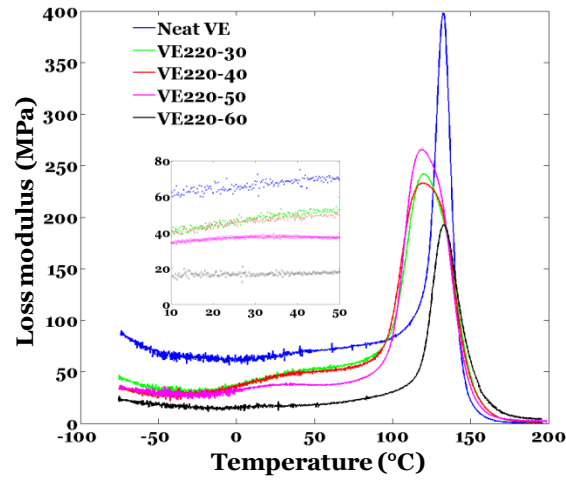
Specimen type	E' at -50°C (MPa)	E' at 30°C (MPa)	E' at 175°C (MPa)
Neat VE	4041±44	3457±42	11±1
VE220-30	2916±76	2548±66	50±2
VE220-40	2841±54	2467±34	72±0
VE220-50	3015±42	2640±44	124±3
VE220-60	2186±65	1998±37	178±2
VE320-30	3554±45	3065±53	46±2
VE320-40	3369±49	2949±55	71±2
VE320-50	3139±73	2810±98	126±3
VE320-60	2935±55	2628±63	213±7
VE460-30	4082±24	3523±36	51±1
VE460-40	3755±143	3311±120	85±9
VE460-50	3557±206	3264±186	137±7
VE460-60	3712±94	3410±36	248±25

Table 6. Maximum use temperature and glass transition temperature for various types of syntactic foams.

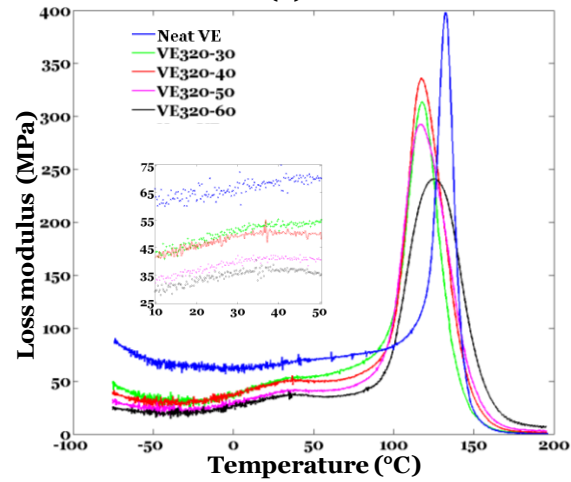
Specimen type	T _{max} (°C)	T _g (°C)
Neat VE	122±1	132±0
VE220-30	96±1	120±0
VE220-40	81±10	123±3
VE220-50	89±1	117±2
VE220-60	119±0	133±0
VE320-30	90±11	116±5
VE320-40	90±9	120±5
VE320-50	89±7	119±2
VE320-60	94±3	126±0
VE460-30	96±5	114±4
VE460-40	93±3	115±1
VE460-50	120±4	133±2
VE460-60	116±9	130±8

Figure 13(a), (b), and (c) show the representative sets of graphs for loss modulus (E'') variation with respect to temperature in the range -75 to 195°C for VE220, VE320, and VE460 syntactic foams, respectively. Neat resin results are also plotted in each figure for comparison. The T_g can be obtained as the temperature corresponding to the maximum of the loss modulus curve and is presented in Table 6 [73, 83]. T_g for the neat resin is found to be higher than most syntactic foams. T_g of syntactic foams increases with Φ and becomes nearly equal to that of the neat resin at $\Phi=0.6$. The values of maximum loss modulus (E''_{\max}) for the neat resin and syntactic foams are presented in Table 7. Some of the notable trends in the loss modulus behavior are:

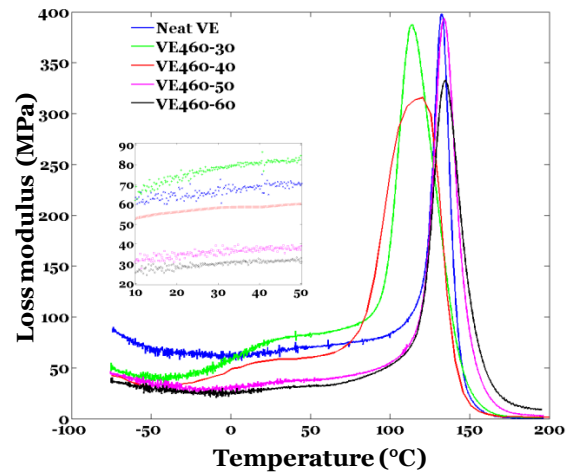
- At room temperature E'' is lower for syntactic foams when compared to the neat resin. The lowest E'' is observed for VE220-60 syntactic foams, which is 73% lower than that of neat resin.
- Increase in Φ results in decrease of E'' for all types of microballoons.
- Increase in the microballoon wall thickness at the same level of Φ results in increased E''_{\max} . The trend between E''_{\max} and Φ is not clearly identified. In general, E''_{\max} decreases with increasing Φ , but there are some exceptions to this trend.
- The E''_{\max} is higher for neat resin when compared to various types of syntactic foams.
- Increase in Φ results in an increasing trend in T_g (Table 6).



(a)



(b)



(c)

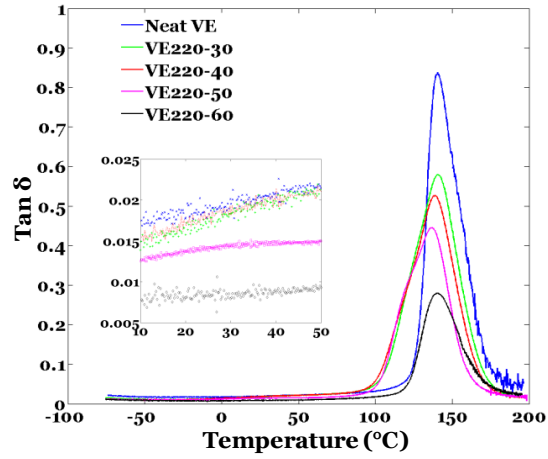
Figure 13. Loss modulus results for (a) VE220, (b) VE320 and (c) VE460 syntactic foams containing $\Phi=0.3-0.6$. The temperature range 10-50°C is magnified in the inset graphs.

Table 7. Loss modulus at room temperature, maximum value over the test temperature range, and temperature at the maximum loss modulus for various syntactic foams.

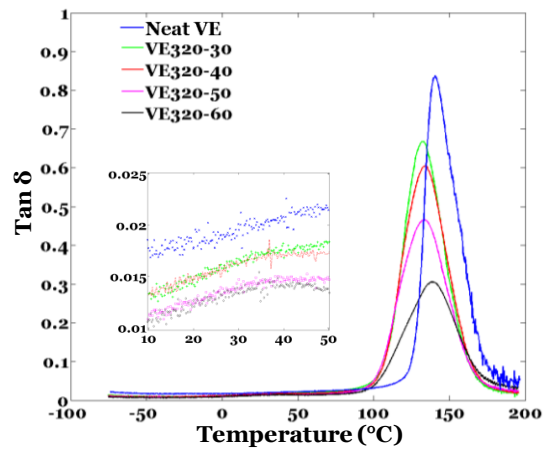
Specimen type	E'' at 30°C (MPa)	Maximum loss modulus (E''_{max}) (MPa)	Temperature at E''_{max} (°C)
Neat VE	66±2	402±4	132±0
VE220-30	47±1	235±5	120±0
VE220-40	47±2	234±4	123±3
VE220-50	38±1	262±16	117±2
VE220-60	18±1	187±2	133±0
VE320-30	59±6	288±22	116±5
VE320-40	52±4	292±35	120±5
VE320-50	41±1	271±20	119±2
VE320-60	37±2	231±13	126±2
VE460-30	71±10	371±28	114±4
VE460-40	56±3	335±17	115±1
VE460-50	34±3	350±18	133±2
VE460-60	35±9	328±6	130±8

Figure 14(a), (b), and (c) show the representative sets of graphs for $\text{Tan } \delta$ variation with respect to temperature for various syntactic foams and neat resin. $\text{Tan } \delta$ is defined as the ratio of the loss modulus to the storage modulus (E'' / E') and is a measure of the damping capability of the material [84]. Increase in Φ results in the decrease of maximum and the room temperature value of $\text{Tan } \delta$ as shown in Table 8. The temperature at which $\text{Tan } \delta$ shows the maximum value is nearly the same for the neat resin and all syntactic foams, which illustrates that it mainly relates to the properties of the matrix resin.

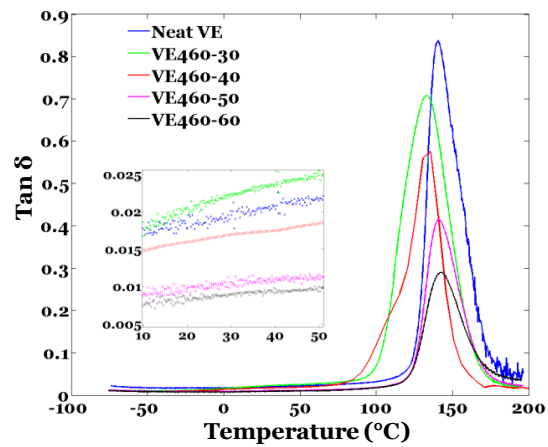
It can be seen from Figure 14 that with the increase in Φ , the area under the $\text{Tan } \delta$ curve decreases. It has been suggested previously that the stability of the polymer materials increases with decrease in the area under the $\text{Tan } \delta$ curve [85]. This implicates that the stability of syntactic foams at higher temperatures increase with increasing Φ .



(a)



(b)



(c)

Figure 14. The damping parameter, $\text{Tan } \delta$, for (a) VE220, (b) VE320 and (c) VE460 syntactic foams containing $\Phi=0.3-0.6$. The temperature range $10-50^\circ\text{C}$ is magnified in the inset graphs.

Table 8. Tan δ at room temperature, maximum value over the test temperature range, and temperature at the maximum Tan δ for syntactic foams.

Specimen type	Tan δ at 30°C ($\times 10^{-3}$)	Maximum Tan δ ($\times 10^{-3}$)	Temperature at Maximum Tan δ (°C)
Neat VE	19±1	814±13	142±1
VE220-30	18±0	574±9	141±1
VE220-40	19±1	512±8	139±0
VE220-50	15±0	440±4	136±0
VE220-60	9±0	282±2	141±0
VE320-30	19±2	623±37	134±1
VE320-40	18±2	570±39	136±2
VE320-50	15±1	445±26	135±2
VE320-60	14±1	323±17	138±2
VE460-30	20±3	700±5	134±1
VE460-40	17±1	582±22	133±2
VE460-50	10±1	435±45	142±1
VE460-60	10±3	311±48	139±5

4.4.2 Combined effect of temperature and frequency

The combined effect of temperature and frequency has been studied on neat resin and four compositions of syntactic foams: VE220-30, VE220-60, VE460-30 and VE460-60. These compositions were selected to account for the particles of the least and highest density in the two extremities of volume fractions. The experiments are conducted in the frequency range of 1-100 Hz and in the temperature range of 30-140°C. TTS schemes can be used to develop master curves for the material over a wide range of temperatures and frequencies from a limited set of data [68].

The E' values for neat resin at different temperatures and frequencies are plotted in Figure 15(a). Although testing is conducted in the temperature range of 30-140°C, this figure includes data only for the temperature range 105-135°C because the lines for lower temperature show the same trend but appear very close to each other. In addition, the master curves are plotted for the useful frequency range of 10^2 - 10^6 Hz, which can be covered by the curves appearing in the 105-135°C range. Two trends can be noticed in this figure: (i) with increasing temperature the E' values decrease, which is similar to the trend observed in Figure 11(a) and (ii) the dependence of E' on the test frequency increases with temperature. The TTS principle can be used to construct master curves in frequency regions that are outside of the test frequency range (1-100 Hz). To construct a master curve, one of the curves in Figure 15(a) is selected as the pivot and the remaining curves are shifted on the frequency axis towards the pivot curve until a continuous plot is obtained, which is called the master curve. The magnitude of shift for each individual curve to superimpose on its neighbor by moving it towards the pivot is termed as shift factor (a_T). The reference temperature was selected as 120°C for the pivot curve in this example and the shift factor a_T for each temperature was determined. Figure 15 (b) shows the master curve for the neat resin at 120°C. The choice of reference temperature does not affect the shift factors. Any desired temperature can be selected as the reference temperature. The master curve is shown in the frequency range 10^2 - 10^6 Hz, which is useful for most applications. In general, the master curve can be constructed for a much wider range of frequencies using the available data. The corresponding shift factor values are presented in Figure 15 (c). The shift factor values for all three specimens matched

closely, as seen by the small error bars in Figure 15 (c). Similar master curves can be constructed for any desired temperature by selecting the appropriate reference temperature for the pivot curve.

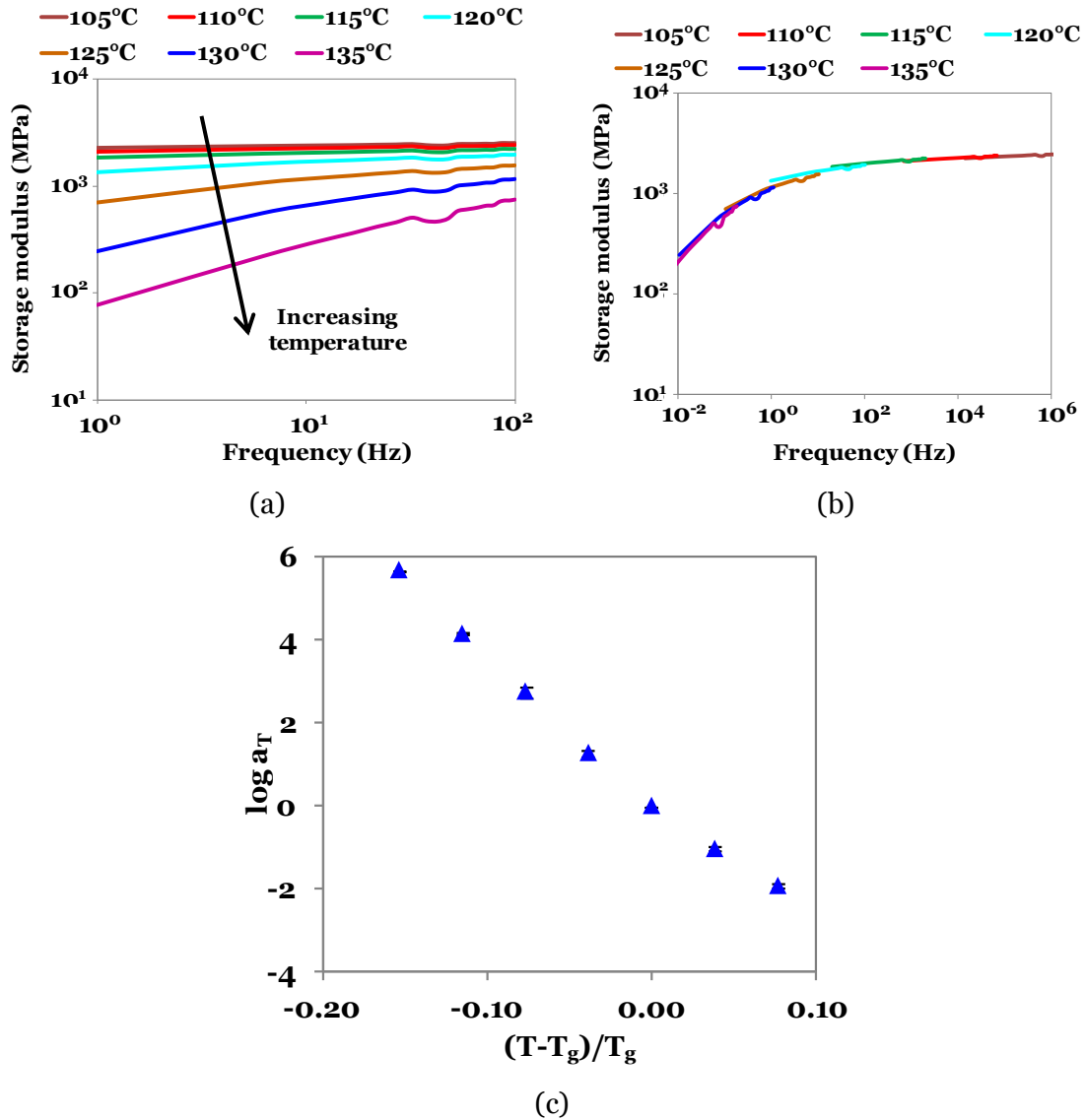


Figure 15. (a) Storage modulus of the neat vinyl ester resin obtained in the frequency range of 1-100 Hz for various temperatures, (b) master curve obtained using TTS at the reference temperature of 120°C and (c) the corresponding shift factors.

The same procedure is used to develop master curves for VE220-30, VE220-60, VE460-30 and VE460-60 syntactic foams. Three specimens for each syntactic foam type are tested and the results are found to be consistent. For simplicity, the curves for only

one specimen of each type are represented here. The master curves are plotted in Figure 16 for various syntactic foams at three different reference temperatures. The curves show that as the frequency is increased the sensitivity of E' for the test frequency reduces. The sensitivity of E' on frequency becomes negligible after 1 MHz frequency for all materials tested in this study. The calculated shift factors for syntactic foams are plotted in Figure 17. It should be noted that the shift factors are independent of the reference temperature of the pivot curve. The shift factors are of the same order for vinyl ester and the syntactic foams as noted in Figure 17.

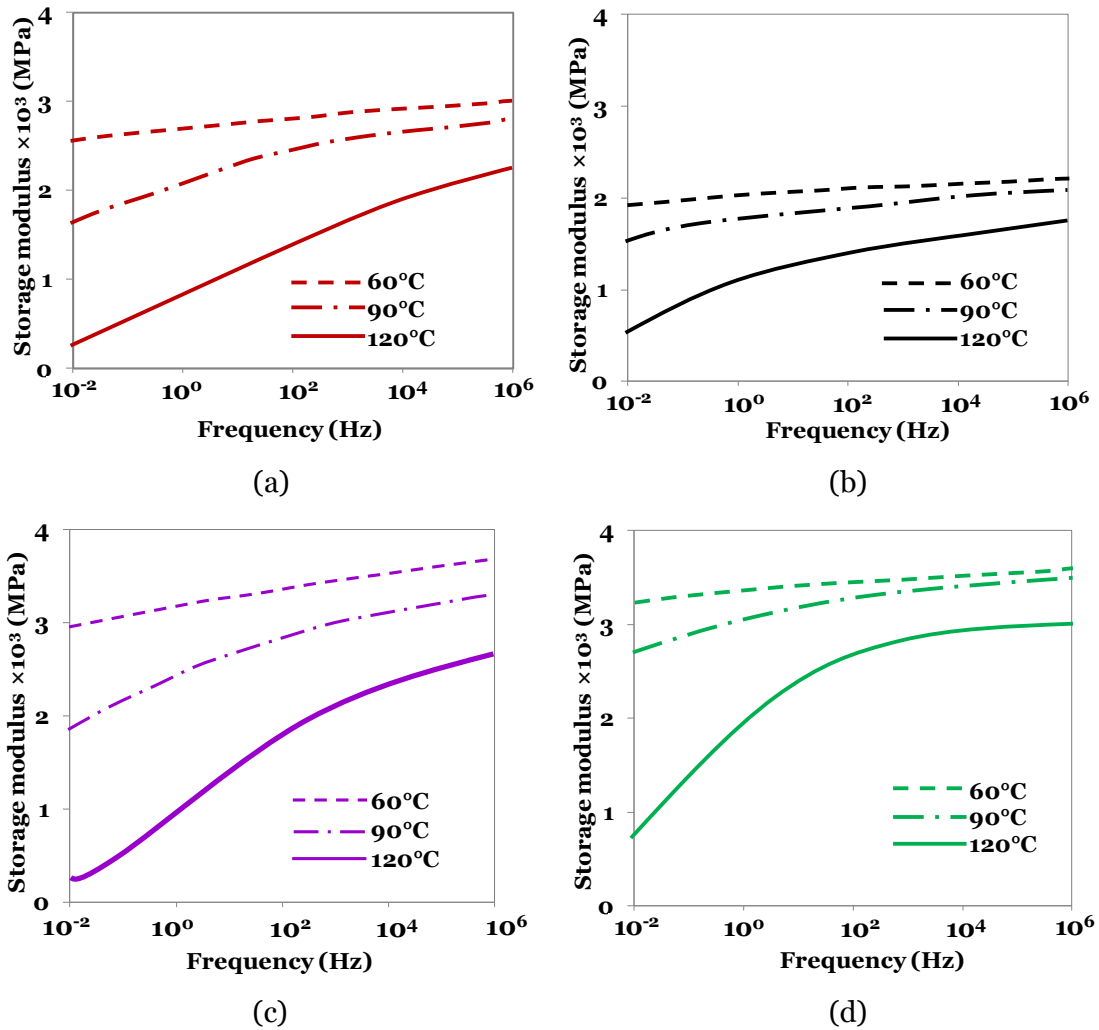
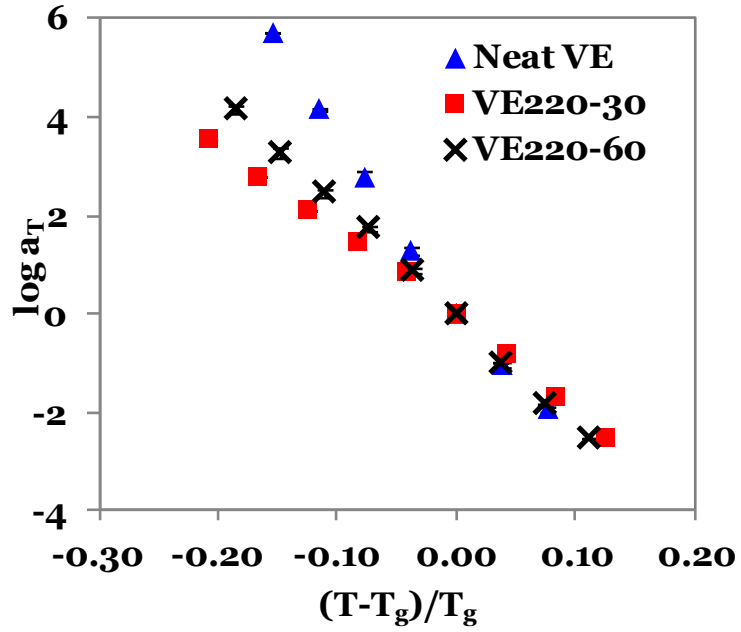
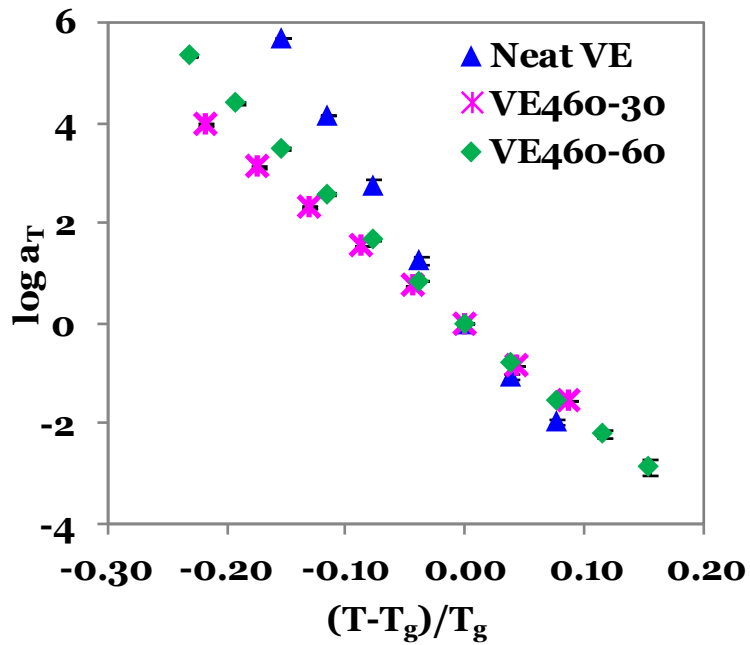


Figure 16. The master curves for (a) VE220-30, (b) VE220-60, (c) VE460-30 and (d) VE460-60 syntactic foams at reference temperatures of 60, 90 and 120°C.



(a)



(b)

Figure 17. The shift factors for (a) VE220 and (b) VE460 syntactic foams, used for obtaining the master curves shown in Figure 16.

4.5 Discussion

4.5.1 Effect of temperature

In syntactic foams, the main parameters for analysis are the microballoon wall thickness and Φ as well as the syntactic foam density. It is important to establish correlations between viscoelastic properties and these parameters. The syntactic foam density can decrease with (i) decreasing wall thickness of microballoons, (ii) increasing microballoon volume fraction, and (iii) increasing matrix porosity. Either the individual effects of these parameters or their combined effects on density may show an identifiable trend with the viscoelastic properties of syntactic foams. The matrix porosity is not a study parameter in the current work. The estimated values are provided only to demonstrate that most syntactic foams have similar levels of matrix porosity. The observed experimental trends are further discussed below.

The E' variation with respect to temperature for various syntactic foams has been studied in Table 6. E' increases with the microballoon wall thickness for a given Φ at temperatures in regions I and II. The variation with respect to the Φ is not the same for all the microballoon types and only weak indications are observed that E' decreases and increases with increasing volume fraction of thin and thick walled particles, respectively.

Syntactic foams are stiffened with the addition of the thicker walled particles while the opposite is observed in the case of thin walled particle reinforcement in studies focused on tensile and the flexural loading of syntactic foams at room temperatures [86-88]. The stiffening or softening effects with increasing Φ depend on the ratio of microballoon to matrix modulus. Hollow particles have an air void inside the glass shell. Therefore, the effective modulus of a hollow particle (E^*) is lower than the modulus of the glass material. For hollow particles, E^* can be estimated by [51]

$$E^* = \frac{E_g(1-2\nu)(1-\eta^3)}{(1-2\nu) + \left(\frac{1+\nu}{2}\right)\eta^3} \quad (3)$$

where E_g is the modulus of glass material (60 GPa) and ν is the Poisson's ratio of glass (0.21). In addition, density of glass is taken as 2540 kg/m³. The average η values calculated from Equation 1, based on the nominal true density of particles, are presented in Table 4. The estimates of \bar{E} for S22, S32, and K46 microballoons are 2.7, 4.0, and 5.9 GPa. These theoretical values assume that the particles are defect free. Presence of defects will further reduce the modulus values. The elastic modulus of neat vinyl ester is 3.4 GPa [47]. Therefore, it can be expected that incorporation of S22 particles will cause softening effect, S32 particles will cause mild stiffening or no effect, and K46 particles will lead to stiffening effect in vinyl ester resin, which is the case for the observed results for E' .

The storage modulus variation with respect to the temperature has been studied previously for many polymers including amorphous and crystalline thermoplastics and thermosets [73, 89, 90]. Mahieux et al. modeled the stiffness variation with respect to temperature [91-93]. This model accounts for the relaxation of the polymer by quantifying the breakage of the secondary bonds. The model is governed by Weibull distribution, which estimates the bond rupture based on the parameters (m_i) referred to as Weibull moduli corresponding to the statistics of bond breakage. These parameters are dependent on various factors such as degree of cross-linking, molecular weight and crystallinity of the polymer [91-93]. Based on the material stiffness transitions with respect to temperature, the general equation for the Weibull distribution can be expressed as [91, 92]

$$E' = (E'_1 - E'_2) \exp\left[-\left(\frac{T}{T_1}\right)^{m_1}\right] + (E'_2 - E'_3) \exp\left[-\left(\frac{T}{T_2}\right)^{m_2}\right] + E'_3 \exp\left[-\left(\frac{T}{T_3}\right)^{m_3}\right] \quad (4)$$

where T corresponds to the temperature, T_1 , T_2 and T_3 correspond to the instantaneous reference temperatures, which are well below T_g , equal to T_g and in the flow region above T_g , respectively. E'_1 , E'_2 and E'_3 correspond to the storage modulus values at each of the three reference temperatures and m_1 , m_2 and m_3 correspond to the Weibull coefficients that govern the decrease in the modulus due to the secondary bond rupture at the three reference temperatures [91]. In the current study, T_1 and T_3 are maintained constant at arbitrarily chosen temperatures 27 and 170°C, respectively, for all syntactic foams and the neat resin. The Weibull coefficients m_1 (corresponding to the low temperature region) and m_3 (corresponding to the flow region above T_g) are selected as 5 and 1, respectively.

Parametric studies were conducted to arrive at the selected values of m_1 and m_3 . Curve fitting is used to obtain the value for m_2 that provides the best fit with the experimental dataset. The best-fit between the Weibull curve with the experimental data for neat resin is obtained at $m_2 = 30$ as shown in Figure 18. It can be observed in Figure 18 that there is some variation between the experimental data and Weibull curve, which can be attributed to the cross-linked structure of thermosetting polymers [91, 92]. Unlike thermoplastic polymers the molecular chains are more restricted in thermosetting polymers due to the presence of cross-links. Therefore, the bond breakage may be underestimated by the Weibull coefficients in thermosetting polymers.

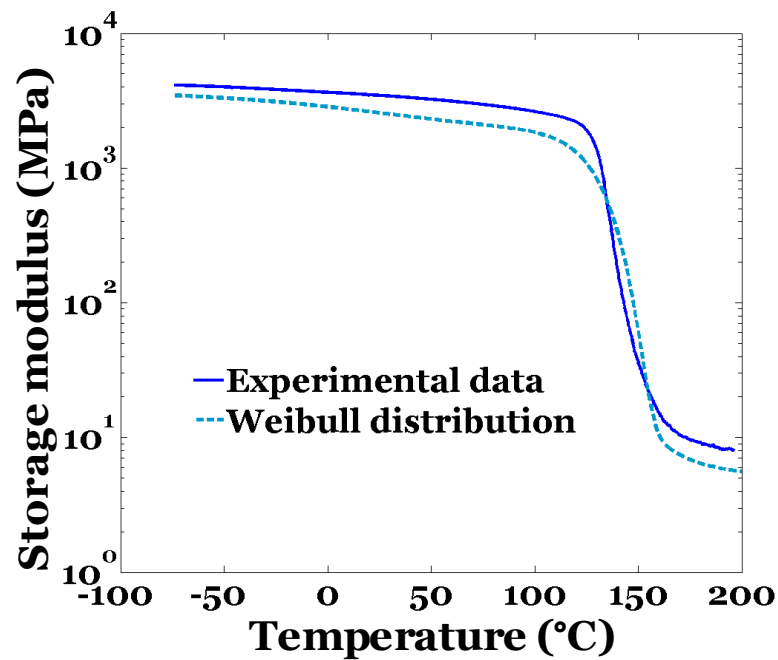


Figure 18. A comparison of Weibull distribution with the experimental data of storage modulus for neat vinyl ester resin.

A similar calculation is conducted to estimate the m_2 values for syntactic foams. Table 9 lists the E' values at the three reference temperatures that are used as inputs in equation 4. A parametric study is performed to estimate the Weibull coefficient m_2 , which are plotted in Figure 19(a). It can be observed that m_2 decreases with increase in Φ . This result corroborates well with the observation made by Mahieux et al, who studied the effect of variation of carbon black content on polybutadiene [91, 93] and showed that with the increasing reinforcement content (0-37.5 wt.% range), the Weibull parameter decreased by up to 50%. It can also be noted that if the m_2 values are plotted with respect

to the syntactic foam density then they fit along a straight line as shown in Figure 19(b). These trends illustrate that with the availability of only a small set of parameters, the behavior of a wide variety of syntactic foam compositions can be determined.

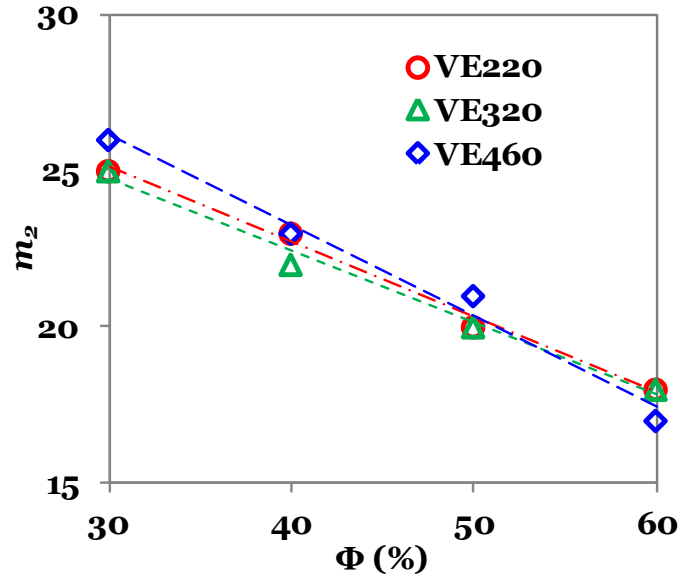
Table 9. Storage moduli values used in the Weibull distribution for syntactic foams.

Specimen type	E'_1 (MPa)*	E'_2 (MPa)**	E'_3 (MPa)***
Neat VE	2936	1616	8
VE220-30	2723	941	136
VE220-40	2451	878	133
VE220-50	2908	979	127
VE220-60	2145	973	202
VE320-30	3085	1155	48
VE320-40	2997	1057	71
VE320-50	2985	1117	133
VE320-60	2785	1093	232
VE460-30	3556	1188	53
VE460-40	3485	1028	76
VE460-50	3285	1634	148
VE460-60	3674	2040	245

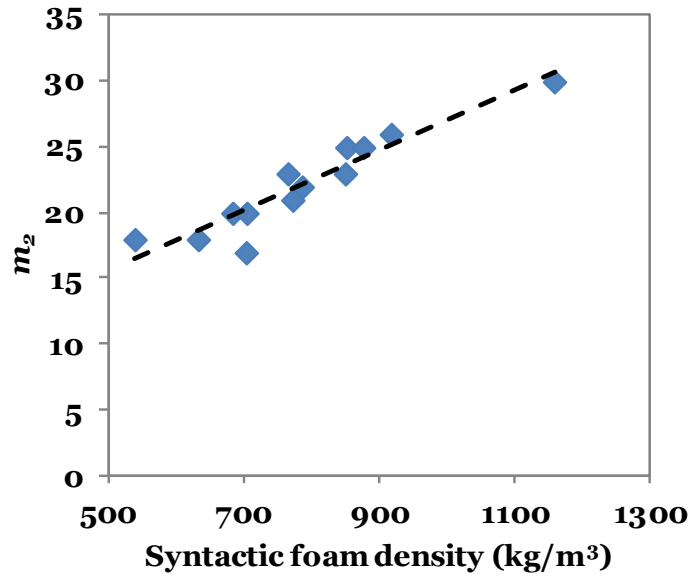
* E'_1 value is selected at constant temperature of 27°C.

** E'_2 value is selected at T_g (given in Table 6).

*** E'_3 value is selected at constant temperature of 170°C.



(a)



(b)

Figure 19. Variation of the Weibull parameter m_2 with respect to (a) Φ and (b) syntactic foam density.

The loss modulus (E'') values at room temperature for most syntactic foams presented in Table 7 show a linear trend with respect to the syntactic foam density for most compositions as seen in Figure 20. Identifying this trend is important because a combination of η and Φ can be used to obtain a range of syntactic foam compositions with the same density. This provides a flexible approach to tailor the viscoelastic properties of syntactic foams with the available material parameters.

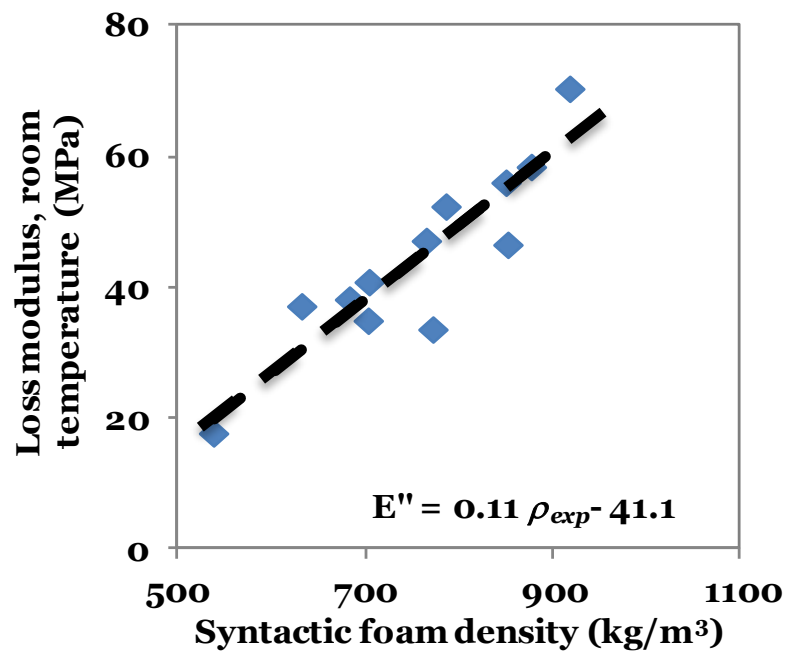


Figure 20. Variation of the loss modulus at 30°C with respect to the syntactic foam density.

The damping parameter, maximum $\text{Tan } \delta$, shows a decrease with increasing Φ . This is related to the brittle nature of microballoons and the viscoelastic nature of the polymeric matrix material. These observations are similar to those made in a previous study on dynamic mechanical behavior of syntactic foams at room temperature [78]. Since $\text{Tan } \delta$ presents a relationship between E' and E'' , it is also analyzed with respect to the syntactic foam density in Figure 21. The maximum $\text{Tan } \delta$ values fit along a straight line in this figure for most syntactic foams. This linear relationship is very useful in

analyzing the weight saving potential through the use of syntactic foams in applications that are based on the damping characteristics.

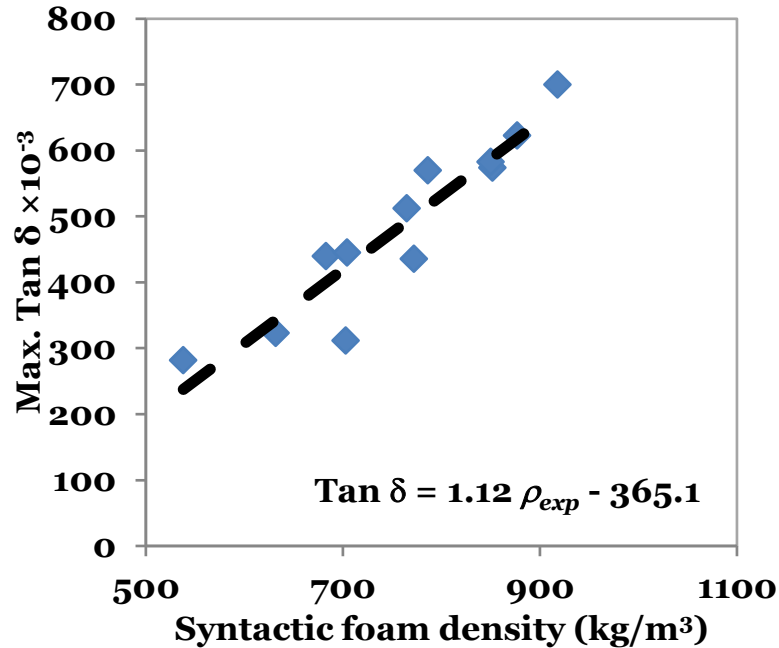


Figure 21. Variation in maximum Tan δ with respect to the syntactic foam density.

T_g of neat resin is higher than any syntactic foam analyzed in this study. This can be related to lower specific heat capacity of glass compared to resin. Increase in T_g is observed with Φ (Table 6). Similar trend was observed in the T_g of epoxy matrix syntactic foams [20]. The increase in T_g with increasing Φ can be attributed to the reduction in the mobility of polymer chains due to the interfacial bonding between microballoons and resin [73]. The microballoon-matrix interfacial area increases with Φ . Although the interfacial bonding in the present syntactic foams does not appear to be very strong as observed through microscopy in Figure 22, the possibility of having higher number of bonds as Φ increases can help in increasing T_g . Characteristics of particle-matrix interfacial bonding are important for thermal properties such as T_g . However, the interfacial bonding has not been of primary focus in existing studies on syntactic foams because syntactic foams are designed for compressive loading conditions in most existing applications and under compression the interfacial bonding is not as important as under tensile loading. The main reason for this observation is that under tension the

interfacial debonds and cracks tend to open up but they tend to close under compression and particles become load bearing element in the material [54, 87, 94].

Several available studies have seen a similar trend in T_g of particle reinforced composites. Robertson et al., analyzed the viscoelastic properties of silica filled polymeric matrix composites and studied the effect of filler on polymeric matrix composite [95]. Using an atomic force microscope, they visualized a stiffening effect adjacent to the filler particle matrix interface, which was responsible for increased T_g .

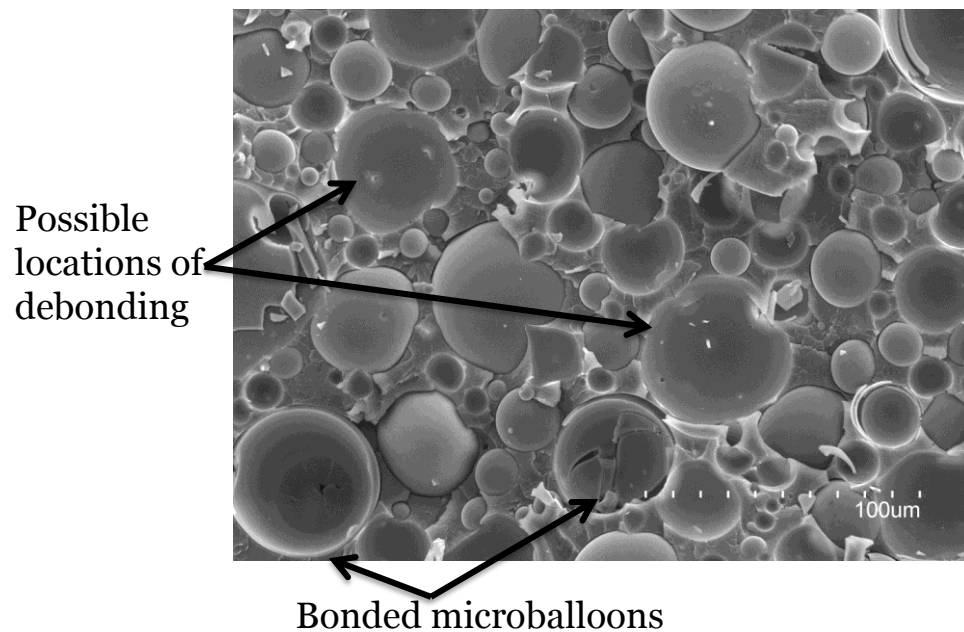


Figure 22. Scanning electron micrograph indicating the presence of particle-matrix interfacial bond, which may be weak.

4.5.2 Temperature and frequency variation

The Cole-Cole plot can be used to interpret trends observed in TTS curves [96]. This plot between $\log E''$ and $\log E'$ is expected to show a semi-circular curve for homogeneous materials. Figure 23 depicts the Cole-Cole plot for the neat resin and syntactic foams. The curves for neat resin and syntactic foams show similar trends and demonstrate the applicability of TTS for syntactic foams. The imperfect semi-circle seen in Figure 23 indicated that there is interfacial bonding between particles and the matrix. Strong interfacial bonding has been attributed to similar deviations from the semi-circular shape of Cole-Cole plots in composites [96].

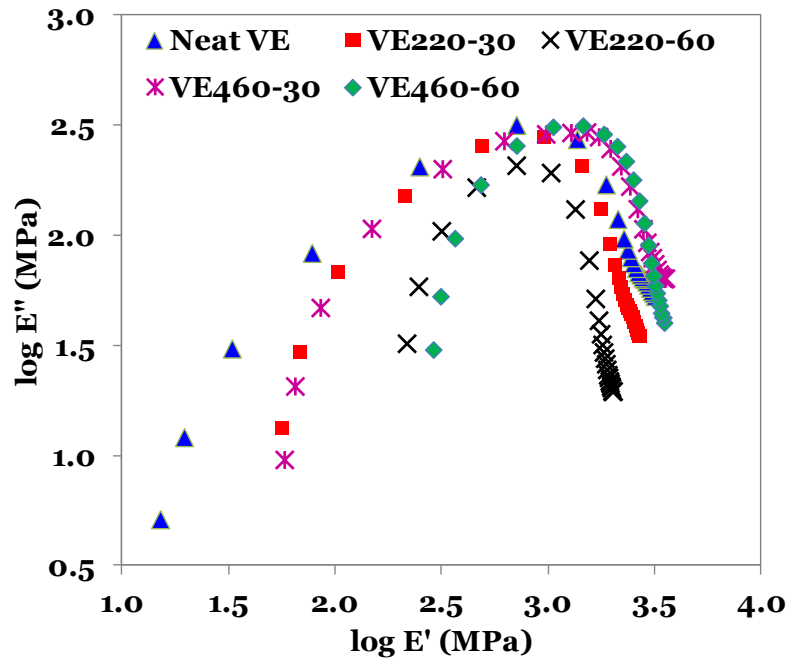


Figure 23. The Cole-Cole plot of syntactic foams and the neat vinyl ester resin.

Further analysis of TTS results can be conducted by the Williams-Landel-Ferry (WLF) equation

$$\log a_T = \frac{-c_1(T-T_0)}{c_2 + (T-T_0)} \quad (5)$$

where T_0 is the reference temperature for which the master curve is constructed (60°C) and c_1 and c_2 are constants [67, 97-99], which are calculated from the slope and the y-intercept of the $(T-T_0)/\log a_T$ versus $(T-T_0)$ plot [67]. The values of c_1 and c_2 are calculated as 96.8 and 357.7, respectively for the neat vinyl ester resin. The values of c_1 and c_2 for various syntactic foams are plotted in Figure 24. Although microballoons of different η and Φ are used in the four syntactic foams, both constants c_1 and c_2 show a linearly increasing trend with the syntactic foam density. The linear trend can help in engineering the new compositions of syntactic foams with required properties.

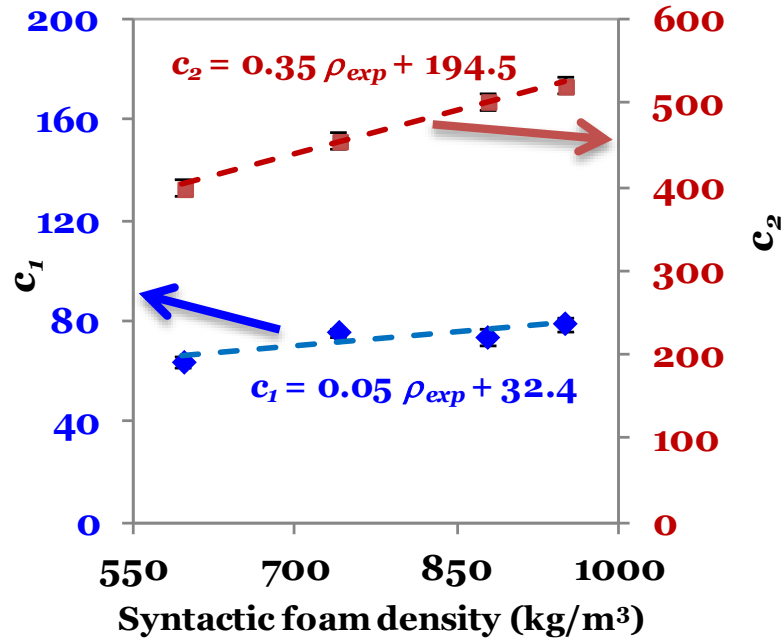


Figure 24. Constants c_1 and c_2 of equation 5 plotted against syntactic foam density.

Finally, the master curves obtained for syntactic foams are compared with the available data from the literature. Tagliavia et al. studied the room temperature dynamic mechanical properties of syntactic foams by using the vibration response of cantilever beam specimens subjected to impulse excitation using an instrumented hammer [78]. Storage modulus values were calculated from these results at certain frequencies, which are plotted in Figure 25. The figure also contains lines for the E' values obtained from the current work at 30°C temperature. The testing in the current work is conducted within the frequency range of 1-100 Hz; the values are extrapolated in the 100-150 Hz range to cover the last data point. The maximum variation of $\pm 14\%$ is observed in both sets of results for all four types of syntactic foams and the neat resin.

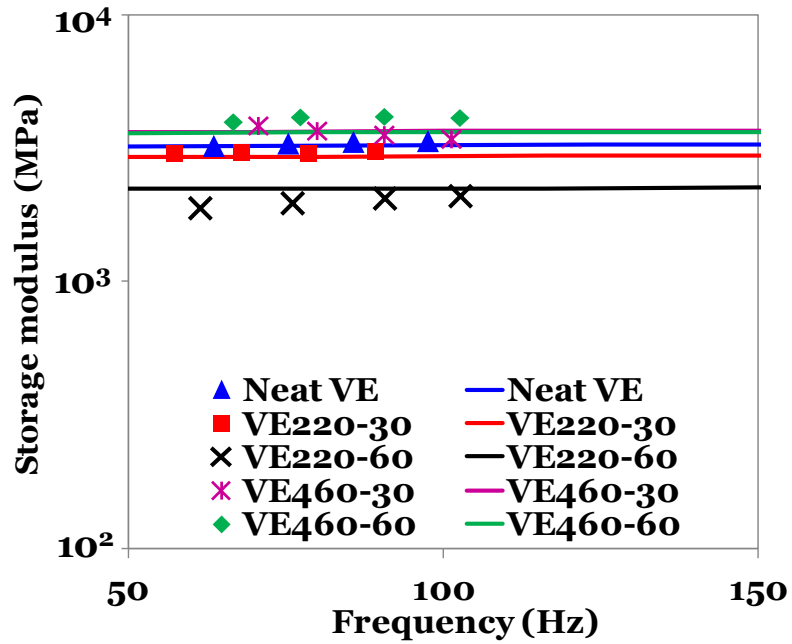


Figure 25. The storage modulus values for syntactic foams and the vinyl ester resin obtained in the present work (represented by lines, extrapolated in the 100-150 Hz range) are compared with the existing data extracted from [78] (symbols).

CHAPTER 5. Electrical properties of syntactic foams

5.1 Introduction

Very large scale integration of electronic circuits has drastically reduced the size of circuit boards used in electronic devices. This has created a challenge to develop materials with low dielectric constant, high specific strength, low density, low moisture absorption and high durability. Integrated circuit boards, which form the heart of computers, require electrical insulators with low and preferably tunable dielectric properties [100]. Polymers and polymeric composites have found applications in such fields due to their low dielectric properties [101, 102].

Epoxy resins, which are often used as matrix materials for composites, are also used in electrical and electronic fields as insulators, dielectrics and as underfills in circuit boards [103, 104]. One of the desirable ways of decreasing the dielectric constant is by introducing porosity in the polymer [105]. Since air has a low dielectric constant of 1, the dielectric constant of polymer foams is low but it also accompanies low strength and stiffness, which are undesirable. In addition, irregular size and distribution of gas voids in polymer foams can lead to mechanical property variation within the material.

Composite materials prepared by embedding hollow filler particles into a continuous matrix are called syntactic foams [11, 60, 106]. This approach ensures low density of the composite with significant volume fraction of porosity but without the penalty on mechanical properties. Hollow particles made of glass, carbon, polymers, and ceramics have been used in syntactic foams [7]. The mechanical and thermal properties such as modulus, coefficient of thermal expansion (CTE) and thermal conductivity of syntactic foam can be tailored [22, 48, 58, 65]. The variables in designing syntactic foams include: particle and matrix materials, volume fraction of particles, and wall thickness of particles. In most existing applications, weight saving is an important consideration in using syntactic foams. Existing studies have shown that a combination of hollow particle wall thickness and volume fraction can be used to independently tailor

the CTE and the density of syntactic foams to achieve weight saving in structural applications[65].

The available studies on electrical properties of syntactic foams characterized with respect to frequency and temperature are summarized in Table 10, whereas Table 11 contains a summary of studies that have included the effect of environmental exposure. This information sets the context for the present work.

Table 10. Existing studies on impedance and dielectric properties of syntactic foams.

Reference	Material used	Test condition	Results
Shahin et al. [107]	Matrix: epoxy, HGM: 0-55 wt.%	f = 100 – 30 kHz	1. The impedance of the composite decreases with the frequency and the increases with Φ_{mb} . 2. The dielectric constant decreases with frequency and Φ_{mb} .
Shahin et al. [108]	Matrix: epoxy, HGM: 0-55 wt.%	f = 100 Hz and 10 kHz Temperature = 20-125°C	1. The syntactic foam impedance decreases with increasing temperature. 2. The dielectric constant increases with increasing temperature.
Park et al. [19]	Matrix: epoxy, HGM: 0-2 wt.%	f = 1 – 10 GHz	Dielectric constant decreased with increasing frequency and Φ_{mb} .
Gupta et al. [109]	Matrix: epoxy, HGM: $\Phi_{mb} = 0.3 - 0.65$	f = 1 - 100 kHz Temperature = 40 - 120°C	1. The dielectric constant decreases with increasing Φ_{mb} . 2. The dielectric constant increases 5-10% with increase in the temperature. 3. The impedance decreased with increasing frequency and the phase angle remained close to -90° , suggesting capacitive behavior.
Andritsch et al. [110]	Matrix: epoxy, HGM: ($\Phi_{mb} = 0.5$) filled with SO ₂	f = 0.5 Hz - 1MHz Temperature = -140 - +120°C	1. The syntactic foams had higher dielectric loss than the neat resin at the tested frequency and temperature. 2. SO ₂ gas inside the microspheres play an important role at <1000 Hz and between -140 and +20°C.
Yung et al. [34]	Matrix: epoxy, HGM: ($\Phi_{mb} = 0-0.51$)	f = 1 kHz – 1 MHz	1. At 1 MHz, the dielectric constant decreased from 3.98 to 2.84 as Φ_{mb} increased from 0-0.51. 2. A maximum decrease of 44% is observed in the dielectric loss at $\Phi_{mb} = 0.51$ compared to neat resin.
Zhu et al. [111]	Matrix: epoxy, HGM: ($\Phi_{mb} = 0.1-0.6$)	f = 1 MHz Temperature = 10°C	1. Maximum 51 decrease % was observed in the dielectric constant at $\Phi_{mb} = 0.60$ compared to neat resin. 2. Maximum 54% decrease in the dielectric loss at $\Phi_{mb} = 0.6$ compared to neat resin.

Table 11. Existing studies on impedance and dielectric properties of syntactic foams, along with environmental effects.

Reference	Material used	Test condition	Results
Ansermet et al. [112]	Matrix: epoxy, HGM: ($\Phi_{mb} = 0.37-0.57$) and Organic (phenolic and copolymer of acrylonitrile-vinylidene chloride) ($\Phi_{mb} = 0.34-0.5$)	f = 100 Hz – 10 MHz (Dried specimens) f = 40 Hz – 1 GHz Water absorption at 85°C and 85% humidity	1. The dielectric constant of resin is lowered with both glass and phenolic microsphere addition. Water absorption deteriorated the dielectric properties of the composites. 2. Microspheres of acrylonitrile-vinylidene chloride copolymer provide both low and water-resistant dielectric properties.
Andritsch et al. [113]	Matrix: epoxy, Hollow particles: Glass ($\Phi_{mb} = 0.5$)	f = $10^{-4} - 10^{-1}$ Hz Temperature = 40 and 70°C (wet: 80% relative humidity at 80°C for 7 days; normal: as obtained; dry: 200°C for 2 days and then kept at 80°C)	1. The difference between the specimens containing microspheres subjected to wet and normal conditions were minimal. 2. A conductive layer is formed due to the moisture absorption in wet specimens which result in DC-conductivity.
Strauchs et al. [114]	Matrix: epoxy, Hollow particles: Glass ($\Phi_{mb} = 0.4$) (Type A: US - Al - 60µm; Type B: silane coated - 60µm; Type C: US - Al - 40µm; Type D: US - 40µm)	f = 50 Hz Temperature = 20°C Water immersion for 0 – 50 days	1. Variation in dielectric properties caused by the water absorption had no relation to microsphere diameter. 2. Specimens with Type A and C microspheres show an increase in the dielectric constant with increasing duration of water storage. 3. Type B specimens show negligible difference, while Type D specimens show increase for the first 10 days of testing, before becoming saturated.
Roggendorf et al. [115]	Matrix: epoxy, Hollow particles: acrylonitrile	f = 50 Hz Aging condition: climatic chamber	Syntactic foam reinforced with 95 µm radius showed lower dielectric constant across the entire aging time,

	copolymer coated with CaCO_3 ($\Phi_{\text{mb}} = 0.4$, $R_o = 40$ and $95 \mu\text{m}$)	(1500 h) and pressure cooker (100 h).	under climatic chamber aging.
--	--	---------------------------------------	-------------------------------

US – untreated surface; Al – Alkali

It can be observed in both tables that all the existing studies have used epoxy resin as the matrix material. In addition, glass hollow particles (also called glass microballoons or HGMs) are the most common type of particles used in syntactic foams. A wide range of material compositions, temperatures, and frequencies have been covered. The results that are summarized in these tables show that the dielectric constant

- decreases with increasing Φ_{mb} of HGMs
- decrease with increasing test frequency
- increases with increasing temperature

Impedance is also found to have a behavior similar to that of dielectric constant with respect to Φ_{mb} and frequency. It is clear from the summary of the available literature that there is a lack of studies on syntactic foams

- with any other matrix except epoxy resin
- understanding the effect of hollow particle wall thickness
- that develop theoretical relations of dielectric constant with Φ_{mb} and microballoon wall thickness. The available studies are mainly experimental.

The present work is aimed at filling this gap by characterizing vinyl ester/HGM syntactic foams for dielectric properties with specific focus on understanding the relation of Φ_{mb} and hollow particle wall thickness with dielectric constant of the syntactic foams. In addition, theoretical models are developed to predict the dielectric constant of syntactic foams. Maxwell-Garnett [116] and Jayasundere-Smith (J-S)[117] equations, applicable to solid particle filled composites, are modified to include the hollow particle wall thickness. The theoretical predictions are validated with experimental results. The models are used to conduct parametric studies to understand the weight saving potential of syntactic foams in applications where the dielectric constant is the primary consideration.

5.2 Materials and Methods

Glass microballoons (3M, MN) and vinyl ester resin (U.S. Composites, FL) are used to fabricate syntactic foam slabs. The neat vinyl ester resin and HGMs are measured in appropriate proportions and mixed in a beaker. To the uniform mixture, the hardener is added and continuously stirred. The slurry is poured into aluminum molds coated with a lubricant (Dow Corning, MI) and allowed to cure at room temperature for at least 24 h. The detailed manufacturing procedure is explained in the published literature [47].

The electrical impedance was measured using a CH Instruments (Austin, TX) 700D potentiostat by the AC impedance method, as schematically represented in Figure 26. The experiments were conducted in a frequency range of 10^{-2} – 10^6 Hz, with applied AC wave amplitude of 500 mV. A specimen size of $18 \times 14 \times 1$ mm³ was used in performing the experiments. The specimens were cut using a low speed precision diamond blade saw (Isomet®; Buehler Ltd, Lake Placid, NY) to ensure that the surfaces were parallel to each other.

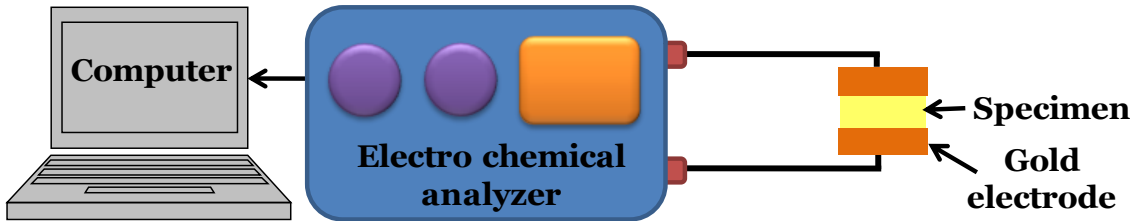


Figure 26. The setup used in the measurement of impedance of syntactic foams.

HGMs of three different nominal true particle densities (220, 320 and 460 kg/m³) are used in four different volume fractions (30, 40, 50 and 60%) to fabricate twelve types of syntactic foams. The HGMs are characterized by radius ratio η as

$$\eta = R_i / R_o \quad (1)$$

where the radius ratio can be related to the HGM wall thickness as

$$w = R_o (1 - \eta) \quad (2)$$

Increasing value of η refers to decreasing hollow particle wall thickness. The HGM properties, including radius ratio, are given in Table 12. The specimen nomenclature starts with VE representing vinyl ester resin, followed by three digit true particle density

and two digits of microballoon volume fraction. Apart from the porosity that exists inside HGMs, some air is entrapped in the matrix during the composite material fabrication and is termed as matrix porosity. Presence of matrix porosity may also affect the composite properties. The volume fraction of matrix porosity is calculated by

$$\Phi_p = \left(\frac{\rho^{th} - \rho^{exp}}{\rho^{th}} \right) \quad (3)$$

The theoretical density calculated using the rule of mixtures and the experimentally measured density of syntactic foams are reported in Table 12. The estimated matrix porosity is low and is between 1 and 4.5 vol.% for most syntactic foam slabs.

Table 12. Theoretical and experimental densities, along with matrix porosity of the syntactic foams used in the study.

Specimen type	Mean particle diameter (μm)*	Wall thickness (μm)*	Radius ratio (η)*	Theo. density (kg/m^3)	Exp. density (kg/m^3)	Matrix porosity (vol.%)
VE220-30	35	0.52	0.970	878	839	4.5
VE220-40				784	774	1.2
VE220-50				690	676	2.0
VE220-60				596	570	4.4
VE320-30	40	0.88	0.956	908	888	2.2
VE320-40				824	787	4.5
VE320-50				740	712	3.8
VE320-60				656	633	3.6
VE460-30	40	1.29	0.936	950	937	1.4
VE460-40				880	843	4.3
VE460-50				810	782	3.4
VE460-60				740	716	3.3

*data taken from [47]

5.3 Results and Discussion

The impedance obtained from the experiment is a complex quantity, containing the real (resistance) and the imaginary (reactance) parts and is defined as

$$|Z| = \sqrt{R^2 + X_c^2} \quad (4)$$

The potentiostat provides measurements of these quantities. The phase angle is given as

$$\phi = \tan^{-1}\left(\frac{X_c}{R}\right) \quad (5)$$

The phase angle is found to be around -90° , which indicates the capacitive nature of the neat resin. The capacitance can be obtained as

$$C = \frac{1}{2\pi f X_c} \quad (6)$$

The dielectric constant is obtained from the calculated capacitance as

$$\varepsilon = \frac{Ct}{\varepsilon_0 A} \quad (7)$$

The values of t , A , and ε_0 are taken as 10^{-3} m, 25.2×10^{-5} m² and 8.854×10^{-12} F/m[118], respectively.

In the first step, the impedance of neat vinyl ester resin used as the matrix in syntactic foams is measured. The variation of impedance with respect to frequency for the vinyl ester resin is shown in Figure 27. The impedance is found to decrease with increasing frequency across the selected range. The impedance values are used to calculate dielectric constant at various frequencies, which are compared with the results obtained for syntactic foams.

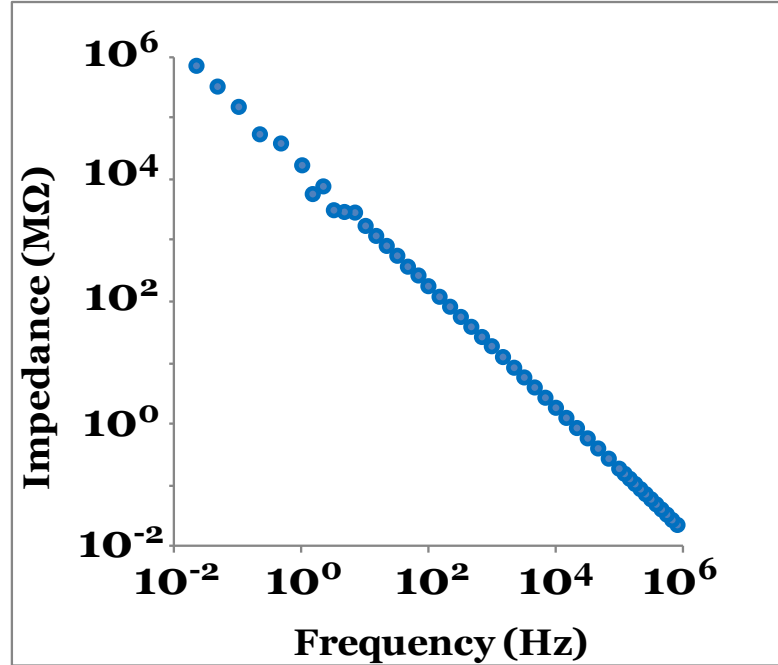


Figure 27. The variation of the impedance of neat vinyl ester resin with respect to frequency.

In the next step, syntactic foams are tested in a similar manner and their dielectric constants are calculated from the experimental results. The impedance-frequency plots of syntactic foams show characteristics similar to that of the neat resin. These plots are used to determine the dielectric constant at various frequencies of interest.

The dielectric constants of the neat resin and the syntactic foams at a representative frequency of 100 kHz are presented in Figure 28. As a general trend, the dielectric constant of syntactic foams is lower than that of the neat resin. It is also observed that HGM volume fraction has a prominent effect on the dielectric constant of syntactic foams. The dielectric constant of syntactic foams decreases with increasing HGM volume fraction. This observation is expected because the air porosity volume fraction increases with HGM volume fraction and air has lower dielectric constant than that of matrix resin and HGM material (glass). The plot of dielectric constant with respect to syntactic foam density, Figure 29, is illustrative because both η and HGM volume fraction affect the density. The neat resin has the highest density in this data set. The dielectric constant varies almost linearly with respect to the syntactic foam density. The figure includes dielectric constant at two different frequencies of 100 Hz and 100

kHz. In both cases the slope of the line is the same. Since the syntactic foam density is dependent on both HGM volume fraction and η , the dependence of dielectric constant on syntactic foam density requires further investigation to understand the individual effect of these parameters. The relations between these parameters can be better understood by theoretical means. Although the interfacial bonding between HGM and vinyl ester is expected to play a role in the measured dielectric constant, this parameter is not included in the study. All syntactic foams use HGMs of the same type of glass material, therefore, the interfacial bonding characteristics are expected to be the same for all syntactic foams. In addition, the mean radius is nearly the same for all types of HGMs used in syntactic foams, which implies that the syntactic foams having the same volume fraction of different types of HGMs will have the same interfacial area and the effect of bonding characteristics will also be the same in these cases. Hence, the attention is focused on evaluating the effect of HGM volume fraction and η in the theoretical models.

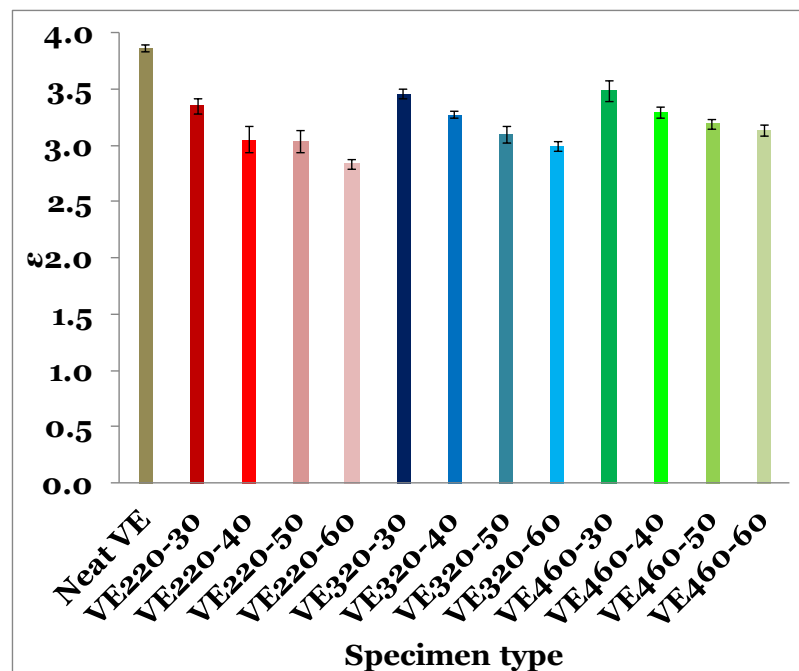


Figure 28. Experimentally measured values (at 100 kHz) of the dielectric constant for the neat resin and twelve types of syntactic foams.

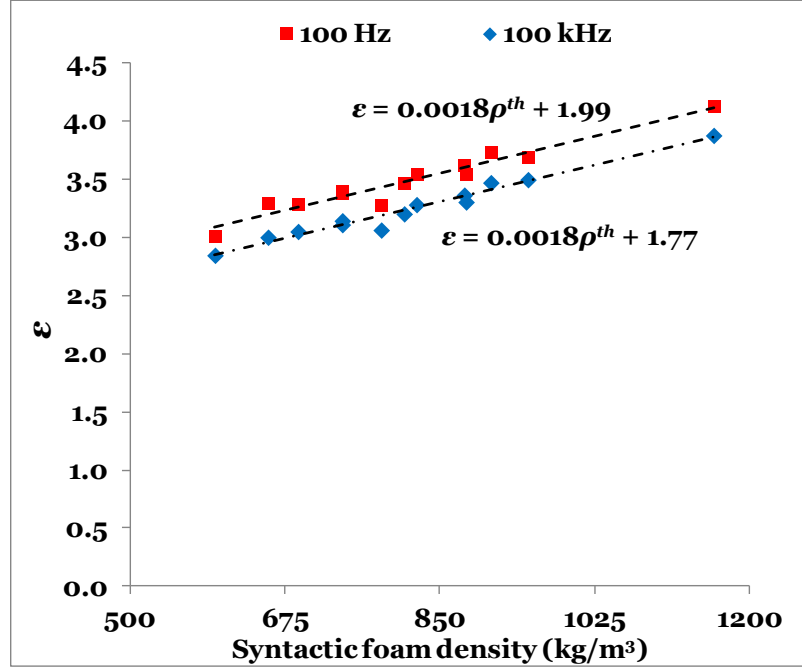


Figure 29. Variation of the experimentally measured dielectric constant at 100 Hz and 100 kHz with respect to the syntactic foams density.

Estimation of the dielectric constant of hollow particles, which comprise a thin shell filled with air, is the first step in obtaining the effective dielectric constant of syntactic foams. In order to find a closed form expression for the dielectric constant of HGMs, Maxwell's theory can be utilized. The polarization of HGMs is equated to the polarization of an equivalent sphere and the dielectric constant of HGM is obtained as follows. The potential ψ of the HGM is obtained by solving the Laplace equation in polar coordinates (Figure 30), given by

$$\nabla^2 \psi = 0 \quad (8)$$

The solution of the Laplace equation is obtained in the form [119]

$$\psi(r, \theta) = \sum_{n=0}^{\infty} (a_n r^{-(n+1)} + b_n r^n) P_n(\cos \theta) \quad (9)$$

where $P_n(\cos \theta)$ is the n^{th} order Legendre polynomial and a_n and b_n are constants. Taking into account the axial symmetry of the sphere, the potential is given by

$$\psi_1(r, \theta) = \sum_{n=1}^{\infty} (D_n r^n) P_n(\cos \theta) \quad (r \leq r_i) \quad (10)$$

$$\psi_2(r, \theta) = \sum_{n=1}^{\infty} (E_n r^{-(n+1)} + G_n r^n) P_n(\cos \theta) \quad (r_i \leq r \leq r_o) \quad (11)$$

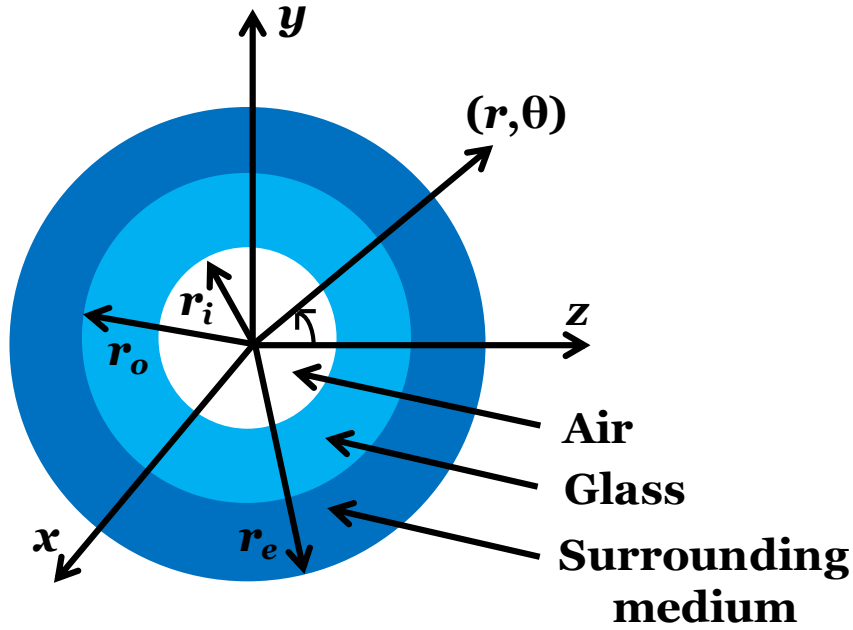


Figure 30. Schematic of hollow glass microballoon to determine the dielectric constant.

$$\psi_3(r, \theta) = \sum_{n=1}^{\infty} (H_n r^{-(n+1)} + I_n r^n) P_n(\cos \theta) \quad (r_o \leq r \leq r_e) \quad (12)$$

$$\psi_4(r, \theta) = -e_0 r P_1(\cos \theta) + \sum_{n=1}^{\infty} J_n r^{-(n+1)} P_n(\cos \theta) \quad (r_e \leq r) \quad (13)$$

The constants D_n , E_n , G_n , H_n , I_n , and J_n are found by applying the following boundary conditions and utilizing the orthogonality property, given by

$$\psi_1(R_i, \theta) = \psi_2(R_i, \theta) \quad (14a)$$

$$\psi_2(R_o, \theta) = \psi_3(R_o, \theta) \quad (14b)$$

$$\psi_3(R_e, \theta) = \psi_4(R_e, \theta) \quad (14c)$$

$$\varepsilon_a (\partial_r \psi_1)_{r=R_i} = \varepsilon_g (\partial_r \psi_2)_{r=R_i} \quad (15a)$$

$$\varepsilon_g (\partial_r \psi_2)_{r=R_o} = \varepsilon_e (\partial_r \psi_3)_{r=R_o} \quad (15b)$$

$$\varepsilon_e (\partial_r \psi_3)_{r=R_e} = (\partial_r \psi_4)_{r=R_e} \quad (15c)$$

$$\int_{\theta=0}^{\pi} P_n(\cos \theta) P_m(\cos \theta) \sin \theta d\theta = \frac{2}{(2m+1)} \delta_{m,n} \quad (16)$$

where $\delta_{m,n}$ is the Kronecker delta function. Applying the above boundary conditions the value of the constant J_1 is found to be

$$J_1 = \left[\frac{(\varepsilon_e - 1)}{(\varepsilon_e + 2)} R_e^3 Q - \frac{(2\varepsilon_e + 1)R_o^3 L}{(\varepsilon_e + 2)(2\varepsilon_e + \varepsilon_g)} \right] S e_0 \quad (17)$$

where the constants Q , L and S are represented by

$$Q = \left[1 + 2 \frac{(\varepsilon_e - \varepsilon_g)(\varepsilon_g - \varepsilon_a)}{(2\varepsilon_e + \varepsilon_g)(2\varepsilon_g + \varepsilon_a)} \frac{R_i^3}{R_o^3} \right]$$

$$L = \left[(\varepsilon_e - \varepsilon_g) + \frac{(\varepsilon_e + 2\varepsilon_g)(\varepsilon_g - \varepsilon_a)}{(2\varepsilon_g + \varepsilon_a)} \frac{R_i^3}{R_o^3} \right]$$

$$S = \left[1 + 2 \frac{(\varepsilon_e - \varepsilon_g)(\varepsilon_g - \varepsilon_a)}{(2\varepsilon_e + \varepsilon_g)(2\varepsilon_g + \varepsilon_a)} \frac{R_i^3}{R_o^3} - 2 \frac{(\varepsilon_e - 1)(\varepsilon_e - \varepsilon_g)}{(\varepsilon_e + 2)(2\varepsilon_e + \varepsilon_g)} \frac{R_o^3}{R_e^3} - 2 \frac{(\varepsilon_e - 1)(\varepsilon_e + 2\varepsilon_g)(\varepsilon_g - \varepsilon_a)}{(\varepsilon_e + 2)(2\varepsilon_e + \varepsilon_g)(2\varepsilon_g + \varepsilon_a)} \frac{R_i^3}{R_e^3} \right]^{-1}$$

The dipole moment induced in the sphere due to the applied external field e_0 is $4\pi\varepsilon_0 J_1$.

In addition, the polarization of the system, χ , is the ratio of the induced dipole moment to the external applied field e_0 . Hence the polarization can be written as

$$\chi = (4\pi\varepsilon_0) r_e^3 \left[\frac{(\varepsilon_e - 1)}{(\varepsilon_e + 2)} K - \frac{(2\varepsilon_e + 1)L}{(\varepsilon_e + 2)(2\varepsilon_e + \varepsilon_g)} \frac{R_o^3}{R_e^3} \right] S \quad (18)$$

The effective dielectric constant of HGM is found by equating the polarization of the system consisting of a hollow glass shell containing the air void to the polarization of an equivalent solid sphere. The dielectric constant of HGMs can be written as

$$\varepsilon_{mb} = \left[\frac{1 - 2\eta^3 \frac{(\varepsilon_g - 1)^2}{(\varepsilon_g + 2)(2\varepsilon_g + 1)} + 2(1 - \eta^3) \frac{(\varepsilon_g - 1)}{(\varepsilon_g + 2)}}{1 - 2\eta^3 \frac{(\varepsilon_g - 1)^2}{(\varepsilon_g + 2)(2\varepsilon_g + 1)} - (1 - \eta^3) \frac{(\varepsilon_g - 1)}{(\varepsilon_g + 2)}} \right] \quad (19)$$

where ε_g and ε_a are taken as 5.6 and 1,[111] respectively. The calculated effective dielectric constants of the three types of HGMs used in the experimental study is plotted with respect to their density in Figure 31. The figure also contains upper and lower bounds obtained by the parallel and the series rule of mixtures, respectively. The values calculated from the model are between the two bounds.

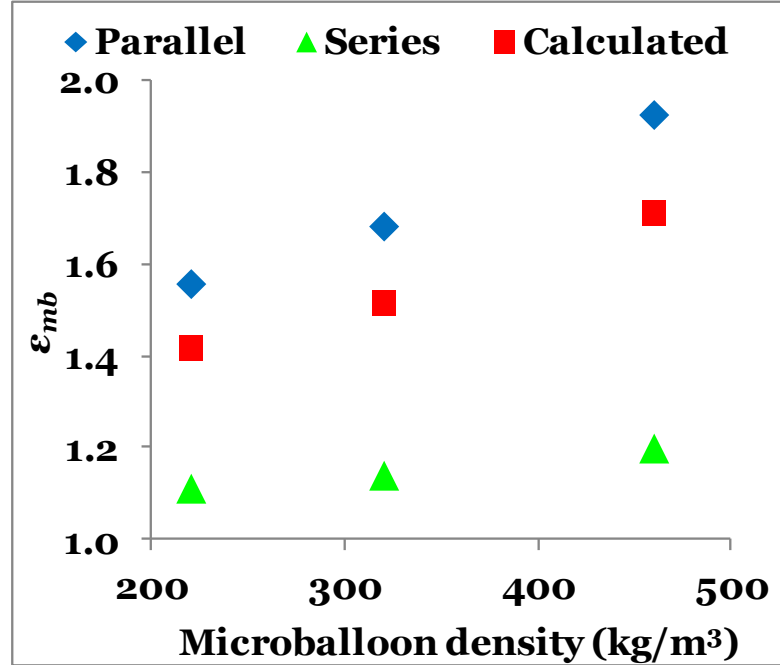


Figure 31. Dielectric constant calculated for the glass microballoon using Equation (19), presented along with values obtained from the parallel and series model.

Although the syntactic foams are assumed to be filled with HGMs that are identical in all respects, polydispersivity exists in their size and radius ratio. Experimental data are available on the size and radius ratio distribution of HGMs used in the present work and can be used in the models to account for polydispersivity[48].

The effective dielectric constant for HGMs is now used in the Maxwell-Garnett and the J-S equations to predict the dielectric properties of particulate reinforced composites [111, 120]. The Maxwell-Garnett equation is given by

$$\varepsilon = \varepsilon_m \left[1 + \frac{3\Phi_{mb} \frac{\varepsilon_{mb} - \varepsilon_m}{\varepsilon_{mb} + 2\varepsilon_m}}{1 - \Phi_{mb} \frac{\varepsilon_{mb} - \varepsilon_m}{\varepsilon_{mb} + 2\varepsilon_m}} \right] \quad (20)$$

The J-S equation is based on the Kerner's equation taking into account the particle-to-particle interaction between HGMs [117] and is given by

$$\varepsilon = \frac{\Phi_m \varepsilon_m + \Phi_{mb} \varepsilon_{mb} \left(\frac{3\varepsilon_m}{\varepsilon_{mb} + 2\varepsilon_m} \right) \left(1 + \frac{3\Phi_{mb} (\varepsilon_{mb} - \varepsilon_m)}{\varepsilon_{mb} + 2\varepsilon_m} \right)}{\Phi_m + \Phi_{mb} \left(\frac{3\varepsilon_m}{\varepsilon_{mb} + 2\varepsilon_m} \right) \left(1 + \frac{3\Phi_{mb} (\varepsilon_{mb} - \varepsilon_m)}{\varepsilon_{mb} + 2\varepsilon_m} \right)} \quad (21)$$

The dielectric constants predicted by the Maxwell-Garnett and J-S equations are given in Table 13. These predictions use the experimentally measured dielectric constant of the neat resin as an input parameter. Since the dielectric constant is dependent on the frequency, selection of dielectric constant of the neat resin at appropriate frequency helps in obtaining predictions for syntactic foams at that frequency. The theoretically obtained dielectric constant values are compared with the experimental values to calculate the prediction error. The Maxwell-Garnett model predictions show a larger deviation from experimental values ($\pm 22\%$) than that obtained from the J-S model ($\pm 12\%$), as listed in Table 13. Further validation of these models is conducted with data obtained from a study published by Yung et al. [34].

Table 13. Dielectric constant for the various types of syntactic foams along with the prediction from Maxwell-Garnett equation and J-S equation.

Specimen type	Average experimental ϵ	Maxwell-Garnett model		J-S model	
		ϵ	Error (%)	ϵ	Error (%)
VE220-30	3.36	3.01	10.4	3.15	6.0
VE220-40	3.05	2.75	10.1	2.98	2.6
VE220-50	3.04	2.50	17.9	2.81	7.6
VE220-60	2.84	2.26	20.3	2.65	6.5
VE320-30	3.46	3.05	12.0	3.18	8.2
VE320-40	3.27	2.80	14.5	3.00	8.2
VE320-50	3.10	2.56	17.5	2.84	8.4
VE320-60	2.99	2.33	22.1	2.68	10.4
VE460-30	3.49	3.12	10.4	3.23	7.3
VE460-40	3.30	2.90	12.1	3.06	7.0
VE460-50	3.19	2.68	16.1	2.91	9.0
VE460-60	3.13	2.47	21.2	2.75	12.4

Figure 32 shows that both the J-S and the Maxwell-Garnett model predictions closely match with the experimental results with only $\pm 6\%$ and $\pm 5\%$ deviation, respectively. This experimental data was obtained on syntactic foams containing HGM of 600 kg/m^3 density tested at 1 MHz frequency. After validation with experimental results obtained from the present study and also with the data obtained from previously

published study, the modified J-S model is used for conducting a parametric study to understand the effect of HGM volume fraction and η on the dielectric constant of syntactic foams. The dielectric constant of the neat resin is taken as 3.87 at 100 kHz frequency in the parametric study.

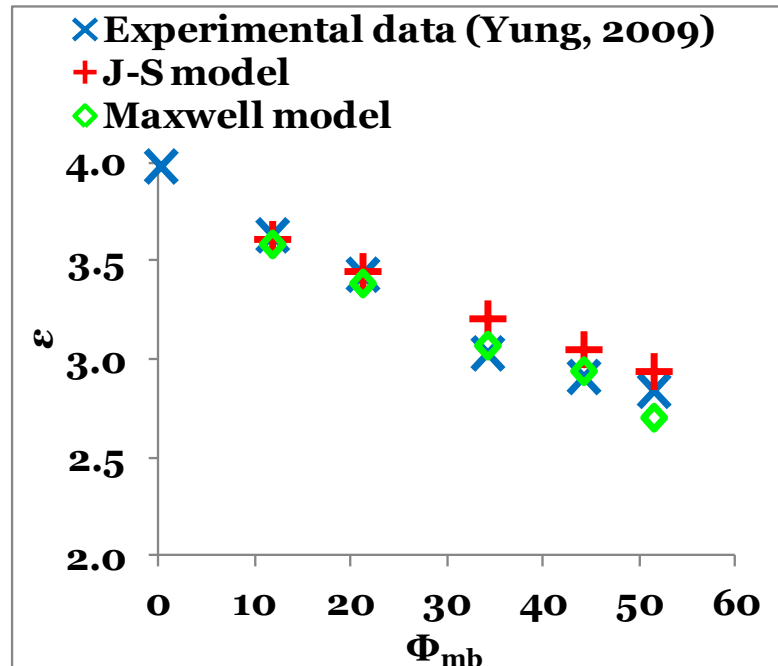
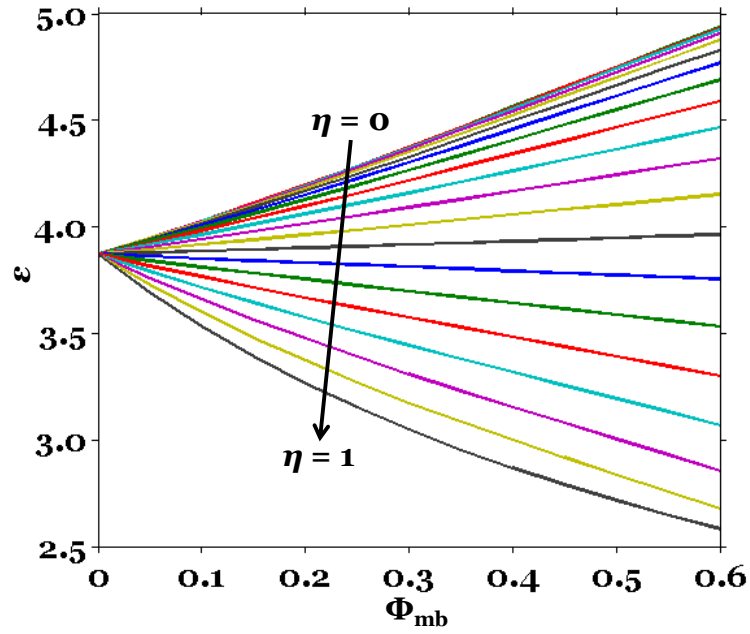
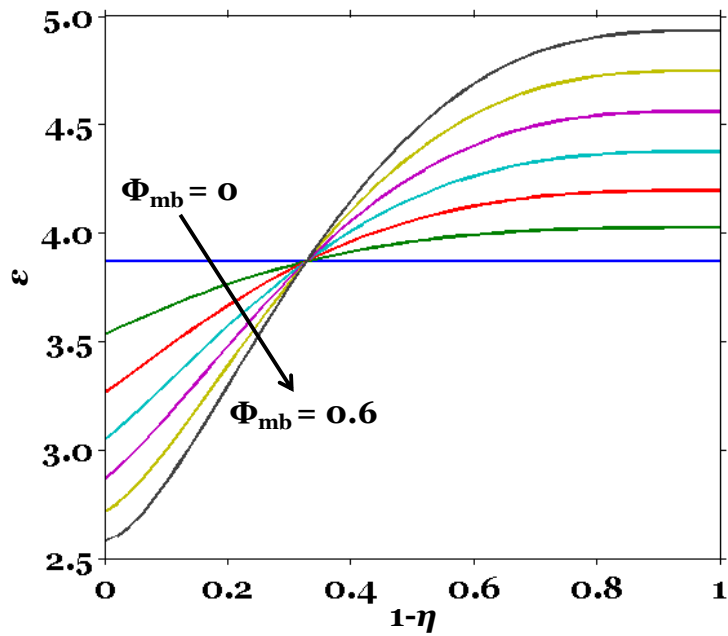


Figure 32. Comparison of theoretically calculated ϵ using J-S and Maxwell-Garnett model's with the experimental values (taken from [34]), at 1 MHz, for epoxy/HGM syntactic foams.

Figure 33(a) and (b) show the variation of the dielectric constant of syntactic foams with respect to the HGM volume fraction and wall thickness, respectively. It can be observed that with the appropriate selection of HGM volume fraction and η , the dielectric constant of syntactic foams can be tailored over a wide range of 2.6-4.9. Thin walled HGMs, especially at $\eta > 0.7$, can result in syntactic foams with dielectric constant lower than that of the neat resin. This trend reverses for HGMs of $\eta < 0.7$.



(a)

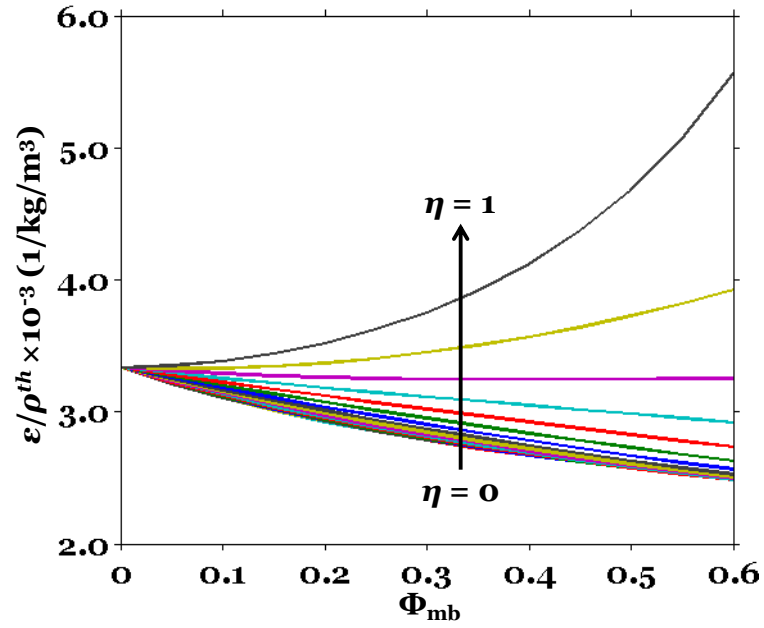


(b)

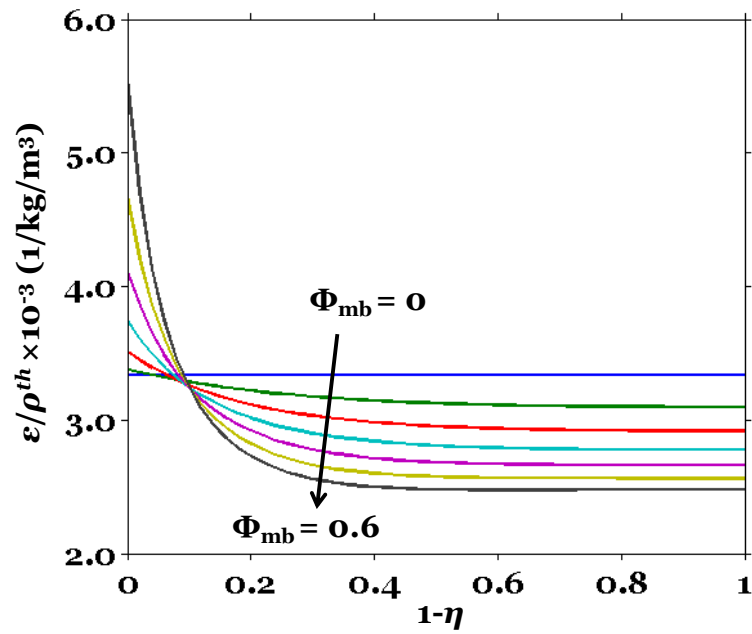
Figure 33. Dielectric constant of syntactic foams as a function of (a) volume fraction and (b) radius ratios of HGMs.

The specific dielectric constant normalized with respect to the syntactic foam density is presented in Figure 34. The figure shows that the density decreases more rapidly than the dielectric constant of syntactic foams. Therefore, HGMs of lower wall thickness provide higher specific dielectric constant. Figure 34 (b) also shows that the effect of wall thickness variation on specific dielectric constant becomes negligible at $\eta > 0.7$ for all HGM volume fractions. This observation is very important in evaluating the weight saving obtained by using certain combination of HGM volume fraction and η . In syntactic foams, Φ_{mb} and η can be independently varied. Several combinations of Φ_{mb} and η can provide the same syntactic foam density. Therefore, the relation between dielectric constant, Φ_{mb} and η is further evaluated in Figure 34.

Figure 35(a) shows a 3D contour plot of dielectric constant variation along the vertical axis, whereas the floor of the graph contains a 2D contour plot of syntactic foam density variation with respect to HGM volume fraction and η marked on two different axes. The 2D contour plot is shown again in Figure 35 (b) for clarity, where axes are marked in terms of Φ_{mb} and η to be more illustrative of the contribution of these parameters on syntactic foam density. The scale bar in Figure 35 (a) represents both dielectric constant and density of syntactic foams in their appropriate units for parity.

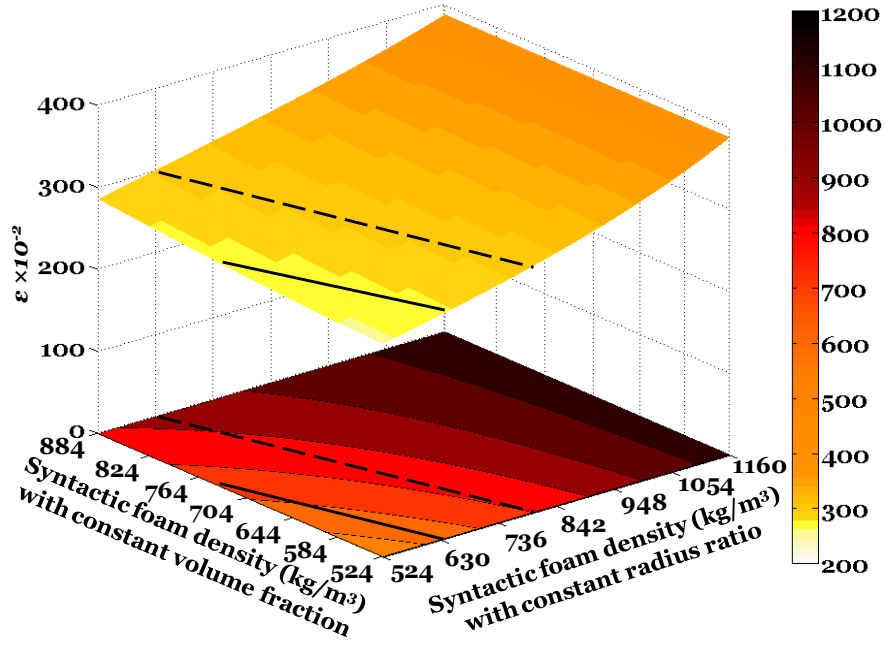


(a)

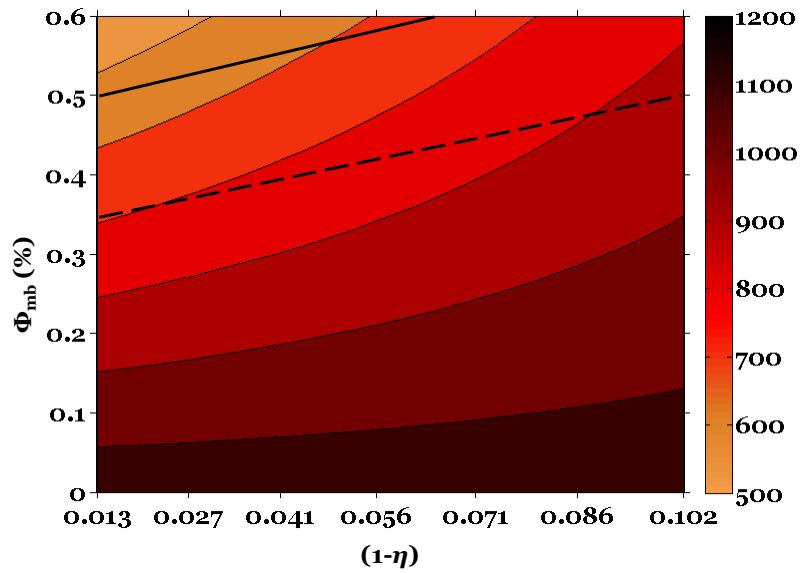


(b)

Figure 34. Variation of specific dielectric constant (normalized with respect to the syntactic foam density) as a function of (a) volume fraction and (b) the radius ratios of HGMs.



(a)



(b)

Figure 35. (a) Contour plot of variation of the dielectric constant with respect to the syntactic foam density. The syntactic foam density is varied with respect to both the volume fraction and the radius ratio of the microballoons. The scale bar represents both the dielectric constant and the foams density in their respective units. (b) The syntactic foams density plotted as a function of volume fraction and the radius ratio of the microballoons. The scale bar represents density in kg/m^3 .

Two representative values of the dielectric constant, namely $\epsilon = 2.75$ and 3 , are denoted by a solid and a dashed line, respectively, in Figure 35 (a). All the syntactic foam compositions along a given line have the same dielectric constant. These two lines are also projected on the density contour plot. It is noted that syntactic foams having densities in the range $630\text{-}740\text{ kg/m}^3$ can be selected to have the same dielectric constant of 2.75 . The syntactic foams having this range of densities have HGM volume fraction in the range of $0.5\text{-}0.6$ and η in the range $0.987\text{-}0.936$. Since the mechanical properties of syntactic foams are also related to Φ_{mb} and η ; the flexibility of selecting these parameters in a range, instead of a fixed value, provides the possibility of independently tailoring the dielectric constant and modulus within the ranges given by such charts. Similar observations can also be made for the second representative value of dielectric constant of 3 , where syntactic foam density can vary in the range $790\text{-}930\text{ kg/m}^3$, which can be obtained by HGM volume fractions of $0.3\text{-}0.5$ and η of $0.987\text{-}0.898$. Most widely used HGMs in syntactic foams are within these ranges of Φ_{mb} and η . Appropriate combinations of Φ_{mb} and η can be selected to have the same syntactic foam density and dielectric constant, while having the desired mechanical properties. Extensive literature is also available for the variation of mechanical properties such as the modulus and Poisson's ratio with respect to Φ_{mb} and η [22, 47, 55]. This knowledge of both mechanical and electrical properties will be helpful in designing the syntactic foams based on the desired application.

CHAPTER 6. Unnotched Izod impact properties of syntactic foams

Syntactic foams are used as energy absorbing materials in several existing marine and aerospace applications. Understanding the impact properties of syntactic foams and relating them to various material parameters is important for these applications. A literature review on the available studies on impact properties of polymer matrix syntactic foams is presented in Tables 15 and 15 for pendulum and drop weight impact, respectively. Table 14 shows that epoxy, vinyl ester, polyester, polypropylene and polyvinylchloride (PVC) matrix syntactic foams have been studied under notched Izod and Charpy impact conditions. The following is a brief overview of the existing literature on the impact properties of syntactic foams.

In the existing literature, studies have characterized the impact strength of syntactic foams based on the Φ_{mb} and the size of the filler. The addition of 5 vol.% of hollow glass microballoons (HGM) decreased the impact strength by 20% and 70% for epoxy [121] and PVC [122] matrix syntactic foams, respectively, in comparison to the neat resin. The addition of phenolic hollow microspheres resulted in increase of the impact strength by up to 300% at 10 wt.% of the filler [123]. The addition of 5 wt.% of hollow epoxy microspheres in polyester matrix resulted in 32% increase in the impact strength [124]. A clear trend between Φ_{mb} and the impact strength of syntactic foam is not observed in the existing literature because the type of filler and the matrix chosen also affect the impact properties.

The effect of particle size on the impact properties of the syntactic foams has also been analyzed. An increase in HGM diameter from 10 to 70 μm , resulted in a linear decrease in the notched impact strength by a maximum of 12% [125]. Another study with three different size (10, 35 and 70 μm) HGMs filled in polypropylene matrix observed that the 35 μm particles showed the lowest U-notched, V-notched and unnotched impact strength [126]. A clear trend of the variation of the impact properties with respect to the reinforcing hollow particle size cannot be established with the current available studies. In the case of glass fiber reinforced syntactic foams containing a constant 43 vol.% HGMs, the absorbed impact energy increased with the fiber content [127].

Table 14. Existing studies on pendulum impact testing of syntactic foams.

Reference	Materials used*	Test conditions	Results
[122]	PVC, HGM** ($\Phi_{mb} = 0-0.2$)	Notched Izod impact	1. The addition of 5% of 24 μm HGM resulted in the decrease in the impact strength by 70%.
[125]	Polypropylene, HGM ($\Phi_{mb} = 0-0.2$)	V-notched Izod impact	1. The notched impact strength increased slightly until $\Phi_{mb}=0.15$ and then decreased. 2. For $\Phi_{mb}=0.1$, as the particle size increased from 10 to 70 μm , the impact strength decreased by 12%.
[126]	Polypropylene, HGM ($\Phi_{mb} = 0.1$)	V-notched, U-notched and unnotched Izod impact	1. The 35 μm sized HGM showed the lowest value for the V-notched, U-notched and unnotched impact strength.
[123]	Vinyl ester, phenolic hollow microsphere (0-15 wt.%), silica	Izod impact	1. Impact strength increased by 300% with up to 10 wt.% of the filler addition and then decreased with further addition of fillers. 2. The silane treated silica reinforced syntactic foam showed better impact strength than untreated silica syntactic foam at all weight fractions.
[124]	Polyester, hollow epoxy microspheres (0-9 wt.%)	Charpy impact	1. Impact strength increased by 32% with addition of 5 wt.% of filler, in comparison to the neat resin.
[127]	Epoxy, HGM ($\Phi_{mb} = 0-0.5$), glass and carbon fiber	Charpy impact	1. Compared to neat resin, absorbed impact energy of syntactic foams decreased by up to 40% as Φ_{mb} increased to 0.5.

			2. At $\Phi_{mb}=0.45$, glass fiber reinforced syntactic foams showed higher absorbed impact energy than carbon fiber reinforced syntactic foams.
[128]	Epoxy, HGM ($\Phi_{mb} = 0-0.55$)	Charpy impact	1. The critical stress intensity factor and the energy release rate decreased slightly as the volume fraction of the HGM increased. 2. The increase in testing temperature from 20 to 80 °C had very little effect on the stress intensity factor and the energy release rate.
[121]	Epoxy, HGM ($\Phi_{mb} = 0-0.2$)	Charpy impact	1. The impact resistance decreased by 20% at 5 vol.% of HGM in comparison to the neat resin, beyond which the addition of HGM had very little effect on the impact resistance.

* Φ_{mb} represents volume fraction of hollow particles in the syntactic foam.

**HGM – hollow glass microballoons

Table 15. Existing studies on drop weight impact testing of syntactic foams.

Reference	Materials used	Test conditions	Results
[129]	Vinyl ester, HGM, ($\Phi_{mb} = 0.39$)	Drop weight impact with a flat-ended striker	<ol style="list-style-type: none"> 1. For specimen diameter of 5 mm, the peak load on the syntactic foams is nearly 75% lower than the neat resin. 2. For specimen diameter of 5 mm, the impact stress decreased by about 70% for the syntactic foam in comparison to the neat resin.
[130]	Epoxy, HGM, ($\Phi_{mb} = 0-0.65$)	Drop weight impact, flat-ended striker	<ol style="list-style-type: none"> 1. Peak load decreased by 83% as the Φ_{mb} increased to 65%.
[131]	Epoxy, HGM ($\Phi_{mb} = 0.6$) and nanoclay	DynaTup 8250 HV drop weight impact, hemispherical tup	<ol style="list-style-type: none"> 1. Specimens containing 1 vol.% nanoclay show the highest peak load and the initiation energy because the propagating crack is arrested by nanoclay. 2. Upon increase in the content of nanoclay, the load and energy decreases due to the intercalation of the nanoclay.
[132]	Epoxy, HGM ($\Phi_{mb} = 0.35-0.6$), rubber, nanoclay and milled glass fiber	DynaTup 8250 HV drop weight impact, hemispherical tup	<ol style="list-style-type: none"> 1. The addition of HGM decreases the initiation energy while increasing the propagation energy. 2. Also the addition of nanoclay and glass fiber leads to further decrease in initiation energy while increasing the propagation energy. 3. An optimal content of rubber addition (10 vol.%) provided the highest energy absorption characteristics.
[51]	Epoxy, HGM ($\Phi_{mb} = 0.417-$	DynaTup 8250 HV	<ol style="list-style-type: none"> 1. With the addition of CaO, the initiation energy decreased by 4.6% and the

	0.45), rubber, milled glass fiber, nanoclay and CaO	drop weight impact, hemispherical tup	propagation energy increased by 8.3%, in comparison to rubberized syntactic foam.
[133]	Epoxy, HGM ($\Phi_{mb} = 0.376-0.576$), rubber, nanoclay and milled glass fiber	DynaTup 8250HV low velocity drop weight impact	1. The initiation energy increased by 414% as Φ_{mb} decreased from 0.576 to 0.376. 2. The propagation energy was found to decrease by 34% as Φ_{mb} decreased.

Studies related to drop weight impact have mainly focused on characterizing multiphase syntactic foams containing another phase in addition to hollow particles, as listed in Table 15. In the case of plain syntactic foams, drop weight impact using a flat end impactor has been conducted [129, 130]. The effect of Φ_{mb} and variation of the specimen diameter on the impact strength of syntactic foam is evaluated. The 5 mm diameter specimens are found to have 75% lower peak load in comparison to the neat resin [129] and the increase in Φ_{mb} resulted in decrease of the peak load [130]. Impact testing using a hemispherical tup on plate specimens has been performed on syntactic foams containing additional reinforcement such as nanoclay, rubber, CaO, and milled glass fibers. The addition of 1 vol.% of nanoclay improved the impact properties, while a higher nanoclay content resulted in reduced exfoliation, which was detrimental to the impact properties [131]. In the case of rubber reinforcement on syntactic foams, the optimum addition of rubber content to improve the impact strength was found to be 10 vol.% [132]. Most of these studies focused on the effect of Φ_{mb} and the secondary reinforcement on the impact properties of syntactic foams [134]. Syntactic foam core sandwich composites with laminated glass fiber skin have also been studied for impact characteristics [135]. Syntactic foam cores are useful in keeping the damage localized around the impact zone.

Although Φ_{mb} is the main parameter in several existing studies, the effect of variation of η on impact properties of syntactic foams has not been studied. It is the combination of these two parameters that can effectively tailor the properties of syntactic

foams, as observed for tensile, compressive and dynamic properties [47, 136]. The goal of the present study is to understand the impact properties of syntactic foams with respect to η and Φ_{mb} . Unnotched specimens are tested under Izod impact conditions.

6.1 Materials and Methods

Syntactic foams containing HGMs (3M, MN) in vinyl ester (U.S. Composites, FL) matrix were fabricated. The properties of the three types of HGMs used in fabricating syntactic foams are provided in Figure 36, along with an illustration of the geometrical characteristics of the hollow particles. Desired quantities of matrix resin and the HGMs are measured and stir-mixed in a beaker. Methyl ethyl ketone peroxide catalyst is added to this uniform mixture and stirred continuously. The composite slurry is cured at room temperature in aluminum molds for at least 24 h and then post cured in a convection oven at 70°C for 3 h. The detailed fabrication procedure is available in a previous published paper [47]. The naming convention of the specimen is: VEXXX-YY, where VE represent the resin vinyl ester matrix, and XXX and YY represent HGM true particle density and HGM volume percentage, respectively.

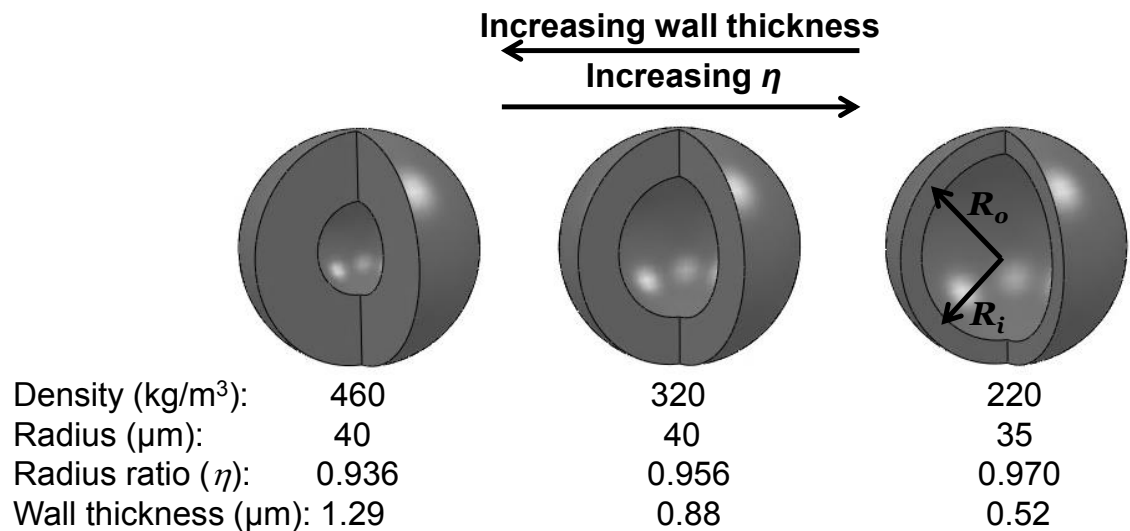


Figure 36. Properties of hollow glass microballoons used in syntactic foams.

The Izod unnotched impact testing is performed using an Instron Dynatup POE2000 instrumented impact tester (Figure 37). The test specimens are prepared in accordance with ASTM standard D4812-11 [137], with nominal dimensions as 12.7±0.15 mm × 62±1 mm × 3.17±0.13 mm (depth×length×width) [137]. The specimens were cut

using a low speed precision diamond blade saw (Isomet®; Buehler Ltd, Lake Placid, NY). At least five specimens were tested for each type of syntactic foam. The load, displacement and energy data are recorded during the test.

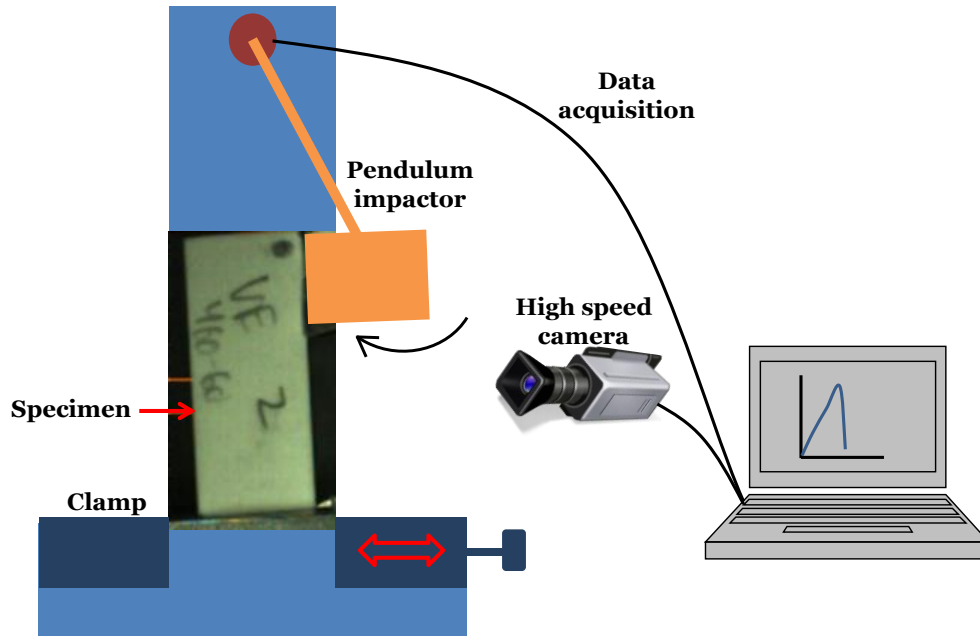


Figure 37. Schematic of the impact test setup along with the high speed camera used in the study.

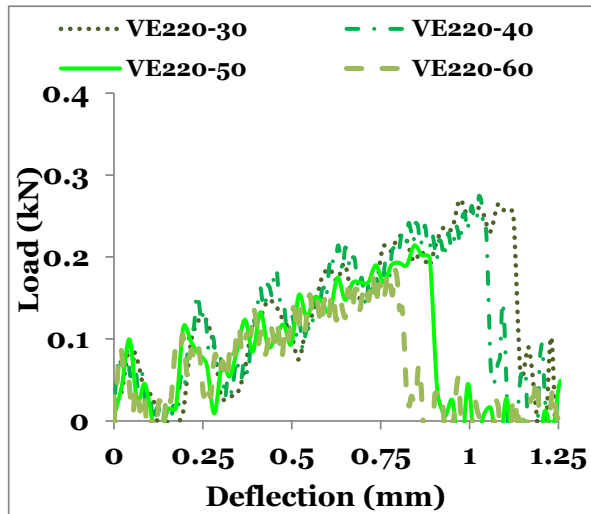
Macroscopic examination of the specimens was performed using a Nikon D7000 camera. The microscopic examination of the fracture surface is carried out using Hitachi S-3400N scanning electron microscope (SEM). Specimens were sputter coated with gold using a Leica EM-SCD050 (Leica, Buffalo Grove, IL) coater before SEM analysis. A high speed image acquisition system (Redlake V-3 camera IDT, Tallahassee, FL) was utilized to capture the failure of the specimens during impact testing. All images were acquired at a rate of 5375 frames/sec.

6.2 Results

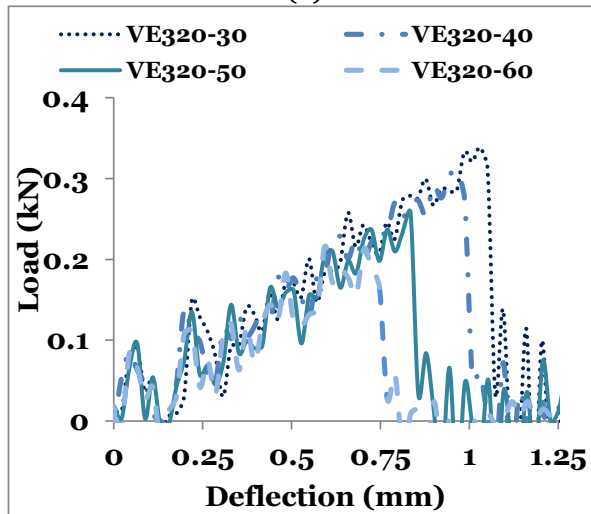
The load-displacement plots for the VE220, VE320 and VE460 syntactic foams are shown in Figure 38a, b and c, respectively. The oscillations observed in these graphs can be ascribed to the specimens vibrations during impact [138]. The vibration amplitude is initially large but decreases with time as the specimen deformation increases. The peak load obtained for the various syntactic foam specimens is normalized

with their corresponding cross-sectional area and is represented as the impact strength. The variation of the impact strength for the various syntactic foam compositions is shown in Figure 39a. The results show that the impact strength decreases with increasing Φ_{mb} . The HGM volume fraction is found to have a more profound effect on the impact strength than the wall thickness. All the Syntactic foam compositions show lower impact strength in comparison to the neat vinyl ester impact strength of 15.08 MPa. For the impact strength, a maximum decrease of 70% is observed for VE220-60 type syntactic foam in comparison to the neat vinyl ester resin. The impact strength with respect to density is shown in Figure 39b. The impact strength for syntactic foams containing the same type of particle increase almost linearly with Φ_{mb} . Most data points for all syntactic foams fit within a narrow range with respect to syntactic foam density.

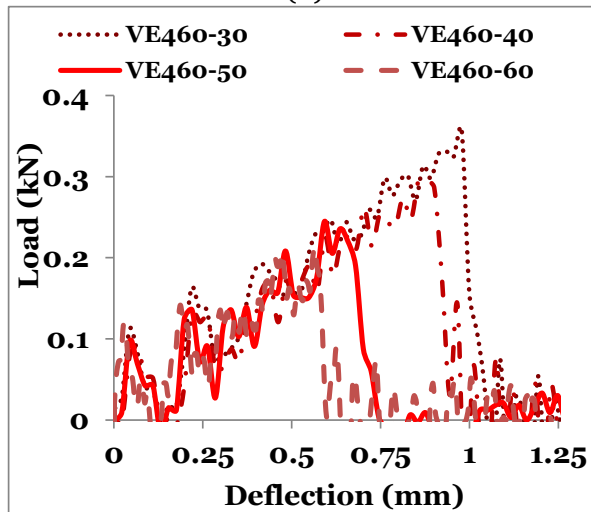
The area under the load-deflection curve is recorded as the energy absorbed and is plotted as a function of displacement for the VE220, VE320 and VE460 syntactic foams as shown in Figure 40a, b and c, respectively. The energy absorbed until the failure of the specimen under impact loading is noted as the impact energy for syntactic foams and is presented in Figure 41. The impact energy shows an increasing trend with increasing HGM wall thickness at $\Phi_{mb}=0.3$. However at $\Phi_{mb}=0.6$, a decrease in impact energy is observed as the HGM wall thickness increases. For $\Phi_{mb}=0.4$ and 0.5, a clear trend in impact energy with respect to the HGM wall thickness is not observed. Increase in Φ_{mb} from 0.3 to 0.6, leads to decrease in the impact energy by up to 50%, 58.8% and 72.2% for VE220, VE320 and VE460 syntactic foams. The standard deviations are observed to be relatively larger in absorbed energy compared to the strength values because the deflection values may vary due to the presence of localized defects in the crack path.



(a)

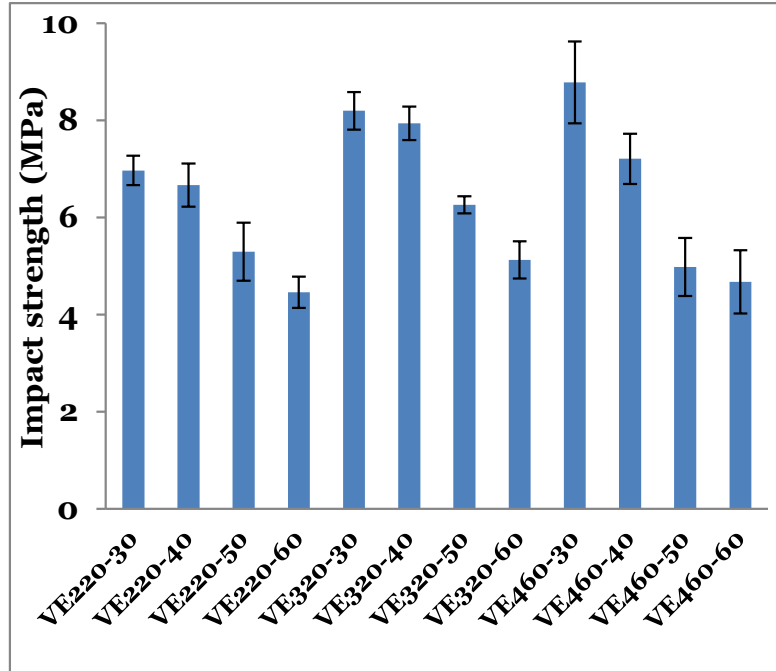


(b)

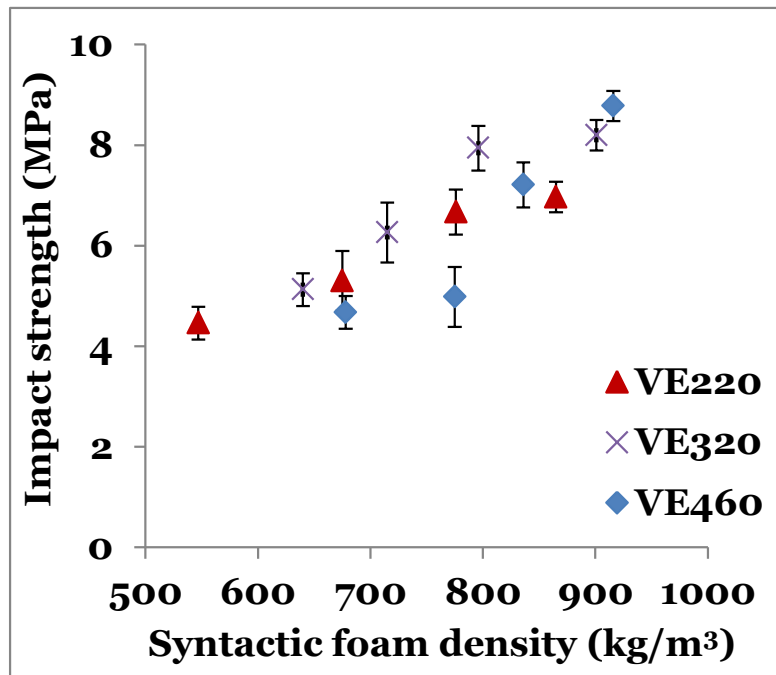


(c)

Figure 38. Load-deflection plots for various types of syntactic foams containing microballoons of (a) 220, (b) 320 and (c) 460 kg/m³ density, in $\Phi_{mb} = 0.3-0.6$.

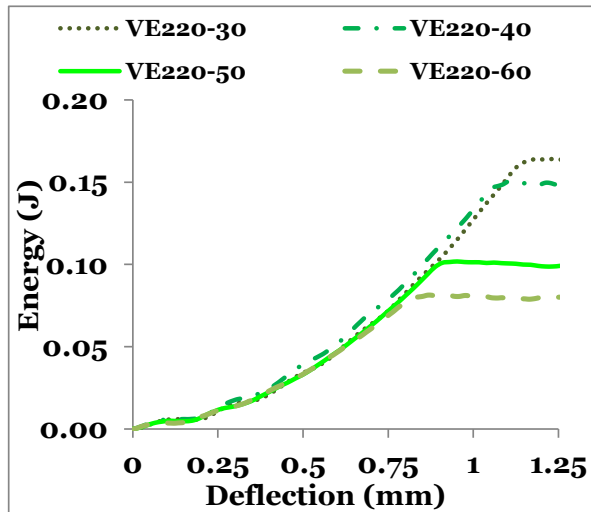


(a)

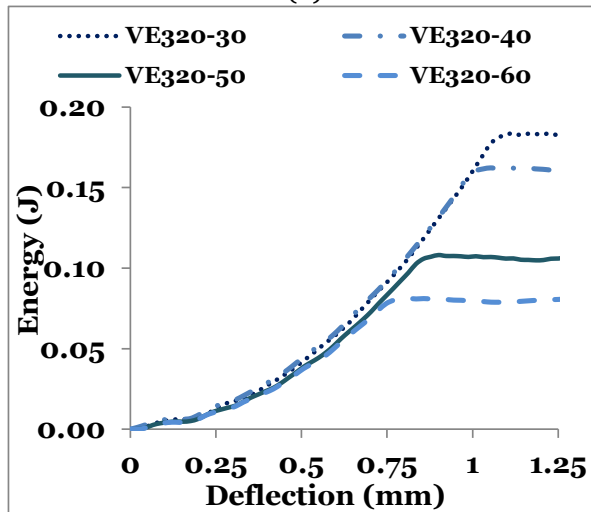


(b)

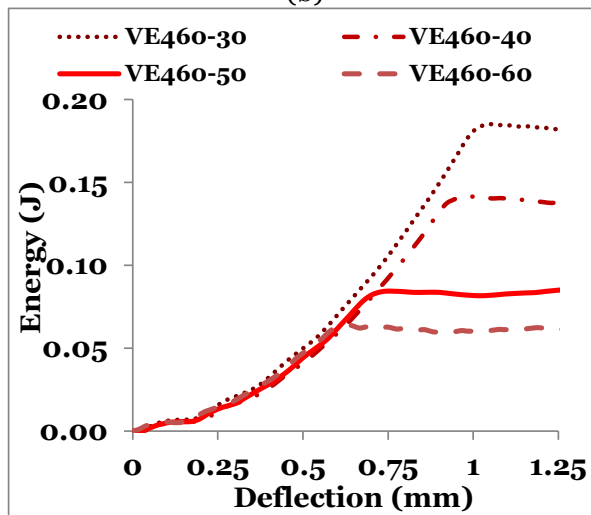
Figure 39. Experimentally measured (a) impact strength and (b) impact strength with respect to syntactic foam density for the various syntactic foams tested.



(a)



(b)



(c)

Figure 40. Energy-deflection plots of for various types of syntactic foams containing microballoons of (a) 220, (b) 320 and (c) 460 kg/m³ density, in $\Phi_{mb} = 0.3-0.6$.

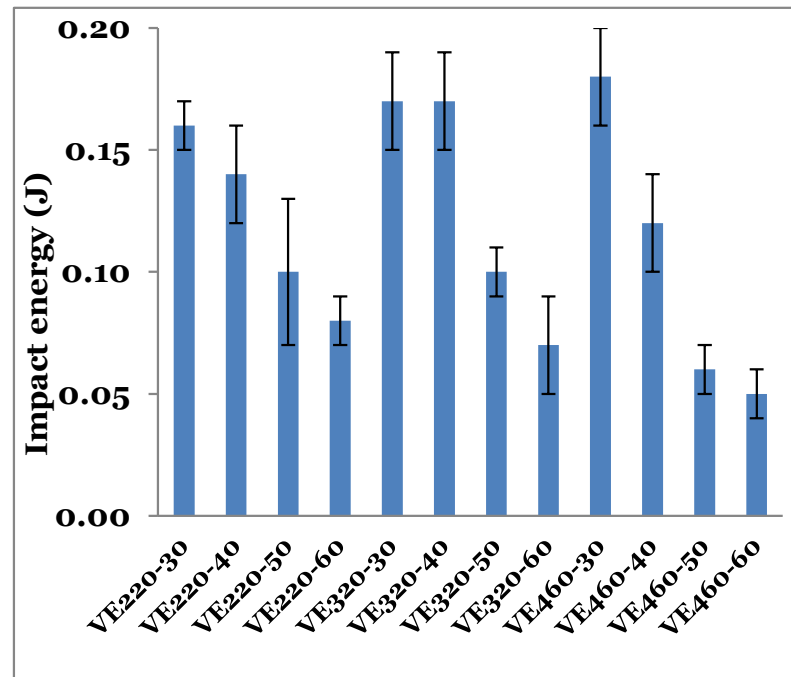


Figure 41. Impact energy for various syntactic foams tested.

6.3 Discussion

The impact testing resulted in complete failure of all syntactic foam specimens. The syntactic foams showed a single crack that initiated from the tensile side of the specimen and propagated to the compression side. Some of the representative fracture specimens are shown in Figure 42. In each specimen, consistently a kink is observed near the compression edge of the specimen, which provides evidence of change in the crack propagation direction. Finite element analysis (FEA) is used to understand the mechanism that results in this kind of crack pattern.

A static two-dimensional structural analysis was performed using Ansys Workbench 14.0 (ANSYS, Inc., Canonsburg, PA). Actual specimen dimensions are used in simulations. The specimen was modeled as a 2D surface of length 6.3 cm and width 1.27 cm. The fixed loading conditions were applied on the specimen such that 3.5 cm of the specimen was unconstrained. The loading and the boundary conditions are shown in Figure 43a and the meshing was performed using one level of refinement. Previous studies have shown that the compressive and tensile moduli for syntactic foams are different [47]. Therefore, the compressive and the tensile moduli values were taken as 2.8 GPa and 3.0 GPa, respectively, in the simulation. The material properties were

assigned through the uniaxial test data scheme under hyper-elastic response function. If the tensile and compressive moduli of the material are the same, then the neutral axis of the specimen under bending resides at the midplane of the specimen. However, a difference in the modulus values causes the neutral axis to shift, which will affect the results. Figure 43b shows the stress profile obtained under the applied load and the boundary condition for elastic analysis. Based on the stress profile, it can be expected that the crack that originates from the tensile side and propagates towards the compression side and encounters a compression zone of high stress near the compression edge of the specimen. The crack is deflected around this region of high compressive stress and results in the crack profile that is observed experimentally.

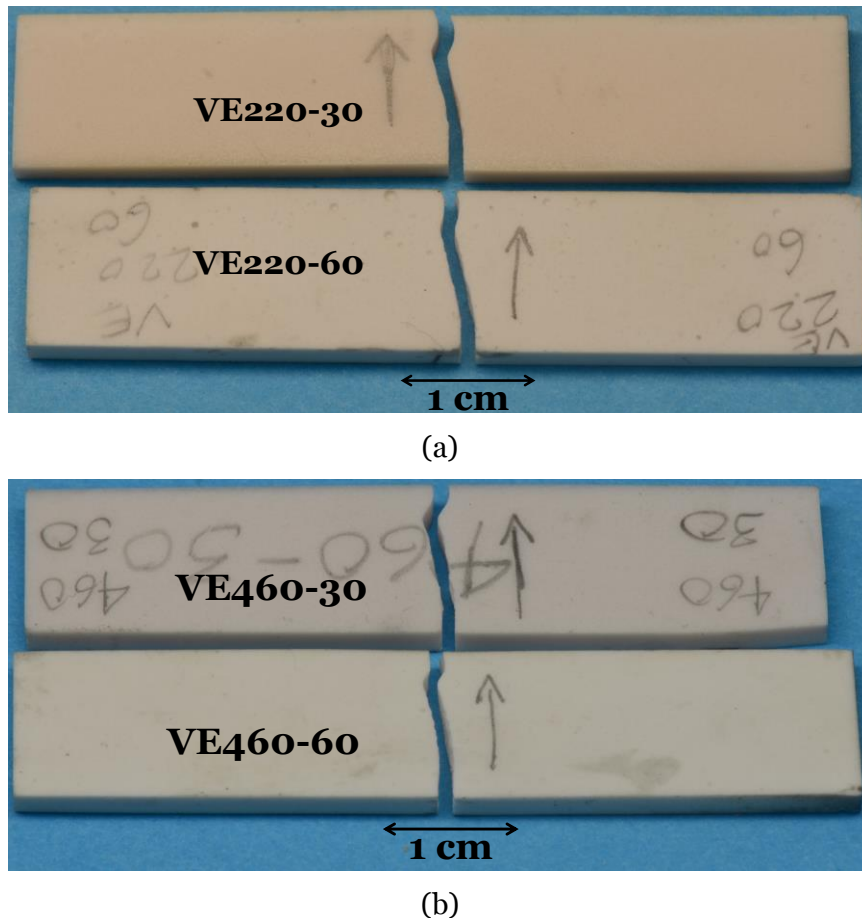
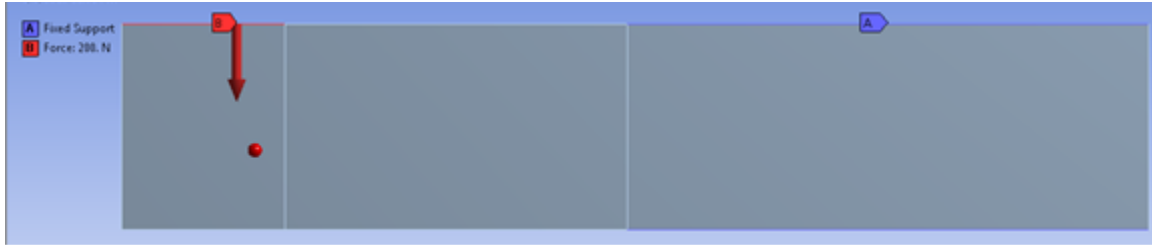
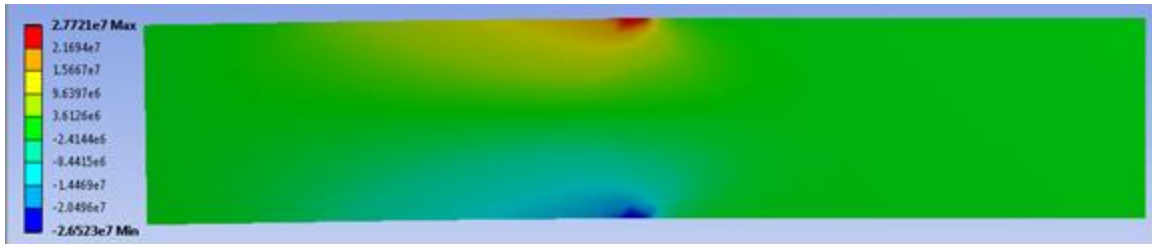


Figure 42. Macroscopic failure features of representative specimens of (a) VE220-30 and VE220-60 and (b) VE460-30 and VE460-60 syntactic foams tested under unnotched Izod impact test. The arrows indicate the direction of crack propagation.



(a)



(b)

Figure 43. (a) The model setup used in the simulation showing the loading and the boundary condition and (b) the normal stress distribution. The stress values shown in (b) are in Pa.

Figure 44 shows the failure mechanisms in syntactic foams that lead to energy absorption. The total energy absorption depends on the relative extents of these mechanisms. For example, for syntactic foams containing low volume fraction of HGMs, the energy absorbed in matrix cracking will dominate, whereas in syntactic foams containing high HGM volume fraction the particle-matrix debonding and particle crushing may absorb significant amount of energy. A combination of absorbed energy values (Figure 41) and failure microstructure can provide information on the role of these mechanisms in various syntactic foam compositions.

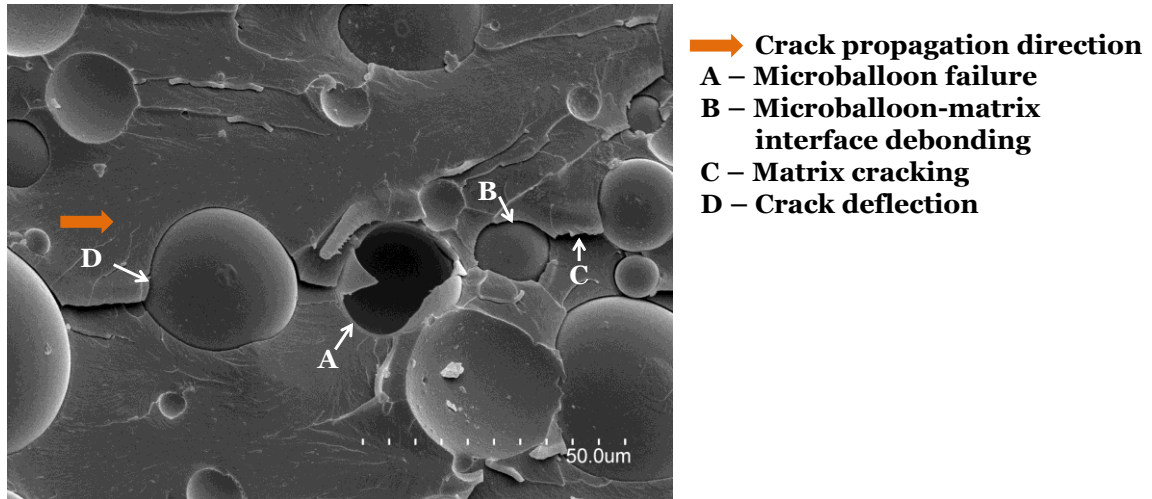


Figure 44. Failure mechanisms observed in syntactic foams under impact loading conditions.

Figure 41 shows that the absorbed energy decreases with increase in Φ_{mb} . The HGM-matrix interface does not seem to be very strong in the micrograph of the failed specimen. In such case, a higher volume fraction of the matrix in the syntactic foam specimens leads to a higher impact failure energy. Although a higher Φ_{mb} may lead to greater instances of crack deflection and increased matrix fracture surface area, the reduced amount of matrix material still leads to lower absorbed energy.

The SEM images of VE220-30, VE220-60, VE460-30 and VE460-60 specimens are shown in Figure 45-Figure 48, respectively. The arrows in the picture of these figures indicate the direction of the crack propagation and the SEM images are obtained on the initial and the final ends of the fracture surface. The failure of the specimens takes place by the crack propagating from the tensile (impacted) side towards the compressive side. All these specimens show similar failure features on tensile and compression sides. It is observed in previous studies on both vinyl ester and epoxy matrix syntactic foams that the tensile failure shows matrix cracking without significant HGM crushing, while the compressive failure is dominated by HGM crushing. In the present case, none of the micrographs show HGM crushing as the main failure feature.

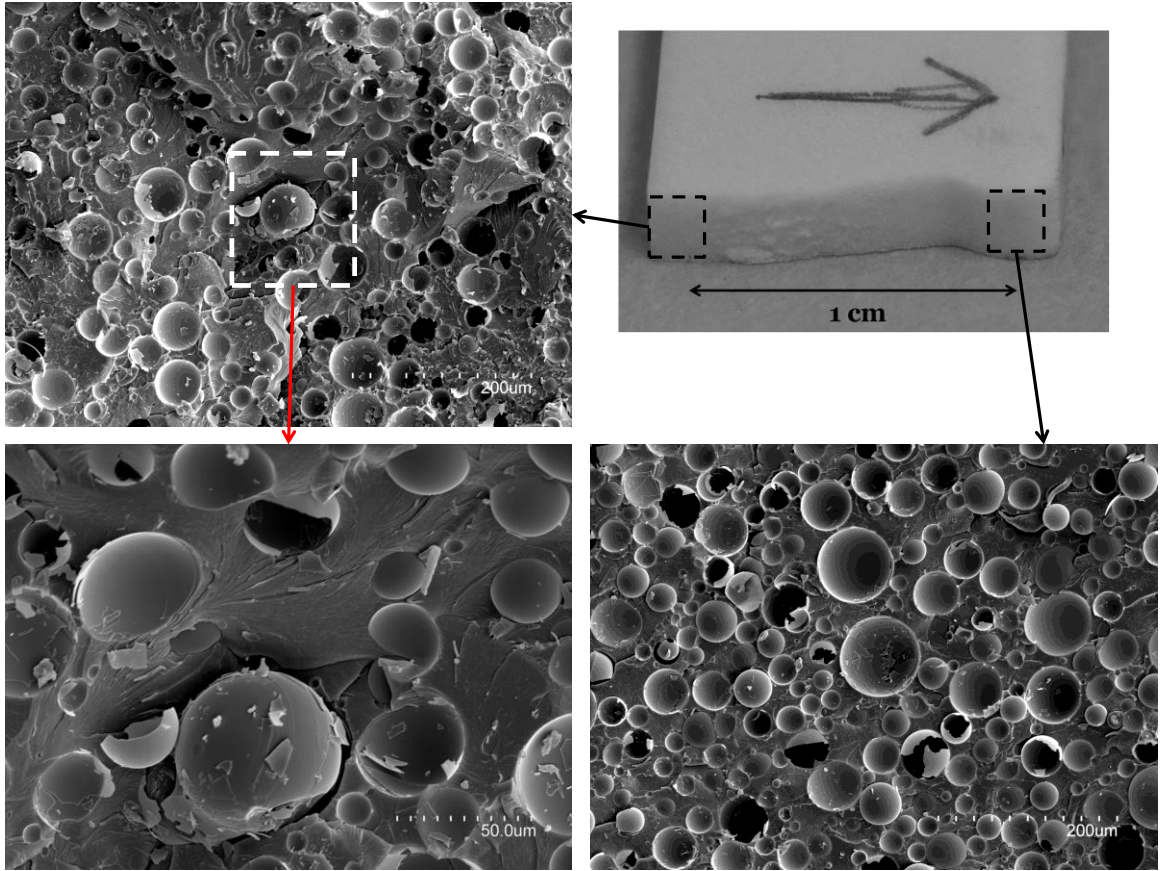


Figure 45. Fractured surface on impact tested VE220-30 syntactic foam. The arrow in the top right image represents the direction of the crack propagation.

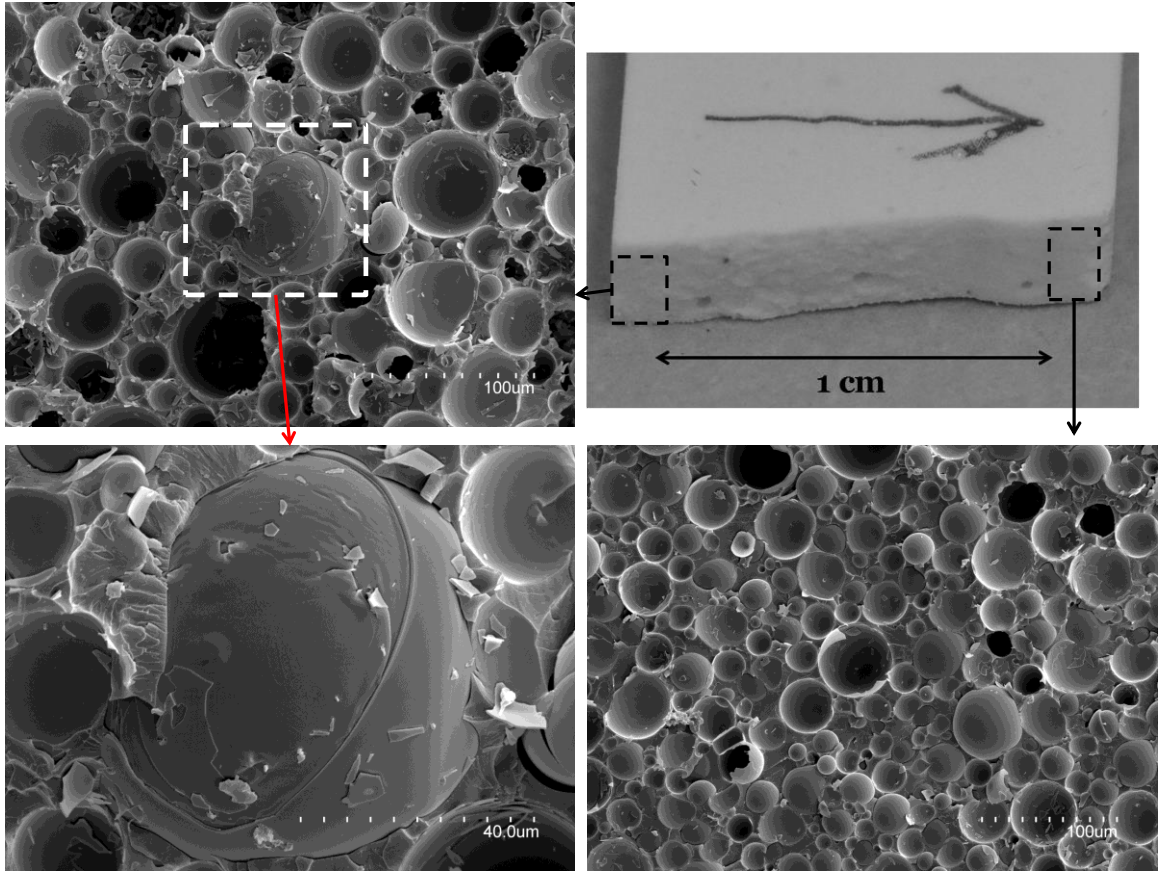


Figure 46. SEM images of the fractured surface on impact tested VE220-60 type syntactic foam.

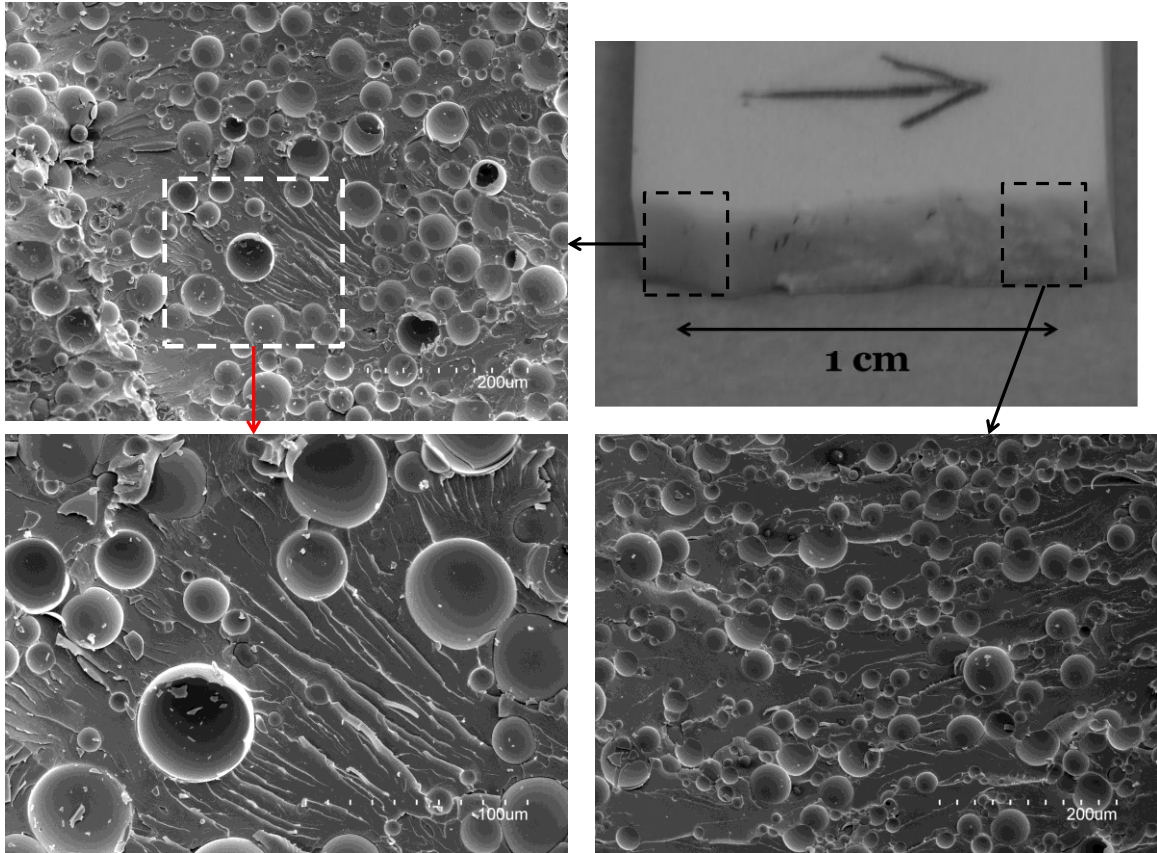


Figure 47. SEM images of the fractured surface on impact tested VE460-30 type syntactic foam.

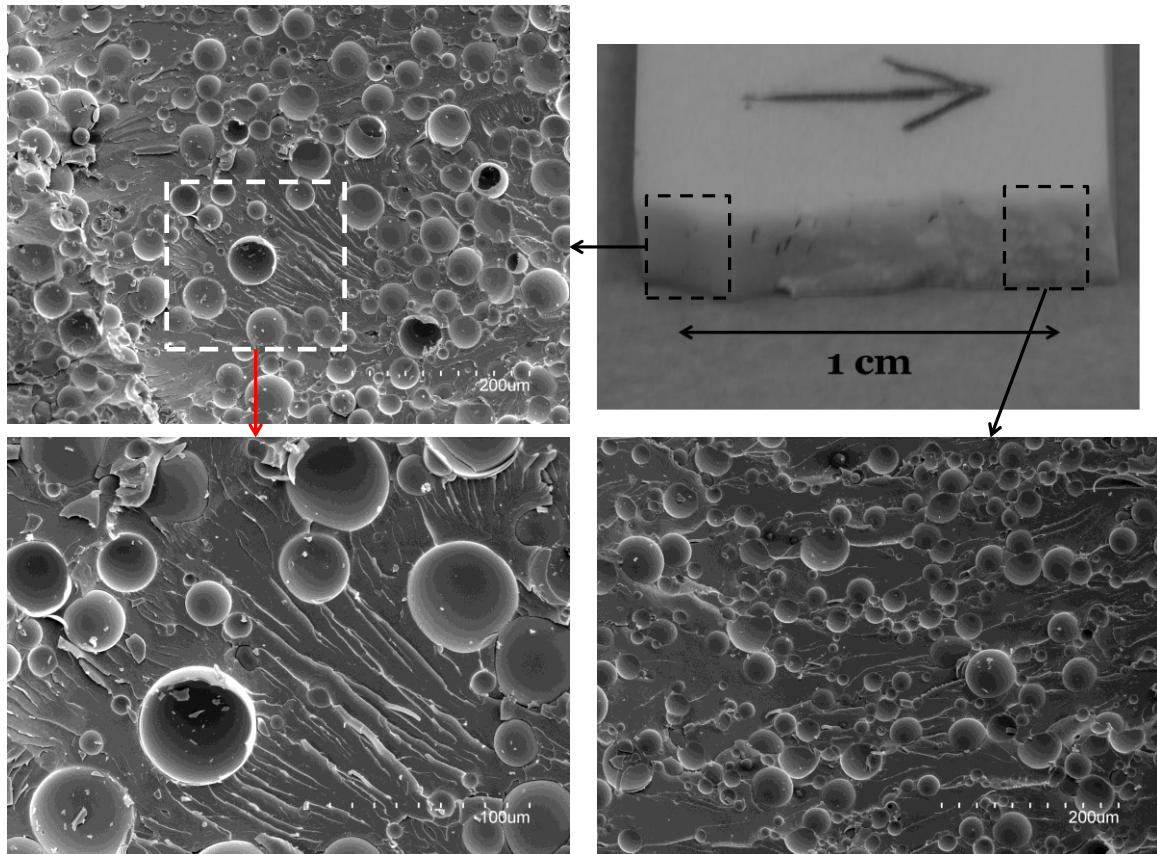


Figure 48. SEM images of the fractured surface on impact tested VE460-60 type syntactic foam.

The high speed camera images of the specimens failing during the impact testing is shown in Figure 49 and Figure 50 for the neat resin, VE220-30, VE220-60 and VE460-30 and VE460-60 syntactic foams, respectively. All the high speed images are obtained at a constant rate of 5375 frames/sec. It can be observed that the total time taken for the failure of the syntactic foams specimens is lower in comparison to the neat resin because of lower energy absorption. Also, as the HGM volume fraction increases to 0.6, the time taken for failure of the specimen decreases, which is corroborated with the lower impact energy, absorbed for the 0.6 volume fraction specimens.

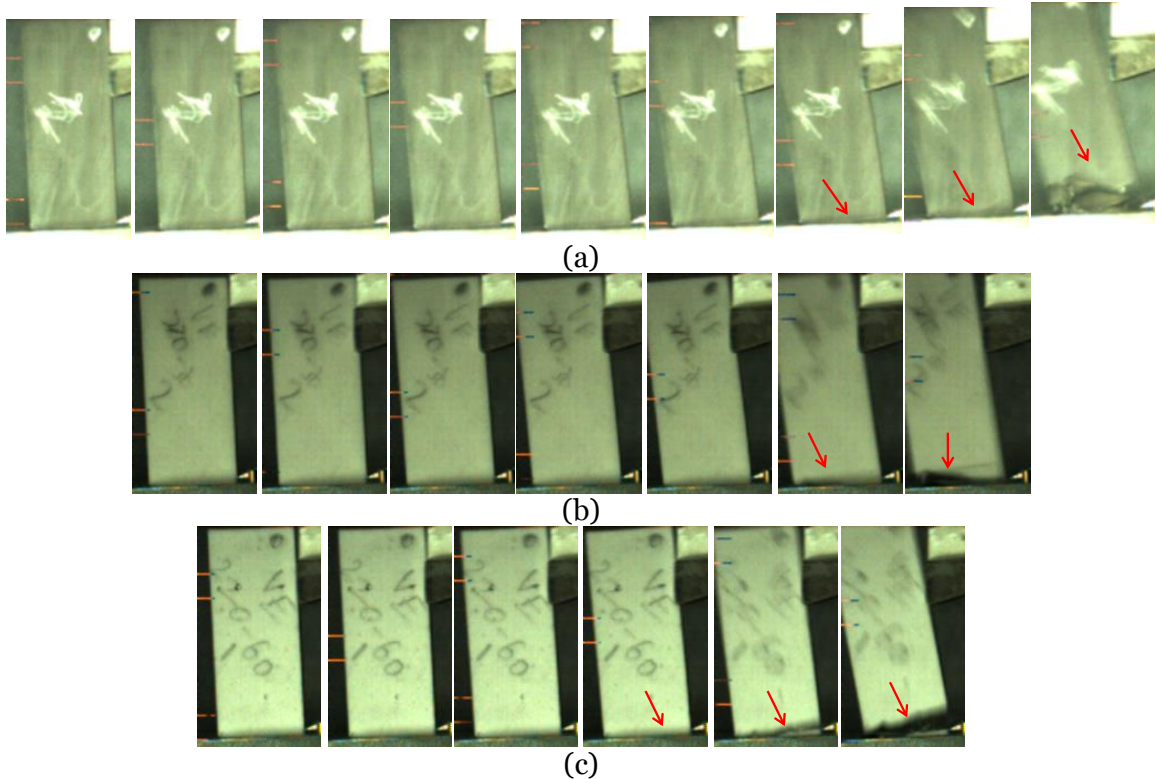


Figure 49. High speed images for (a) neat vinyl ester, and (b) VE220-30 and (c) VE220-60 syntactic foams. The time gap between two successive images in the sequence is 186 μ s. The arrows in the images indicate the crack propagating through the specimen.

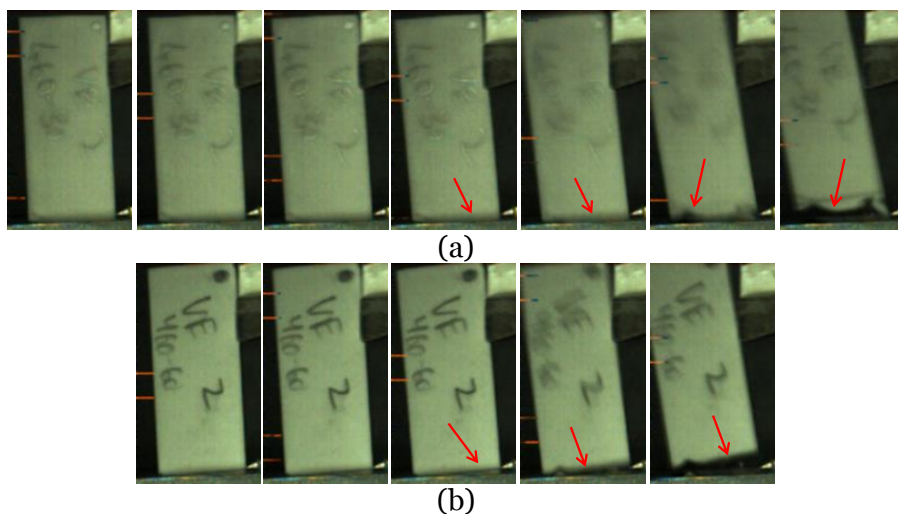


Figure 50. High speed images for (a) VE460-30 and (b) VE460-60 syntactic foams. The time gap between two successive images in the sequence is 186 μ s. The arrows in the images indicate the crack propagating through the specimen.

CHAPTER 7. Multifunctionality in syntactic foams

7.1 Multifunctionality modeling

The tailorability of syntactic foam properties with respect to the microballoon wall thickness and the volume fraction has been shown. To utilize syntactic foams in weight saving applications, the multifunctionality in syntactic foams need to be understood.

In this chapter the multifunctionality of syntactic foams is explained by utilizing the models developed in the current study for the electrical and the thermal properties and combining them with the modulus and density for the same compositions. As the illustrative example, syntactic foam compositions are found that have a particular dielectric constant, which is randomly chosen for this example. In the next step, the range of CTE, modulus, and density are calculated for those compositions to understand the possible variation in these properties for the same dielectric constant. Such scheme can allow selection of material parameters to tailor more than one property at the same time.

Figure 51 shows the variation of both the CTE and the dielectric constant with respect to the microballoon volume fraction and the density. The variation of syntactic foam density is also plotted in the figure to show the weight saving potential. To tailor a syntactic foam of dielectric constant of $\epsilon=3$, it can be shown that apart from the choosing not only based on the foam density, the models for CTE [65] and elastic modulus [57] can also be utilized and from a wide choice of the values the best possible syntactic foam combination can be selected. Figure 52 show the selection of elastic modulus and CTE values available to be chosen for a constant dielectric constant of $\epsilon=3$. Table 16 summarizes the density, modulus and CTE values available for the constant dielectric constant of 3.

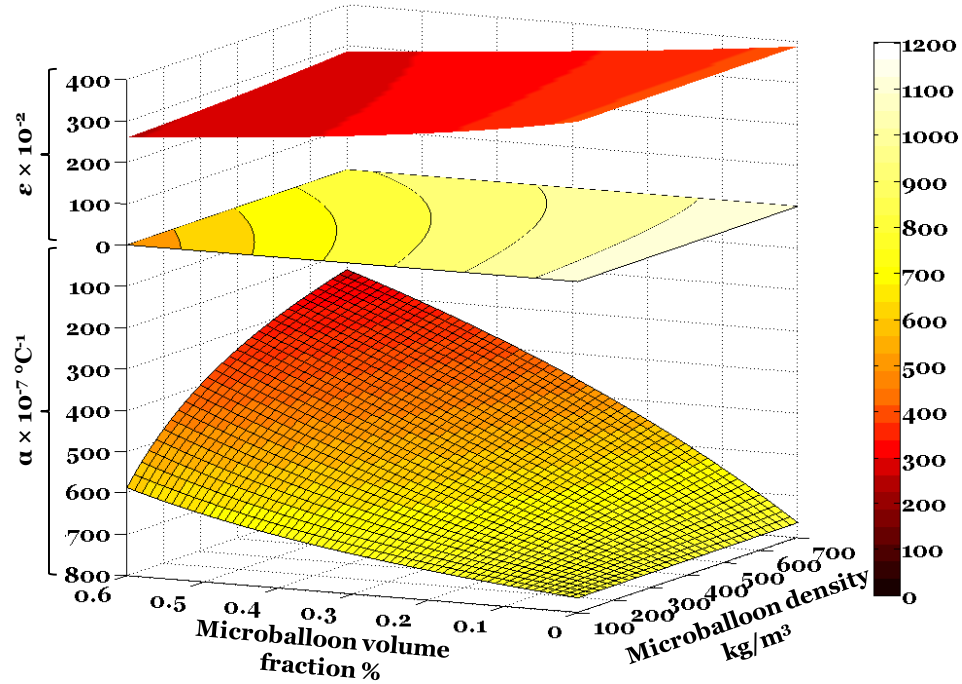


Figure 51. The variation of the dielectric constant and the coefficient of thermal expansion of syntactic foams is plotted as a 3D-contour plot, while the syntactic foams density is plotted as a 2D-contour plot. The scale represents the CTE, dielectric constant and the syntactic foam density in their corresponding units.

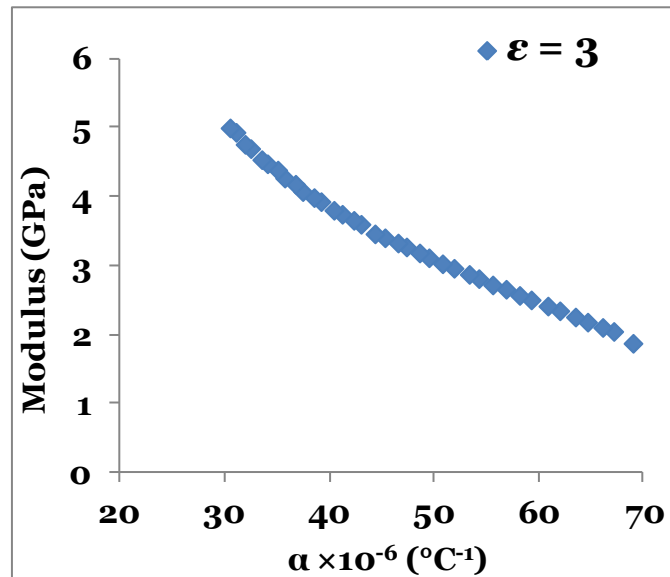


Figure 52. Selection of the elastic modulus and the CTE available in syntactic foams, for a constant dielectric value of $\epsilon=3$.

Table 16. Density, coefficient of thermal expansion and modulus of syntactic foams having a constant dielectric constant value of 3.

Φ_{mb} (%)	η	ρ_{mb} (kg/m ³)	ρ_c (kg/m ³)	E_c (GPa)	α (10 ⁻⁶ / °C)
34	0.987	100	800	1.9	69.2
36	0.973	200	814	2.4	62.1
38	0.959	300	833	2.8	55.2
41	0.944	400	848	3.3	48.2
44	0.929	500	870	3.7	41.6
47	0.914	600	897	4.3	35.8
51	0.898	700	925	5.1	29.9

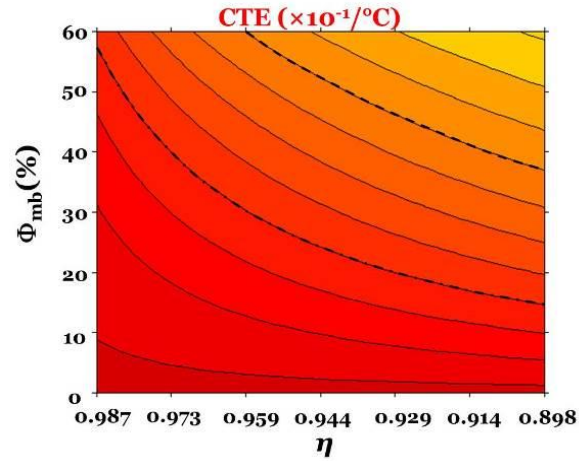
It can be observed in Table 16 that the choice of parameters to get the same dielectric constant of 3 is very wide. HGMs of 100-700 kg/m³ can be selected in appropriate volume fraction to obtain syntactic foams of this dielectric constant. The elastic modulus for such compositions can range from 1.9-5.1 GPa. Similar large variation is also observed in CTE values. Such opportunities of tailoring the properties exist in syntactic foams due to independent variation in two parameters, which are HGM wall thickness and volume fraction. Traditional solid reinforcement filled composites do not provide such flexibility of approach.

In addition to the above illustration, as a next step, syntactic foam combinations containing a constant CTE value is explored. The variation in the CTE for HGM filled vinyl ester matrix syntactic foam system is calculated in Figure 53a using the modified Turner's model developed in the study. This figure is developed utilizing the material parameters of hollow glass microballoon vinyl ester matrix syntactic foam. The HGM density is varied between 100-700 kg/m³ through change in the wall thickness for the same outer radius of particles and the HGM volume fraction (Φ_{mb}) is varied between 0 to 60% for the theoretical calculation.

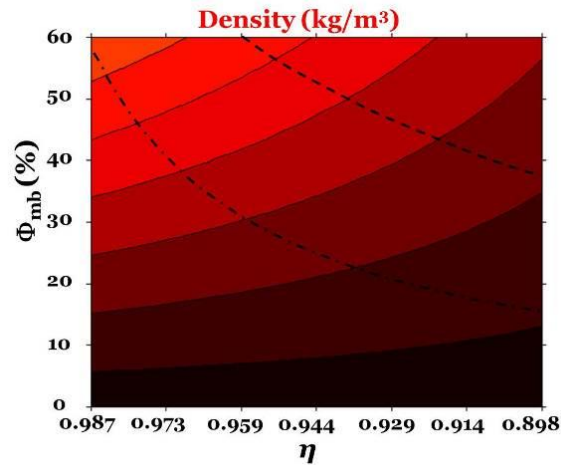
The dashed line marked in Figure 53a indicates all the compositions of syntactic foams that have the same CTE of 40×10⁻⁶/°C. Similarly, as another case, the dashed-dotted line marks the compositions that have the same CTE of 60 ×10⁻⁶/°C A theoretical

model developed by Porfiri and Gupta [57] is used to obtain the syntactic foam modulus for the same range of HGM volume fraction and wall thickness and is shown in Figure 53c. Further, the density map of the syntactic foams having the same range of HGM volume fraction and wall thickness is developed using rule of mixtures and is plotted in Figure 53b. Since the variation of the CTE, modulus and the density 2D-maps are based on the same range of η and Φ_{mb} , These 2D plots can be superimposed on each other to find the range of modulus and densities for the same values of CTE and the corresponding η and Φ_{mb} can be determined. Table 17 and Table 18 provide the compositions, densities, and modulus of syntactic foams corresponding to the CTE values of 40 and $60 \times 10^{-6}/^{\circ}\text{C}$, respectively.

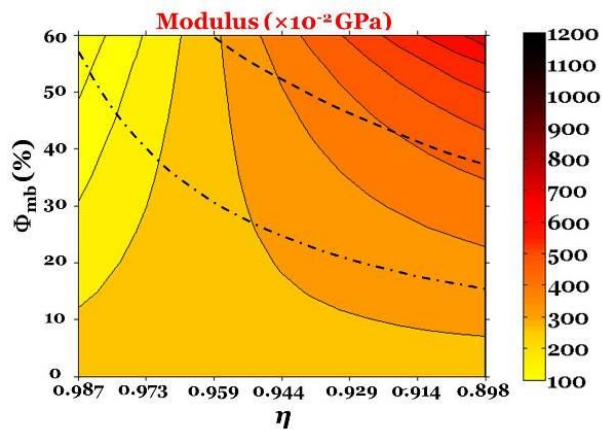
Table 18, where the density ranges between $556 - 1091 \text{ kg/m}^3$ and the modulus ranges between $1.226 - 3.231 \text{ GPa}$ by tailoring the combination of η and Φ_{mb} . Depending on the requirements of an application, either syntactic foams of lowest density or desired modulus can be selected from this available composition range. This possibility of obtaining multifunctionality in the syntactic foam properties provides greater flexibility than solid reinforcement filled composites.



(a)



(b)



(c)

Figure 53. Variation of the (a) CTE ($\mu\text{m}/\text{m}/^\circ\text{C}$), (b) density (kg/m^3) and (c) modulus (GPa) of syntactic foams with respect to the HGM density and Φ_{mb} . The scale in (c) is the cumulative representation of the CTE, density and modulus in their corresponding units. The dashed and dash-dotted lines represent CTE values of 40 and 60 ($\mu\text{m}/\text{m}/^\circ\text{C}$), respectively.

Table 17. Density and modulus of syntactic foams having a constant CTE value of 40 ($\mu\text{m}/\text{m}/^\circ\text{C}$).

Φ_{mb} (%)	η	ρ_{mb} (kg/m^3)	ρ_c (kg/m^3)	E_c (GPa)
60	0.959	300	644	2.8
53	0.944	400	757	3.5
47	0.929	500	850	3.9
41	0.914	600	930	4.0
37	0.898	700	990	4.1

Table 18. Density and modulus of syntactic foams having a constant CTE value of 60 ($\mu\text{m}/\text{m}/^\circ\text{C}$).

Φ_{mb} (%)	η	ρ_{mb} (kg/m^3)	ρ_c (kg/m^3)	E_c (GPa)
57	0.987	100	556	1.2
40	0.973	200	776	2.3
30	0.959	300	902	2.8
24	0.944	400	978	3.0
20	0.929	500	1028	3.1
17	0.914	600	1065	3.2
15	0.898	700	1091	3.2

CHAPTER 8. Conclusions

The conclusions drawn from the thermal, mechanical and electrical characterization of syntactic foams are summarized in this section. These results are helpful in understanding the multi-functional modality of syntactic foam composite materials to be used in marine, electronics and aerospace applications.

8.1 Thermal study

- The CTE of the syntactic foams is studied with respect to the hollow microballoon wall thickness and volume fraction.
- The Kerner and the Turner models are modified to account for the wall thickness parameter of the microballoon and the predicted results are within $\pm 18\%$ and $\pm 15\%$, respectively.
- The microballoon volume fraction is found to more profound effect in controlling the CTE.
- Parametric studies performed using the modified Turner's model shows that a wide range of selection available for the microballoon wall thickness and the volume fraction, to obtain syntactic foams with the same CTE. This demonstrates the tailorability of the thermal properties of syntactic foams.

8.2 Dynamic mechanical study

- The effect of temperature and the combined effects of temperature and the loading frequency on the dynamic mechanical properties of syntactic foams have been studied.
- At sub-zero and room temperatures, increase in microballoon wall thickness at the same level of volume fraction results in increase in storage modulus for all types of microballoons.
- In the flow region after T_g , the storage modulus is for the neat resin is 76–96 % lower than any syntactic foam. In this region, the storage modulus increases with the microballoon wall thickness.

- Presence of glass microballoons helps in increasing the retention of mechanical properties of syntactic foams at temperatures beyond T_g .
- Time temperature superposition (TTS) is used to develop master curves over a wide temperature and frequency ranges from the tests conducted in the frequency range 1–100 Hz.

8.3 Electrical study

- The dielectric constant is found to
 - decrease with increase in the volume fraction of the microballoons and
 - increase with increase in the wall thickness of the microballoons.
- A linear relation is found between the dielectric constant and density of the syntactic foams at all testing frequencies.
- An equivalent sphere approach is used to obtain the dielectric constant of the hollow glass microballoons. This closed form expression is used in coherence with the Maxwell-Garnett and the Jayasundere-Smith (J-S) models to obtain predictions of the dielectric constant of the syntactic foams.
- The J-S model is used to perform a parametric study to understand the relations between syntactic foam dielectric constant with microballoon volume fraction and wall thickness.

8.4 Impact study

- The HGM volume fraction is seen to have a more pronounced effect on the peak load than the HGM wall thickness.
- The impact energy decreased as the HGM volume fraction increases. As the volume fraction increased from 0.3 to 0.6 the impact energy decreases by 50%, 58.8% and 72.2% for VE220, VE320 and VE460 type syntactic foams respectively.
- Brittle mode of failure was observed in the resin and the syntactic foam specimens. SEM evaluation of the fractured surface showed crack branching and matrix failure without evidence of extensive HGM crushing. This kind of failure is typical of tensile failure of syntactic foams. Finite element analysis showed that

the possible crack deflection around the compression zone can lead to the type of failure that is observed in these specimens.

8.5 Development of multifunctional syntactic foams

The approach of tailoring the syntactic foams based on the wall thickness and the volume fraction of the microballoons has been shown in the present study for thermal and electrical properties. This approach is extended in the present work to obtain multifunctionality in the syntactic foams by simultaneous tailoring dielectric constant, CTE, elastic modulus and density. This concept of multifunctionality can help in selecting material properties that aid in weight saving in engineering structural applications, while enhancing the performance.

CHAPTER 9. Recommendations for future work

Syntactic foams are characterized for mechanical, electrical and thermal properties in the present study. Utilizing the composites in marine and aerospace applications requires understanding the long term behavior of these materials. The following are some of the suggestions for possible future studies on these materials.

9.1 Fatigue testing

The fatigue behavior of the composite under compression and tension needs to be studied. The effect of the volume fraction and the wall thickness parameter on the fatigue behavior helps in designing the syntactic foams for cyclic loading patterns encountered in energy absorbing structures and vibration dampers.

9.2 Environmental study

Syntactic foams find application in marine field in the form of buoyancy aids and floatation aids. These structures are subjected to sea water and ultraviolet light throughout their lifespan. Studying the properties of syntactic foams subjected to environmental effects helps in maintain the structures over their life-term usage.

9.3 High strain rate tensile behavior

Syntactic foams can be utilized in armors as energy absorbing members, which are subjected to high strain rate loading conditions. The high strain rate testing under compression testing helped in understanding the strain rate sensitivity and the failure mechanisms with increasing strain rates. Similar study can be performed for tensile behavior, which can help in designing these composites for armors applications.

9.4 Shock testing

Syntactic foams can find applications in blast mitigation structures in marine and armor applications. These applications need the material to be subjected to shock waves.

Understanding the shock behavior based on the volume fraction and the wall thickness of the filler helps in designing the composites for these applications.

These are some of the possibilities that can be explored to understand the properties of syntactic foams under additional loading conditions. The understanding derived through these additional studies can help in developing syntactic foams tailored for a given application and ensuring the safety and high performance.

REFERENCES

1. Kaw, A.K., 2006. *Mechanics of composite materials*. Boca Raton, Fl: CRC Press. pp.
2. Fu, S.-Y., X.-Q. Feng, B. Lauke, and Y.-W. Mai, "Effects of particle size, particle/matrix interface adhesion and particle loading on mechanical properties of particulate-polymer composites," *Composites Part B: Engineering*, 2008. 39(6): 933-961.
3. Alexandre, M. and P. Dubois, "Polymer-layered silicate nanocomposites: preparation, properties and uses of a new class of materials," *Materials Science and Engineering: R: Reports*, 2000. 28(1-2): 1-63.
4. Coleman, J.N., U. Khan, W.J. Blau, and Y.K. Gun'ko, "Small but strong: A review of the mechanical properties of carbon nanotube-polymer composites," *Carbon*, 2006. 44(9): 1624-1652.
5. Ku, H., H. Wang, N. Pattarachaiyakoop, and M. Trada, "A review on the tensile properties of natural fiber reinforced polymer composites," *Composites Part B: Engineering*, 2011. 42(4): 856-873.
6. Hodge, A.J., R.K. Kaul, and W.M. McMahon. May 21-25, 2000. "Sandwich composite, syntactic foam core based application for space structures." in Proceedings of the 45th International SAMPE Symposium, . May 21-25, 2000 of Conference.
7. Gupta, N. and V.C. Shunmugasamy, "High strain rate compressive response of syntactic foams: Trends in mechanical properties and failure mechanisms," *Materials Science and Engineering: A*, 2011. 528(25-26): 7596-7605.
8. Rutz, B.H. and J.C. Berg, "A review of the feasibility of lightening structural polymeric composites with voids without compromising mechanical properties," *Advances in Colloid and Interface Science*, 2010. 160(1-2): 56-75.
9. Montminy, M.D., A.R. Tannenbaum, and C.W. Macosko, "The 3D structure of real polymer foams," *Journal of Colloid and Interface Science*, 2004. 280(1): 202-211.
10. Jang, W.-Y., A.M. Kraynik, and S. Kyriakides, "On the microstructure of open-cell foams and its effect on elastic properties," *International Journal of Solids and Structures*, 2008. 45(7-8): 1845-1875.
11. Shutov, F.A., 1991. *Syntactic polymeric foams*. Handbook of polymeric foams and foam technology, ed. D. Klemperer and K.C. Frisch. New York Hanser Publishers. pp.

12. Rohatgi, P.K., N. Gupta, B.F. Schultz, and D.D. Luong, "The synthesis, compressive properties and applications of metal matrix syntactic foams," *Journal of Minerals, Metals and Materials Society*, 2011. 63(2): 36-42.
13. John, B. and C.P.R. Nair, 2010. *Update on syntactic foams*. Shropshire, UK: iSmithers Rapra. pp.
14. Vo, H.T. and F.G. Shi, "Towards model-based engineering of optoelectronic packaging materials: dielectric constant modeling," *Microelectronics Journal*, 2002. 33(5-6): 409-415.
15. Gupta, N., E. Woldesenbet, and P. Mensah, "Compression properties of syntactic foams: effect of cenosphere radius ratio and specimen aspect ratio," *Composites Part A: Applied Science and Manufacturing*, 2004. 35(1): 103-111.
16. Gupta, N. and E. Woldesenbet, "Microballoon wall thickness effects on properties of syntactic foams," *Journal of Cellular Plastics*, 2004. 40(6): 461-480.
17. Devi, K.A., B. John, C.P.R. Nair, and K.N. Ninan, "Syntactic foam composites of epoxy-allyl phenol-bismaleimide ternary blend - Processing and properties," *Journal of Applied Polymer Science*, 2007. 105(6): 3715-3722.
18. Wang, W.-T. and L. Watkins. 2002. "Syntactic foam thermal insulation for ultradeep high temperature applications." in The 21nd International Conference on Offshore Mechanics And Arctic Engineering. 2002 of Conference.
19. Park, S.-J., F.-L. Jin, and C. Lee, "Preparation and physical properties of hollow glass microspheres-reinforced epoxy matrix resins," *Materials Science and Engineering: A*, 2005. 402(1-2): 335-340.
20. Lin, T., N. Gupta, and A. Talalayev, "Thermoanalytical characterization of epoxy matrix-glass microballoon syntactic foams," *Journal of Materials Science*, 2009. 44(6): 1520-1527.
21. Shabde, V., K. Hoo, and G.M. Gladysz, "Experimental determination of the thermal conductivity of three-phase syntactic foams," *Journal of Materials Science*, 2006. 41(13): 4061-4073.
22. Porfiri, M., N. Nguyen, and N. Gupta, "Thermal conductivity of multiphase particulate composite materials," *Journal of Materials Science*, 2009. 44(6): 1540-1550.
23. Zweben, C., "Advances in composite materials for thermal management in electronic packaging," *JOM Journal of the Minerals, Metals and Materials Society*, 1998. 50(6): 47-51.

24. Lerch, B.A. and R.M. Sullivan. 2006. "Thermal expansion of polyurethane foam." in 43rd Annual Technical Meeting of the Society of Engineering Science. 2006 of Conference.
25. Deng, D.Q. and L. Xu, "Measurements of thermal expansion coefficient of phenolic foam at low temperatures," *Cryogenics*, 2003. 43(8): 465-468.
26. Yang, C.G., L. Xu, and N. Chen, "Thermal expansion of polyurethane foam at low temperature," *Energy Conversion and Management*, 2007. 48(2): 481-485.
27. Li, G. and D. Nettles, "Thermomechanical characterization of a shape memory polymer based self-repairing syntactic foam," *Polymer*, 2010. 51(3): 755-762.
28. Wouterson, E.M., F.Y.C. Boey, X. Hu, and S.-C. Wong, "Effect of fiber reinforcement on the tensile, fracture and thermal properties of syntactic foam," *Polymer*, 2007. 48(11): 3183-3191.
29. Rohatgi, P.K., N. Gupta, and S. Alaraj, "Thermal expansion of aluminum–fly ash cenosphere composites synthesized by pressure infiltration technique," *Journal of Composite Materials*, 2006. 40(13): 1163-1174.
30. Zhang, Q., G. Chen, G. Wu, Z. Xiu, and B. Luan, "Property characteristics of a AlNp/Al composite fabricated by squeeze casting technology," *Materials Letters*, 2003. 57(8): 1453-1458.
31. Yusriah, L., M. Mariatti, and A. Abu Bakar, "The properties of vinyl ester composites reinforced with different types of woven fabric and hollow phenolic microspheres," *Journal of Reinforced Plastics and Composites*, 2010. 29(20): 3066-3073.
32. Wong, C.P. and R.S. Bollampally, "Thermal conductivity, elastic modulus, and coefficient of thermal expansion of polymer composites filled with ceramic particles for electronic packaging," *Journal of Applied Polymer Science*, 1999. 74(14): 3396-3403.
33. McGrath, L.M., R.S. Parnas, S.H. King, J.L. Schroeder, D.A. Fischer, and J.L. Lenhart, "Investigation of the thermal, mechanical, and fracture properties of alumina–epoxy composites," *Polymer*, 2008. 49(4): 999-1014.
34. Yung, K.C., B.L. Zhu, T.M. Yue, and C.S. Xie, "Preparation and properties of hollow glass microsphere-filled epoxy-matrix composites," *Composites Science and Technology*, 2009. 69(2): 260-264.
35. Budiansky, B., "Thermal and thermoelastic properties of isotropic composites," *Journal of Composite Materials*, 1970. 4(3): 286-295.

36. Kerner, E.H., "The elastic and thermo-elastic properties of composite media " *Proceedings of the Physical Society. Section B*, 1956. 69(8): 808-813.
37. Tummala, R.R. and A.L. Friedberg, "Thermal expansion of composite materials," *Journal of Applied Physics*, 1970. 41(13): 5104-5107.
38. Turner, P.S., "Thermal-expansion stresses in reinforced plastics " *Journal of Research of the National Bureau of Standards*, 1946. 37(4): 239.
39. Vaidya, R.U. and K.K. Chawla, "Thermal expansion of metal-matrix composites," *Composites Science and Technology*, 1994. 50(1): 13-22.
40. Schapery, R.A., "Thermal expansion coefficients of composite materials based on energy principles," *Journal of Composite Materials*, 1968. 2(3): 380-404.
41. Lee, K.Y., K.H. Kim, S.K. Jeoung, S.I. Ju, J.H. Shim, N.H. Kim, S.G. Lee, S.M. Lee, J.K. Lee, and D.R. Paul, "Thermal expansion behavior of composites based on axisymmetric ellipsoidal particles," *Polymer*, 2007. 48(14): 4174-4183.
42. Lee, K.-Y., S.R. Hong, S.K. Jeoung, N.H. Kim, S.G. Lee, and D.R. Paul, "Thermal expansion behavior of composites based on non-axisymmetric ellipsoidal particles," *Polymer*, 2008. 49(8): 2146-2152.
43. Gunes, I.S., F. Cao, and S.C. Jana, "Effect of thermal expansion on shape memory behavior of polyurethane and its nanocomposites," *Journal of Polymer Science Part B: Polymer Physics*, 2008. 46(14): 1437-1449.
44. Nielsen, L.E., "Mechanical properties of particulate-filled systems," *Journal of Composite Materials*, 1967. 1(1): 100-119.
45. Balch, D.K., T.J. Fitzgerald, V. Michaud, A. Mortensen, Y. Shen, and S. Suresh, "Thermal expansion of metals reinforced with ceramic particles and microcellular foams," *Metallurgical and Materials Transactions A*, 1996. 27 A(11): 3700-3717.
46. Uju, W.A. and I.N.A. Oguocha, "A study of thermal expansion of Al-Mg alloy composites containing fly ash," *Materials & Design*, 2012. 33(0): 503-509.
47. Gupta, N., R. Ye, and M. Porfiri, "Comparison of tensile and compressive characteristics of vinyl ester/glass microballoon syntactic foams," *Composites Part B: Engineering*, 2010. 41(3): 236-245.
48. Aureli, M., M. Porfiri, and N. Gupta, "Effect of polydispersivity and porosity on the elastic properties of hollow particle filled composites," *Mechanics of Materials*, 2010. 42(7): 726-739.

49. Shunmugasamy, V.C., N. Gupta, N.Q. Nguyen, and P.G. Coelho, "Strain rate dependence of damage evolution in syntactic foams," *Materials Science and Engineering: A*, 2010. 527(23): 6166-6177.
50. Sideridis, E., V.N. Kytopoulos, E. Kyriazi, and G. Bourkas, "Determination of thermal expansion coefficient of particulate composites by the use of a triphase model," *Composites Science and Technology*, 2005. 65(6): 909-919.
51. Nji, J. and G. Li, "A CaO enhanced rubberized syntactic foam," *Composites Part A: Applied Science and Manufacturing*, 2008. 39(9): 1404-1411.
52. Li, G., Y. Zhao, and S.-S. Pang, "Analytical modeling of particle size and cluster effects on particulate-filled composite," *Materials Science and Engineering: A*, 1999. 271(1-2): 43-52.
53. Li, G., Y. Zhao, and S.S. Pang, "A three-layer built-in analytical modeling of concrete," *Cement and Concrete Research*, 1998. 28(7): 1057-1070.
54. Tagliavia, G., M. Porfiri, and N. Gupta, "Analysis of hollow inclusion-matrix debonding in particulate composites," *International Journal of Solids and Structures*, 2010. 47(16): 2164-2177.
55. Poveda, R., N. Gupta, and M. Porfiri, "Poisson's ratio of hollow particle filled composites," *Materials Letters*, 2010. 64(21): 2360-2362.
56. Saha, M.C., S. Nilufar, M. Major, and S. Jeelani, "Processing and performance evaluation of hollow microspheres filled epoxy composites," *Polymer Composites*, 2008. 29(3): 293-301.
57. Porfiri, M. and N. Gupta, "Effect of volume fraction and wall thickness on the elastic properties of hollow particle filled composites," *Composites Part B: Engineering*, 2009. 40(2): 166-173.
58. Shabde, V., K. Hoo, and G. Gladysz, "Experimental determination of the thermal conductivity of three-phase syntactic foams," *Journal of Materials Science*, 2006. 41(13): 4061-4073.
59. Gladysz, G., B. Perry, G. McEachen, and J. Lula, "Three-phase syntactic foams: structure-property relationships," *Journal of Materials Science*, 2006. 41(13): 4085-4092.
60. Gupta, N., K. Kishore, E. Woldesenbet, and S. Sankaran, "Studies on compressive failure features in syntactic foam material," *Journal of Materials Science*, 2001. 36(18): 4485-4491.

61. Poveda, R., S. Achar, and N. Gupta, "Thermal Expansion of Carbon Nanofiber-Reinforced Multiscale Polymer Composites," *JOM Journal of the Minerals, Metals and Materials Society*, 2012. 64(10): 1148-1157.
62. Dimchev, M., R. Caeti, and N. Gupta, "Effect of carbon nanofibers on tensile and compressive characteristics of hollow particle filled composites," *Materials & Design*, 2010. 31(3): 1332-1337.
63. Grosjean, F., N. Bouchonneau, D. Choqueuse, and V. Sauvante-Moynot, "Comprehensive analyses of syntactic foam behaviour in deepwater environment," *Journal of Materials Science*, 2009. 44(6): 1462-1468.
64. Bouchonneau, N., V. Sauvante-Moynot, D. Choqueuse, F. Grosjean, E. Poncet, and D. Perreux, "Experimental testing and modelling of an industrial insulated pipeline for deep sea application," *Journal of Petroleum Science and Engineering*, 2010. 73(1-2): 1-12.
65. Shunmugasamy, V., D. Pinisetty, and N. Gupta, "Thermal expansion behavior of hollow glass particle/vinyl ester composites," *Journal of Materials Science*, 2012. 47(14): 5596-5604.
66. Yasmin, A. and I.M. Daniel, "Mechanical and thermal properties of graphite platelet/epoxy composites," *Polymer*, 2004. 45(24): 8211-8219.
67. Ferry, J.D., 1980. *Viscoelastic properties of polymers* New York: John Wiley & Sons. pp.
68. Menard, K.P., 1999. *Dynamic mechanical analysis a practical introduction*. Boca Raton, Florida: CRC Press. pp.
69. Gupta, N. and R. Nagorny, "On the tensile properties of glass microballoon-epoxy resin syntactic foam," *Journal of Applied Polymer Science*, 2006. 102(2): 1254-1261.
70. Rizzi, E., E. Papa, and A. Corigliano, "Mechanical behavior of a syntactic foam: experiments and modeling," *International Journal of Solids and Structures*, 2000. 37(40): 5773-5794.
71. Bardella, L. and F. Genna, "On the elastic behavior of syntactic foams," *International Journal of Solids and Structures*, 2001. 38(40-41): 7235-7260.
72. Capela, C., J.A.M. Ferreira, and J.D. Costa, "Viscoelastic properties of syntactic foams by dynamic mechanical analysis," *Materials Science Forum*, 2010. 636-637: 280-286.

73. Sankaran, S., K. Sekhar, G. Raju, and M. Kumar, "Characterization of epoxy syntactic foams by dynamic mechanical analysis," *Journal of Materials Science*, 2006. 41(13): 4041-4046.
74. Hu, G. and D. Yu, "Tensile, thermal and dynamic mechanical properties of hollow polymer particle-filled epoxy syntactic foam," *Materials Science and Engineering: A*, 2011. 528(15): 5177-5183.
75. Ferreira, J.A.M., C. Capela, and J.D. Costa, "Dynamic mechanical analysis of hybrid fibre/glass microspheres composites," *Strain*, 2011. 47(3): 275-280.
76. John, B., C.P.R. Nair, and K.N. Ninan, "Effect of nanoclay on the mechanical, dynamic mechanical and thermal properties of cyanate ester syntactic foams," *Materials Science and Engineering: A*, 2010. 527(21–22): 5435-5443.
77. Lefebvre, X., V. Sauvart-Moynot, D. Choqueuse, and P. Chauchot, "Durability of syntactic foams for deep offshore insulation: Modelling of water uptake under representative ageing conditions in order to predict the evolution of buoyancy and thermal conductivity," *Oil & Gas Science and Technology - Revue d'IFP Energies Nouvelles*, 2009. 64 (2): 165-178.
78. Tagliavia, G., M. Porfiri, and N. Gupta, "Vinyl ester—glass hollow particle composites: Dynamic mechanical properties at high inclusion volume fraction," *Journal of Composite Materials*, 2009. 43(5): 561-582.
79. Asif, A., V.L. Rao, and K.N. Ninan, "Nanoclay reinforced thermoplastic toughened epoxy hybrid syntactic foam: Surface morphology, mechanical and thermo mechanical properties," *Materials Science and Engineering: A*, 2010. 527(23): 6184-6192.
80. Guo, Z., T. Pereira, O. Choi, Y. Wang, and H.T. Hahn, "Surface functionalized alumina nanoparticle filled polymeric nanocomposites with enhanced mechanical properties," *Journal of Materials Chemistry*, 2006. 16(27): 2800-2808.
81. Guo, Z., S. Wei, B. Shedd, R. Scaffaro, T. Pereira, and H.T. Hahn, "Particle surface engineering effect on the mechanical, optical and photoluminescent properties of ZnO/vinyl-ester resin nanocomposites," *Journal of Materials Chemistry*, 2007. 17(8): 806-813.
82. Guo, Z., H.W. Ng, G.L. Yee, and H.T. Hahn, "Differential scanning calorimetry investigation on vinyl ester resin curing process for polymer nanocomposite fabrication " *Journal of Nanoscience and Nanotechnology*, 2009. 9(5): 3278–3285.

83. Ray, D., B.K. Sarkar, S. Das, and A.K. Rana, "Dynamic mechanical and thermal analysis of vinyl ester resin matrix composites reinforced with untreated and alkali-treated jute fibres," *Composites Science and Technology*, 2002. 62(7–8): 911-917.
84. Zhu, J., S. Wei, J. Ryu, M. Budhathoki, G. Liang, and Z. Guo, "In situ stabilized carbon nanofiber (CNF) reinforced epoxy nanocomposites," *Journal of Materials Chemistry*, 2010. 20(23): 4937-4948.
85. Dow Corning, 2004. *FSRs in extreme applications: Proof of the new paradigm*: A Dow Corning Publication, Midland, MI. pp. 1-16.
86. Huang, J.S. and L.J. Gibson, "Elastic moduli of a composite of hollow spheres in a matrix," *Journal of the Mechanics and Physics of Solids*, 1993. 41(1): 55-75.
87. Tagliavia, G., M. Porfiri, and N. Gupta, "Analysis of flexural properties of hollow-particle filled composites," *Composites Part B: Engineering*, 2010. 41(1): 86-93.
88. Karthikeyan, C.S., S. Sankaran, and Kishore, "Flexural behaviour of fibre-reinforced syntactic foams," *Macromolecular Materials and Engineering*, 2005. 290(1): 60-65.
89. Brennan, A.B., Y.Q. Wang, J.M. DeSimone, S. Stempel, and E.T. Samulski, "Thiophene-based poly(arylene ether ketone)s: 2. Thermal and mechanical properties of amorphous systems using bis(p-fluorobenzoyl)aryl monomers," *Polymer*, 1993. 34(4): 807-812.
90. Xia, Z., H.-J. Sue, A.J. Hsieh, and J.W.L. Huang, "Dynamic mechanical behavior of oriented semicrystalline polyethylene terephthalate," *Journal of Polymer Science Part B: Polymer Physics*, 2001. 39(12): 1394-1403.
91. Mahieux, C.A. and K.L. Reifsnider, "Property modeling across transition temperatures in polymers: a robust stiffness–temperature model," *Polymer*, 2001. 42(7): 3281-3291.
92. Mahieux, C.A. and K.L. Reifsnider, "Property modeling across transition temperatures in polymers: application to thermoplastic systems," *Journal of Materials Science*, 2002. 37(5): 911-920.
93. Mahieux, C.A. and K.L. Reifsnider, "Property modeling across transition temperatures in polymers: application to filled and unfilled Polybutadiene," *Journal of Elastomers and Plastics*, 2002. 34(1): 79-89.
94. Tagliavia, G., M. Porfiri, and N. Gupta, "Elastic interaction of interfacial spherical-cap cracks in hollow particle filled composites," *International Journal of Solids and Structures*, 2011. 48(7–8): 1141-1153.

95. Robertson, C.G., C.J. Lin, M. Rackaitis, and C.M. Roland, "Influence of particle size and polymer–filler coupling on viscoelastic glass transition of particle-reinforced polymers," *Macromolecules*, 2008. 41(7): 2727-2731.
96. Pothan, L.A., Z. Oommen, and S. Thomas, "Dynamic mechanical analysis of banana fiber reinforced polyester composites," *Composites Science and Technology*, 2003. 63(2): 283-293.
97. Williams, M.L., R.F. Landel, and J.D. Ferry, "The temperature dependence of relaxation mechanism in amorphous polymers and other glass-forming liquids," *Journal of the American Chemical Society*, 1955. 77: 3701–3707.
98. Bozorg-Haddad, A. and M. Iskander, "Comparison of accelerated compressive creep behavior of virgin HDPE using thermal and energy approaches," *Journal of Materials Engineering and Performance*, 2011. 20(7): 1219-1229.
99. Bozorg-Haddad, A. and M. Iskander, "Predicting compressive creep behavior of virgin HDPE using thermal acceleration," *Journal of Materials in Civil Engineering*, 2011. 23(8): 1154-1162.
100. Volksen, W., R.D. Miller, and G. Dubois, "Low dielectric constant materials," *Chemical Reviews*, 2010. 110(1): 56-110.
101. Zhao, X.-Y. and H.-J. Liu, "Review of polymer materials with low dielectric constant," *Polymer International*, 2010. 59(5): 597-606.
102. Gonon, P., A. Sylvestre, J. Teyseyre, and C. Prior, "Dielectric properties of epoxy/silica composites used for microelectronic packaging, and their dependence on post-curing," *J Mater Sci: Materials in Electronics*, 2001. 12(2): 81-86.
103. Miller, K.J., K.N. Collier, H.B. Soll-Morris, R. Swaminathan, and M.E. McHenry, "Induction heating of FeCo nanoparticles for rapid rf curing of epoxy composites," *Journal of Applied Physics*, 2009. 105: 07E714-1-3.
104. Kohl, P.A., 2011. *Low-dielectric constant insulators for future integrated circuits and packages*. Annual Review of Chemical and Biomolecular Engineering, ed. J.M. Prausnitz. Vol. 2. Palo Alto, CA: Annual Reviews. pp.
105. Maier, G., "Low dielectric constant polymers for microelectronics," *Progress in Polymer Science*, 2001. 26(1): 3-65.
106. Ashida, K., 1995. *Syntactic foams*. Handbook of plastic foams: types, properties, manufacture and applications, ed. A.H. Landrock. New Jersey: Noyes Publications. pp.
107. Shahin, M., M. Al-Haj Abdallah, and A. Zihlif, "Dielectric properties of epoxy-glass microballoons composite," *Journal of Polymer Materials*, 1995. 12: 151-156.

108. Shahin, M., M. Al-Haj Abdallah, and A. Zihlif, "Temperature dependence of electrical properties of epoxy-glass microballoons composite," *Journal of Polymer Materials*, 1996. 13: 253-257.
109. Gupta, N., S. Priya, R. Islam, and W. Ricci, "Characterization of mechanical and electrical properties of epoxy-glass microballoon syntactic composites," *Ferroelectrics*, 2006. 345(1): 1-12.
110. Andritsch, T.M., A. Lunding, P.H.F. Morshuis, H. Negle, and J.J. Smit. *Dielectric behavior of syntactic foams at low temperatures and frequencies*. in *2007 Annual Report Conference on Electrical Insulation and Dielectric Phenomena*, (Vancouver, BC, 2007). 2007. Vancouver, BC.
111. Zhu, B., J. Ma, J. Wang, J. Wu, and D. Peng, "Thermal, dielectric and compressive properties of hollow glass microsphere filled epoxy-matrix composites," *Journal of Reinforced Plastics and Composites*, 2012. 31(19): 1311-1326.
112. Ansermet, J.P. and E. Baeriswyl, "Dielectric study of hollow microsphere composites," *J Mater Sci*, 1994. 29(11): 2841-2846.
113. Andritsch, T., A. Lunding, P.H.F. Morshuis, H. Negle, and J.J. Smit. *The investigation of the permittivity of syntactic foam under varying humidity*. in *2008 Annual Report Conference on Electrical Insulation Dielectric Phenomena*, (Quebec, QC, 2008). 2008. Quebec, QC.
114. Strauchs, A., A. Mashkin, A. Schnettler, and J. Podlazly. *The impact of water absorption on the dielectric properties of syntactic foam*. in *Solid Dielectrics (ICSD), 2010 10th IEEE International Conference on Solid Dielectrics*, (Potsdam, Germany, 2010). 2010. Potsdam.
115. Roggendorf, C. and A. Schnettler, "Accelerated hydrothermal aging of epoxy resin based syntactic foams with polymeric microspheres," *IEEE Transactions on Dielectrics and Electrical Insulation*, 2012. 19(3): 973-980.
116. Dang, Z.M., Y. Shen, and C.W. Nan, "Dielectric behavior of three-phase percolative Ni-BaTiO₃/polyvinylidene fluoride composites," *Applied Physics Letters*, 2002. 81(25): 4814-4816.
117. Jayasundere, N. and B.V. Smith, "Dielectric constant for binary piezoelectric O₃ composites," *Journal of Applied Physics*, 1993. 73(5): 2462-2466.
118. Zhang, W. and K. Bhattacharya, "A computational model of ferroelectric domains. Part I: model formulation and domain switching," *Acta Materialia*, 2005. 53(1): 185-198.

119. Scaife, B.K.P., 1998. *Principles of dielectrics*. Oxford, U.K.: Clarendon press. pp.
120. Zhu, B.L., J. Ma, J. Wu, K.C. Yung, and C.S. Xie, "Study on the properties of the epoxy-matrix composites filled with thermally conductive AlN and BN ceramic particles," *Journal of Applied Polymer Science*, 2010. 118: 2754-2764.
121. Wouterson, E.M., F.Y.C. Boey, X. Hu, and S.-C. Wong, "Fracture and impact toughness of syntactic foam," *Journal of Cellular Plastics*, 2004. 40(2): 145-154.
122. Liang, J.-Z., "Tensile and impact properties of hollow glass bead-filled PVC composites," *Macromolecular Materials and Engineering*, 2002. 287(9): 588-591.
123. Yusriah, L. and M. Mariatti, "Effect of hybrid phenolic hollow microsphere and silica-filled vinyl ester composites," *Journal of Composite Materials*, 2013. 47(2): 169-182.
124. Low, L.F. and A. AbuBakar, "Fracture toughness and impact strength of hollow epoxy particles toughened polyester composites," *Sains Malaysiana*, 2013. 42(4): 443-448.
125. Liang, J.-Z., "Impact fracture toughness of hollow glass bead-filled polypropylene composites," *Journal of Materials Science*, 2007. 42(3): 841-846.
126. Liang, J.Z. and C.B. Wu, "Gray relational analysis between size distribution and impact strength of polypropylene/hollow glass bead composites," *Journal of Reinforced Plastics and Composites*, 2009. 28(16): 1945-1955.
127. Ferreira, J.A.M., C. Capela, and J.D. Costa, "A study of the mechanical behaviour on fibre reinforced hollow microspheres hybrid composites," *Composites Part A: Applied Science and Manufacturing*, 2010. 41(3): 345-352.
128. Zihlif, A.M. and G. Rastoga, "Yielding and fracture toughness of glass microballoon-filled epoxy composites," *Polymers and Polymer Composites*, 2001. 9(5): 345-350.
129. Kim, H.S. and H.H. Oh, "Manufacturing and impact behavior of syntactic foam," *Journal of Applied Polymer Science*, 2000. 76(8): 1324-1328.
130. Kim, H.S. and M.A. Khamis, "Fracture and impact behaviours of hollow microsphere/epoxy resin composites," *Composites Part A: Applied Science and Manufacturing*, 2001. 32(9): 1311-1317.
131. Woldesenbet, E., "Low velocity impact properties of nanoparticulate syntactic foams," *Materials Science and Engineering: A*, 2008. 496(1-2): 217-222.
132. Li, G. and N. Jones, "Development of rubberized syntactic foam," *Composites Part A: Applied Science and Manufacturing*, 2007. 38(6): 1483-1492.

133. Li, G. and M. John, "A crumb rubber modified syntactic foam," *Materials Science and Engineering: A*, 2008. 474(1-2): 390-399.
134. Li, G. and V.D. Muthyala, "A cement based syntactic foam," *Materials Science and Engineering: A*, 2008. 478(1-2): 77-86.
135. Kim, H.S. and C. Mitchell, "Impact performance of laminates made of syntactic foam and glass fiber reinforced epoxy as protective materials," *Journal of Applied Polymer Science*, 2003. 89: 2306-2310.
136. Shunmugasamy, V., D. Pinisetty, and N. Gupta, "Viscoelastic properties of hollow glass particle filled vinyl ester matrix syntactic foams: effect of temperature and loading frequency," *Journal of Materials Science*, 2013. 48(4): 1685-1701.
137. ASTM International, W.C., PA, 2011, *Standard test method for unnotched cantilever beam impact resistance of plastics*, in *ASTM Standard D4812*. 2011.
138. Nagendra, N., U. Ramamurty, T.T. Goh, and Y. Li, "Effect of crystallinity on the impact toughness of a La-based bulk metallic glass," *Acta Materialia*, 2000. 48(10): 2603-2615.